International Institute for
Applied Systems Analysis
Schlossplatz 1
A-2361 Laxenburg, Austria

Tel: +43 2236 807 342
Fax: +43 2236 71313
E-mail: publications@iiasa.ac.at
Web: www.iiasa.ac.at

**Interim Report** **IR-08-012**

# Is the Climate Sensitivity Even More Uncertain?

Katsumasa Tanaka (tanaka@iiasa.ac.at)
Thomas Raddatz (thomas.raddatz@zmaw.de)
Brian C. O'Neill (oneill@iiasa.ac.at)
Christian H. Reick (christian.reick@zmaw.de)

**Approved by**

Sten Nilsson (nilsson@iiasa.ac.at)
Director

July 3, 2008

## Contents

## Abstract

Uncertainty in climate sensitivity is a fundamental problem for projections of the future climate. Climate sensitivity is defined as the equilibrium response of global-mean surface air temperature to a doubling of the atmospheric $CO_2$ concentration from the preindustrial level (≈ 280 ppm). In spite of various efforts to estimate its value, climate sensitivity is still not well constrained (IPCC, 2007, pp.718-727 and pp.798-799; Gerard and Baker, 2007), posing a difficulty to informing climate change policy. Here we show that the climate sensitivity is in fact even more uncertain than has been found by earlier studies (Andronova and Schlesinger, 2001; Gregory et al., 2002; Knutti et al., 2002; Forest et al., 2006; Hegerl et al., 2006). Our results suggest that uncertainty in historical radiative forcing has not been sufficiently considered and that including a carbon cycle feedback, which in principle offers an additional constraint on climate sensitivity, does not reduce the uncertainty in climate sensitivity due to the poor knowledge of the global carbon budget before the year 1850.

## Acknowledgments

This study is financially supported by the International Max Planck Research School on Earth System Modelling (IMPRS-ESM), Hamburg, Germany and the International Institute for Applied Systems Analysis (IIASA), Laxenburg, Austria. K. Tanaka presented earlier versions of this study in various occasions, notably the Workshop on Climate Risk Assessment, Tsukuba, Japan on March 6-7, 2007, Ph.D. defense at Hamburg Universität, Germany on April 30, 2007, and European Geosciences Union (EGU) General Assembly 2008, Vienna, Austria on April 13-18, 2008. K. Tanaka acknowledges all who provided useful comments to improve this study.

This paper has been submitted to *Proceedings of the National Academy of Sciences – USA* (PNAS).

## About the Authors

Katsumasa Tanaka is a Postdoc in Population and Climate Change (PCC) Program and Greenhouse Gas Initiative (GGI) at IIASA.

Dr. Thomas Raddatz is a Postdoc in the Research group Global Vegetation Modelling in the Department of Land in the Earth System at Max Planck Institute for Meteorology in Hamburg.

Brian O'Neill is the Leader of the Population and Climate Change (PCC) Program and a Scientist III in the Institute for the Study of Society and Environment (ISSE) at the National Center for Atmospheric Research (NCAR) in Boulder, Colorado.

Dr. Christian H. Reick is the Group Leader of the Research group Global Vegetation Modelling in the Department of Land in the Earth System at Max Planck Institute for Meteorology in Hamburg.

# Is the Climate Sensitivity Even More Uncertain?

Katsumasa Tanaka
Thomas Raddatz
Brian C. O'Neill
Christian H. Reick

## Introduction

Atmosphere-Ocean General Circulation Models (AOGCMs) show different climate sensitivity ranging from 1.9°C to 4.6°C (IPCC, 2007, pp.798-799), reflecting our poor understanding of the Earth's radiation budget and the response of the hydrological cycle and the biosphere to climate change.

Climate sensitivity can be estimated also by an inversion approach using historical observations over various periods and time scales. The uncertainties in existing inversion estimates are dominated by uncertainties in reconstructions of historical surface air temperature. Uncertainty in historical radiative forcing has received much less attention. Previous inversion studies express this forcing uncertainty by introducing an additional parameter to scale a presumed time-evolution of the aerosol forcing, with the exception of one study (Hegerl et al., 2006) that uses different realizations of volcanic and solar forcing. The scaling approach does not fully capture radiative forcing uncertainty, because the influence of its temporal structure on climate may also be relevant for climate sensitivity estimation. Previous inversion studies have not also considered interactions of the climate system with other aspects of the Earth system (e.g. carbon cycle feedbacks and anthropogenic changes in land albedo), despite the recognized importance of these feedbacks for future climate projections (Cox et al., 2000; IPCC, 2007;).

## Methods

Here we investigate the effect of radiative forcing uncertainty and carbon cycle feedback on the estimation of climate sensitivity using an inversion setup of the Aggregated Carbon Cycle, Atmospheric Chemistry, and Climate model (ACC2) (Tanaka et al., 2007; Tanaka, 2008) for the period 1750-2000. In ACC2, the carbon cycle, atmospheric chemistry, and the climate system are linked via feedbacks and therefore jointly affect the estimation of various uncertain parameters in each of these components (Tables S1 and S2 of Supplementary Information).

Radiative forcing is represented as the sum of three types of forcing: calculated radiative forcing subject to uncertainties ($CO_2$, $CH_4$, and $N_2O$ forcing), prescribed/parameterized radiative forcing without uncertainties (other GreenHouse Gas (GHG), aerosol, volcanic, and solar forcing), and "missing forcing." This missing

forcing term accounts for the uncertainty in the prescribed/parameterized radiative forcing and also represents forcings that are not included in other forcing terms in ACC2 (e.g. albedo forcing and mineral dust forcing). Furthermore, it reflects the interannual and decadal variability in the temperature records (except for the ENSO-induced change after 1930). Missing forcing is treated as a parameter in each year. Further discussion on missing forcing is found in Methods.

We obtain a best estimate of the uncertain parameters corresponding to the minimum of a cost function (equation (1) in Methods), in contrast to previous inversion studies which compute the Probability Density Function (PDF) of climate sensitivity. Calculating a PDF can be done for a problem addressing a small number of uncertainties but is infeasible for our approach, which considers more than one thousand uncertain parameters, including those representing missing forcing.

We conduct two sets of simulations:

1) We compare the standard ACC2 inversion (i.e., expressing radiative forcing uncertainty as missing forcing) with two other ACC2 inversions with alternative representations of radiative forcing uncertainty: one in which, similar to previous studies, it is expressed by an uncertain forcing scaling factor applied to the aerosol forcing, and a second that assumes no forcing uncertainty at all. We do not consider the climate-carbon cycle feedback in these cases in order to focus on the effect of radiative forcing uncertainty.

2) We use the standard radiative forcing representation, but carry out two inversions in which the climate-carbon cycle feedback is either included or not, termed coupled or uncoupled inversion experiment, respectively. For further details, see Methods.

For all setups, we calculate the relationship between the minimum value of the cost function and the value of climate sensitivity by performing a series of inversions by which climate sensitivity is fixed at values between 1°C and 10°C at intervals of 0.25°C. The shape of this relationship indicates both the best estimate of climate sensitivity and the uncertainty of such an estimate.

## Results and Discussion

### Uncertainty in Radiative Forcing

Figure 1 (unfilled plots) shows the cost function values for the first set of simulations. It indicates that the climate sensitivity is unlikely to be smaller than 2°C, in line with the results of the PDF studies. More importantly, if the forcing uncertainty is fully addressed as missing forcing, the cost function curve is almost completely flat at values of climate sensitivity above about 2°C. In this case, the inversion indicates little preference for any value of climate sensitivity in the range 2°C–10°C. In contrast, if the forcing uncertainty is represented as an uncertain scaling factor applied to a fixed temporal trend of aerosol forcing as in the PDF studies, the climate sensitivity appears far better constrained, particularly at high values. It is even better constrained if the uncertainty in the radiative forcing is not considered at all. Therefore, our analysis suggests that the well-defined peak of the PDF of climate sensitivity in former studies is a consequence of insufficient treatment of the historical development of radiative

forcing uncertainty. Including these uncertainties implies that climate sensitivity is much less constrained at the high end than previously thought.

We can draw this conclusion even though our results are not expressed as PDFs as in previous studies. According to probabilistic inverse estimation theory (Tarantola, 2005), our best estimate for climate sensitivity can be interpreted as the *peak* of the marginal posterior PDF for *all the parameters*. The previous studies cited above, on the other hand, present the marginal posterior PDF for *climate sensitivity* (obtained by integrating our marginal posterior PDF with respect to the parameters other than climate sensitivity). Thus, the two approaches reduce the full joint posterior PDF differently. Nevertheless, in our case, differences in the value of the cost function qualitatively indicate differences in relative likelihood because the cost function changes monotonically with respect to parameters (Figure S14 of Supplementary Information). In other words, flatter cost function curves mean less constrained PDFs.

More in detail, Figure 2 presents radiative forcing and temperature time series resulting from missing forcing- and forcing scaling-based inversions. Figure 2.1 shows that low climate sensitivity is not supported even with the missing forcing approach because of the difficulty in explaining the warming in the late 20th century. Figure 2.2 demonstrates that high climate sensitivity is not acceptable with the forcing scaling approach, which results in excessively strong cooling after large volcanic eruptions in the 19th century. Such results indicate that the forcing scaling approach is too inflexible to deal with the complexity in forcing uncertainty.

## Carbon Cycle Feedback

If considering temperature and radiative forcing is insufficient to constrain climate sensitivity, including feedbacks with other Earth system components in the inversion may tighten the constraint, a possibility addressed by the second set of simulations.

The cost function curves of the coupled and uncoupled inversions are both nearly flat at high values of climate sensitivity (two lower curves in Figure 1). So, despite the addition of climate-carbon cycle feedback, our inversion still almost equally accepts a wide range of high climate sensitivity.

This result can be explained by examining the relative contributions of different sources of uncertainty to the cost function (Figure 3). Almost all sources display the same flat shape toward high climate sensitivity, with two exceptions: missing forcing in both coupled and uncoupled cases, which has a distinct minimum at a climate sensitivity of 2.5–3.0°C, and land use $CO_2$ emissions in the coupled case, which decreases monotonically toward high climate sensitivity. Thus, Figure 3 suggests that in the uncoupled case, the uncertainty in climate sensitivity is large because about 80% of the cost function is derived from variables that do not contribute to discriminating among higher values of climate sensitivity. In the coupled case, the uncertainty in climate sensitivity is even slightly larger because, although the missing forcing and land use emission terms do discriminate among climate sensitivity values to some extent, they act in opposite directions.

The time series in Figure 4 explain the decreasing land use $CO_2$ emission residuals toward high climate sensitivity in Figure 3. In the early 19th century, the

atmospheric $CO_2$ concentration records stabilized (Figure 4.2) due to the suppression of heterotrophic respiration at the low surface temperature caused by volcanic eruptions. However, the simulated respiration responses to volcanic eruptions are not sufficiently large (Figure 4.3), resulting in a cutoff of the land use $CO_2$ emission (Figure 4.1). The eruption-induced decrease in the heterotrophic respiration is larger with higher climate sensitivity, leading to a smaller reduction in the land use $CO_2$ emission.

The results above depend on the prior estimates and their uncertainties of the land use $CO_2$ emission and land $CO_2$ uptake for the first 100 years of the inversion, which are linearly extrapolated from the later period. Thus, an improvement of data quality before 1850 would be necessary to improve the effectiveness of climate sensitivity estimation with a coupled model.

### Caveats

We have not discussed ocean $CO_2$ uptake as it turned out to be nearly insensitive to the temperature change in our simulations (Figure S1 of Supplementary Information). Also we have not discussed the atmospheric chemistry component because no temperature feedbacks to the atmospheric chemistry processes are included in the model and it therefore did not affect the results of our analysis. We assume a fixed estimate for the ocean diffusivity (Kriegler, 2005) because constraining the ocean diffusivity requires oceanic heat diffusion processes, which are not explicitly modelled in ACC2. Our estimate of the prior range for missing forcing is also uncertain, but the sensitivity analysis in Section S3 of Supplementary Information demonstrates that our overall conclusions hold under various possible assumptions. Our results are based only on a single temperature reconstruction (Jones et al., 1998; Mann and Jones, 2003) as our emphasis lies in considering radiative forcing uncertainty.

### Concluding Remarks

The question still remains as to how to appropriately represent the forcing uncertainty, although it may ultimately depend on the specific research question. Our results support the idea of using the carbon cycle for climate sensitivity estimation. The interplay among the uncertainty estimates in the carbon cycle and climate systems encourages a holistic uncertainty analysis using an Earth system model with more complexity.

## Details in Methods

### Model

We use ACC2, a global-annual-mean Earth system model comprising carbon cycle, atmospheric chemistry, and climate components. The ocean and land carbon cycle processes are represented by the respective four-reservoir box models tuned to Impulse Response Function models (Hooss et al., 2001; Joos et al., 1996). Thermodynamic equilibria for marine carbonate species ($CO_2(aq)$, $HCO_3^-$, and $CO_3^{2-}$) are dynamically computed and are sensitive to the ocean mixed layer temperature, providing temperature effect on ocean $CO_2$ uptake. The temperature sensitivity of large scale ocean circulation

is not accounted for, which is acceptable on the time scale of our model projections. $CO_2$ fertilization for Net Primary Production and temperature-dependency of heterotrophic respiration are parameterized with the beta factor and Q10, respectively. ACC2 incorporates parameterizations of atmospheric chemistry processes (Joos et al., 2001; WMO, 2003; IPCC, 2005) involving direct radiative forcing agents ($CO_2$, $CH_4$, $N_2O$, $O_3$, $SF_6$, 29 species of halocarbons, sulfate aerosols (direct effect), carbonaceous aerosols (direct effect), all aerosols (indirect effect), and stratospheric $H_2O$) and indirect radiative forcing agents (OH, $NO_x$, CO, and VOC), including feedbacks of $CH_4$ and $N_2O$ concentrations on their lifetimes. Volcanic (Ammann et al., 2003) and solar (Krivova et al., 2007) forcings are prescribed. The calculation of surface air temperature is based on the Diffusion Ocean Energy balance CLIMate model (DOECLIM) (Tarantola, 2005), a land-ocean energy balance model. Note that ACC2 version 3.1 (Tanaka, 2008) that we use in this paper slightly differs from ACC2 version 3.0 (Tanaka et al., 2007) mainly in its treatment of Q10. Differences in the inversion results are not significant.

## Inversion

The ACC2 inversion derives a best estimate of major uncertain parameters by synthesizing various knowledge on the Earth system including parameter estimates, observations, and physical-biogeochemical laws on the basis of the probabilistic inverse estimation theory (Tarantola, 2005). The parameters and data used in the ACC2 inversion are summarized in Tables S1 and S2 of Supplementary Information.

Our approach is concerned with the estimates obtained by optimization, corresponding to the minimum of the cost function $S(\mathbf{m})$ as follows:

$$S(\mathbf{m}) = \frac{1}{2}\left( \sum_{i=1}^{a} \left( \frac{g_i(\mathbf{m}) - d_{mes,i}}{\sigma_{d,i}} \right)^2 + \sum_{j=1}^{b} \left( \frac{m_j - m_{prior,j}}{\sigma_{m,j}} \right)^2 \right) \qquad (1)$$

$g_i(\mathbf{m})$ is the forward model projection for data $i$ based on a set of parameter $\mathbf{m}$. $a$ and $b$ are the total numbers of data and parameters, respectively. $d_{mes,i}$ and $m_{prior,j}$ denote measurement $i$ and prior estimate of parameter $j$, respectively. $\sigma_{d,i}$ and $\sigma_{m,j}$ are one-sigma uncertainty ranges for measurement $i$ and for prior estimate of parameter $j$, respectively. In the framework of the probabilistic inverse estimation theory, the cost function is the negative of the argument of the exponential function expressing the marginal posterior PDF for all the parameters. We assume normal distributions for all the prior uncertainties of the parameters and data. It should be noted that all the parameters and data in the ACC2 inversions are treated independently, implying that fits for time series having strong autocorrelations are over-emphasized.

Inverse calculations are performed using the local optimization solver CONOPT3 implemented in GAMS. The solutions for inversions are confirmed by performing the same inversions from different initial points.

Inversions are performed from the year 1750 to 2000. Although the system is not completely equilibrated due to various natural forcings and internal dynamics, we made a steady-state assumption in 1750 on the ground that the energy-intensive machinery,

the key driver for the global warming, emerged in the early 18th century and also that the land use $CO_2$ emission has already been substantial in magnitude by mid 19th century.

## Missing Forcing

The prior estimate of the missing forcing is assumed to be 0.0 W/m$^2$ throughout the inversion period. The 2σ prior uncertainty range is assumed to be constant at 0.5 W/m$^2$ before 1900 primarily to explain the natural variability in the temperature (rationales explained below). Then the uncertainty range increases linearly to 1.0 W/m$^2$ in 2000 to account mainly for the uncertainty in the aerosol forcing, which is consistent with the corresponding IPCC range (IPCC, 2007, Figure SPM.2). The prior uncertainty range of the missing forcing is assumed to be larger by four-fold when volcanic forcing is stronger than -0.5 W/m$^2$ in consideration of associated processes not resolved in the model.

Below are the rationales for the 2σ prior missing forcing range before 1900 (±0.5 W/m$^2$). Our model simulations indicate that a constant radiative forcing of at least 0.5 W/m$^2$ is required to produce a temperature rise of 0.5°C on a decadal time scale with various climate sensitivity (Figure S5 of Supplementary Information). We assume that natural variability of the global-mean temperature is at most 0.5°C, based on the followings: 1) The global-mean surface temperature has risen about 0.5°C in the first half of the 20th century. Attribution/detection studies have so far not agreed upon whether such warming was due to natural variability or anthropogenic interference. 2) The temperature projection in the 1000-year control run of Community Climate System Model (CSM-1.4) (a coupled GCM) indicates a temperature variability of about 0.5°C (Doney et al., 2006).

## Coupled/Uncoupled Inversion Setups

The coupled inversion experiment uses the standard inversion setup, where the climate component is fully coupled with the ocean and land carbon cycle components, so that the feedback between these Earth system components is fully accounted for. More specifically, in ACC2 this feedback is acting via the following two loops: a) Thermodynamic equilibria for the marine carbonate species ($CO_2(aq)$, $HCO_3^-$, and $CO_3^{2-}$) depend on the ocean mixed layer temperature (linearly related to the ocean surface air temperature), which in turn controls the $CO_2$ uptake from the atmosphere, thereby influences indirectly the ocean surface air temperature. b) The land surface air temperature influences heterotrophic respiration of the soil, and thus the land $CO_2$ flux to the atmosphere, thereby indirectly feeding back on the land surface air temperature. In the second experiment, uncoupled inversion experiment, this climate-carbon cycle feedback has been suppressed, by setting artificially the temperature as seen by ocean and land carbon cycle fixed to its preindustrial value. $CO_2$ exchange between the three compartments atmosphere, ocean, and land is thus uncoupled from changes in surface air temperature in this second type of experiment.

## References


Ammann C. M., Meehl, G. A., Washington, W. M., and C. S. Zender. 2003. A monthly and latitudinally varying volcanic forcing dataset in simulations of 20th century climate. Geophysical Research Letters 30(12): 1,657, doi:10.1029/2003GL016875

Andronova, N. G. and M. E. Schlesinger. 2001. Objective estimation of the probability density function for climate sensitivity. Journal of Geophysical Research 106, D19: 22,605-22,611.

Cox, P. M., Betts, R. A., Jones, C. D, Spall, S. A., and I. J. Totterdell. 2000. Acceleration of global warming due to carbon-cycle feedbacks in a coupled climate model. Nature 408: 184-187.

Doney, S. C., Lindsay, K., Fung, I., and J. John. 2006. Natural variability in a stable, 1000-yr global coupled climate–carbon cycle simulation. Journal of Climate 19: 3,033-3,054.

Etheridge, D. M., Steele, L. P., Langenfelds, R. L., and R. J. Fransey. 1996. Natural and anthropogenic changes in atmospheric CO2 over the last 1000 years from air in Antarctic ice and firn. Journal of Geophysical Research 101, D2: 4,115-4,128.

Forest, C. E., Stone, P. H., and A. P. Sokolov. 2006. Estimated PDFs of climate system properties including natural and anthropogenic forcings. Geophysical Research Letters 33: L01705, doi:10.1029/2005GL023977.

Friedlingstein, P., Cox, P., Betts, R., Bopp, L., von Bloh, W., Brovkin, V., Cadule, P., Doney, S., Eby, M., Fung, I., Bala, G., John, J., Jones, C., Joos, F., Kato, T., Kawamiya, M., Knorr, W., Lindsay, K., Matthews, H. D., Raddatz,T., Rayner, P., Reick, C., Roeckner, E., Schnitzler, K.-G., Schnur, R., Strassmann, K., Weaver, A. J., Yoshikawa, C., and N. Zeng. 2006. Climate–carbon cycle feedback analysis: Results from the C4MIP model intercomparison. Journal of Climate 19: 3,337–3,353.

Gerard, H. R. and M. B. Baker. 2007. Why is climate sensitivity so unpredictable? Science 318: 629-632.

Gregory, J. M., Stouffer, R. J., Raper, S. C. B., Stott, P. A., and N. A. Rayner. 2002. An observationally based estimate of the climate sensitivity. Journal of Climate 15: 3,117-3,121.

Hegerl, G. C., Crowley, T. J., Hyde, W. T., and D. J. Frame. 2006. Climate sensitivity constrained by temperature reconstructions over the past seven centuries. Nature 440: 1,029-1,032.

Hooss, G., Voss, R., Hasselmann, K., Maier-Reimer, E., and F. Joos. 2001. A nonlinear impulse response model of the coupled carbon cycle-climate system (NICCS). Climate Dynamics 18: 189-202.

Houghton, R. A. 2003. Revised estimates of the annual net flux of carbon to the atmosphere from changes in land use and land management 1850-2000. Tellus B 55: 378-390.

Intergovernmental Panel on Climate Change (IPCC). 2007. Climate change 2007: the physical science basis. Contribution of Working Group I to the Fourth Assessment Report of the Intergovernmental Panel on Climate Change [Solomon, S., Qin, D., Manning, M., Chen, Z., Marquis, M., Averyt, K. B., Tignor, M., and H.L. Miller (eds.)]. Cambridge, UK and New York, NY, USA: Cambridge University Press, 996 pp.

Intergovernmental Panel on Climate Change (IPCC). 2005. IPCC special report on safeguarding the ozone layer and the global climate system: Issues related to hydrofluorocarbons and perfluorocarbons. Cambridge: Cambridge University Press.

Jones, P. D., Parker, D. E., Osborn, T. J., and K. R. Briffa. 2006. Global and hemispheric temperature anomalies – land and marine instrumental records. In Trends: A Compendium of Data on Global Change. Oak Ridge, Tennessee, USA: Carbon Dioxide Information Analysis Center, Oak Ridge National Laboratory, U.S. Department of Energy, http://cdiac.ornl.gov/

Joos, F., Bruno, M., Fink, R., Siegenthaler, U., and T. F. Stocker. 1996. An efficient and accurate representation of complex oceanic and biospheric models of anthropogenic carbon uptake. Tellus B 48: 397-417.

Joos, F., Prentice, C., Sitch, S., Meyer, R., Hooss, G., Plattner, G.-K., Gerber, S., and K. Hasselmann. 2001. Global warming feedbacks on terrestrial carbon uptake under the Intergovernmental Panel on Climate Change (IPCC) emission scenarios. Global Biogeochemical Cycles 15: 891–907.

Knutti, R., Stocker, T. F., Joos, F., and G.-K. Plattner. 2002. Constraints on radiative forcing and future climate change from observations and climate model ensembles. Nature 416: 719-723.

Keeling, C. D. and T. P. Whorf. 2005. Atmospheric CO2 records from sites in the SIO air sampling network. In Trends: A Compendium of Data on Global Change. Oak Ridge, Tennessee, USA: Carbon Dioxide Information Analysis Center, Oak Ridge National Laboratory, U.S. Department of Energy, http://cdiac.ornl.gov/

Kriegler, E. 2005. Imprecise probability analysis for Integrated Assessment of climate change. Ph.D. dissertation. Potsdam, Germany: Potsdam Universität, 256 pp. http://opus.kobv.de/ubp/volltexte/2005/561/

Krivova, N. A., Balmaceda, L., and S. K. Solanki. 2007. Reconstruction of solar total irradiance since 1700 from the surface magnetic flux. Astronomy and Astrophysics 467: 335-346.

Mann, M. E. and P. D. Jones. 2003. Global surface temperatures over the past two millennia. Geophysical Research Letters 30(15): 1,820, doi:10.1029/2003GL017814

Tanaka, K., Kriegler, E., Bruckner, T., Hooss, G., Knorr, W., and T. Raddatz. 2007. Aggregated Carbon Cycle, Atmospheric Chemistry, and Climate model (ACC2): Description of the forward and inverse modes. Reports on Earth System Science 40, 188 pp. Hamburg, Germany: Max Planck Institute for Meteorology. http://www.mpimet.mpg.de/wissenschaft/publikationen/erdsystemforschung.html

Tanaka, K. 2008. Inverse estimation for the simple Earth system model ACC2 and its applications. Ph.D. dissertation. Hamburg, Germany: Hamburg Universität, International Max Planck Research School on Earth System Modelling, 296 pp. http://www.sub.uni-hamburg.de/opus/volltexte/2008/3654/

Tarantola, A. 2005. Inverse problem theory and methods for model parameter estimation. Philadelphia, USA : Society for Industrial and Applied Mathematics (SIAM), 342 pp. http://www.ipgp.jussieu.fr/~tarantola/

World Meteorological Organization (WMO). 2003. Scientific assessment of ozone depletion: 2002, Report No. 47. Geneva, Switzerland: Global Ozone Research and Monitoring Project, 498 pp.

## Figures

**Figure 1**. Cost function in the ACC2 inversions under different treatments to radiative forcing uncertainty and climate-carbon cycle feedback

Final values of the cost function are computed by optimizations with climate sensitivity fixed at values between 1°C and 10°C at intervals of 0.25°C. Each plot represents a unique inversion result. In square brackets, best estimates of climate sensitivity are shown.

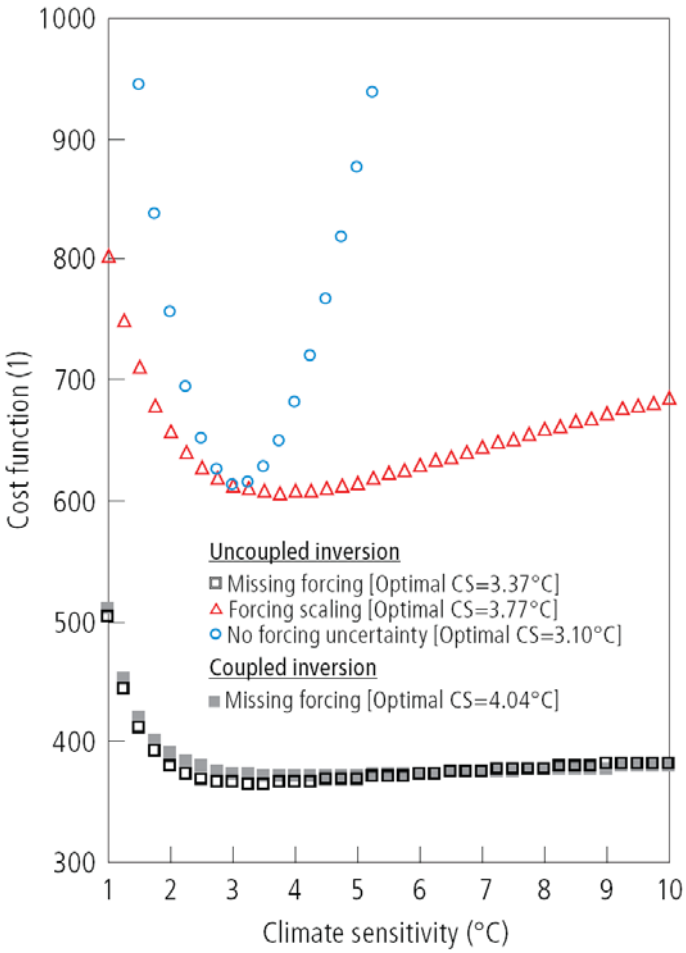


**Figure 2**. Comparison of the results of ACC2 inversions using missing forcing- and forcing scaling-approach

The figures show the results from the uncoupled inversions using the missing forcing- and forcing scaling-approach with climate sensitivity of 1, 3, 5, and 10°C. The prior missing forcing is 0 W/m$^2$ over the entire period. The forcing scaling factor is estimated to be 0.045, 0.999, 1.214, and 1.398 in the forcing scaling-based inversions with climate sensitivity of 1, 3, 5, and 10°C, respectively. Measurements in Figure 2.2 are compilation of temperature reconstruction (Jones et al, 1998; Mann and Jones, 2003) and instrumental records (Jones et al., 2006). Insert of Figure 2.2 shows the "residuals,"

i.e. the difference between prior and posterior values. The residuals are calculated such that the mean measurement during the period 1961-1990 is equal to the corresponding posterior mean. Measurements shown in the main figure are for the missing forcing-based inversion with climate sensitivity of 3°C. Note that the prior uncertainty ranges for the missing forcing and temperature change are assumed four times larger when volcanic forcing is stronger than -0.5 W/m$^2$.

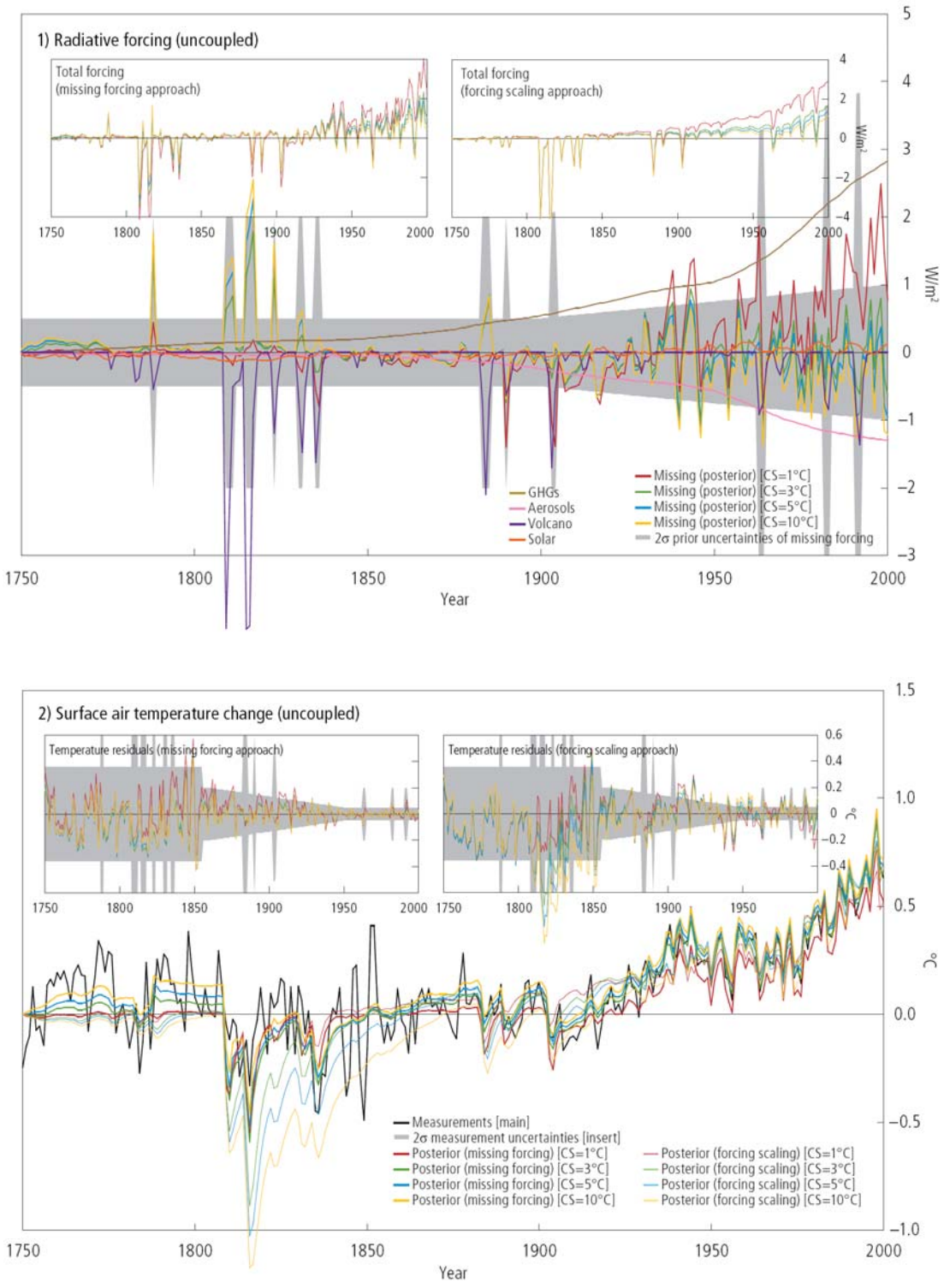

**Figure 3**. Various contributions to the cost function in the ACC2 coupled and uncoupled inversions

Temporal sums of the squares of the residuals weighted by the associated prior uncertainties (σ) are shown. They are obtained from the coupled and uncoupled inversions with climate sensitivity fixed at values between 1°C and 10°C at intervals of 0.25°C. Each plot represents a unique inversion result.

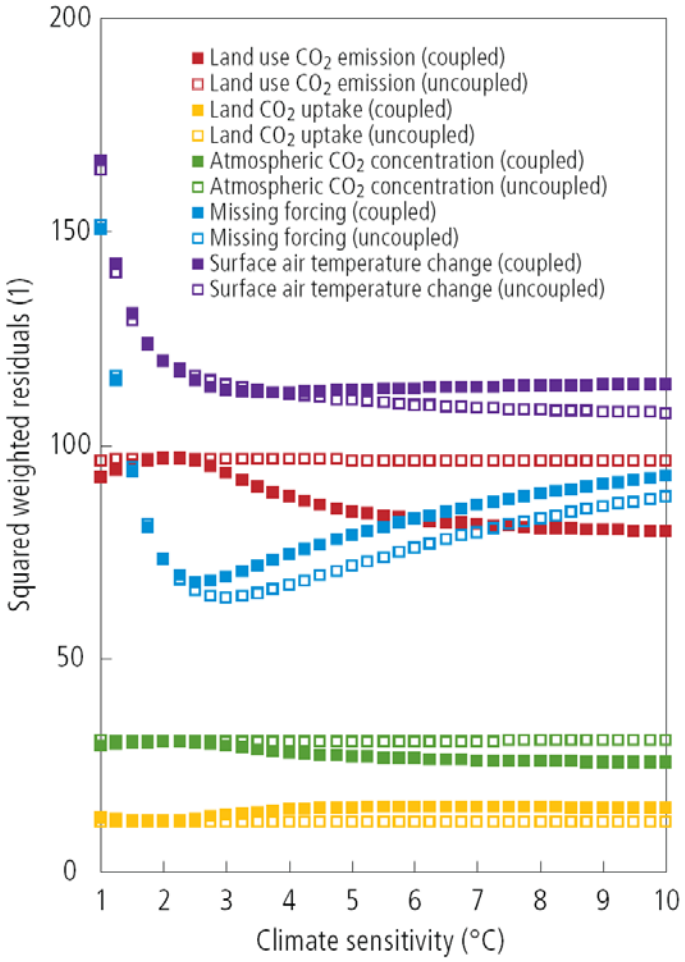

**Figure 4**. Comparison of the ACC2 coupled and uncoupled inversion results

Shown in the figures are the coupled and uncoupled inversion results for optimal climate sensitivity (4.04°C and 3.37°C, respectively). Note that the prior uncertainty range for the atmospheric $CO_2$ concentration is assumed four times larger when volcanic forcing is stronger than -0.5 W/m$^2$. More details of the prior for the land use $CO_2$ emission (Houghton, 2003), atmospheric $CO_2$ concentration (Etheridge et al., 1996; Keeling and Whorf, 2005), and land $CO_2$ uptake (Friedlingstein et al., 2006) are shown in Tables S1 and S2 of Supplementary Information.

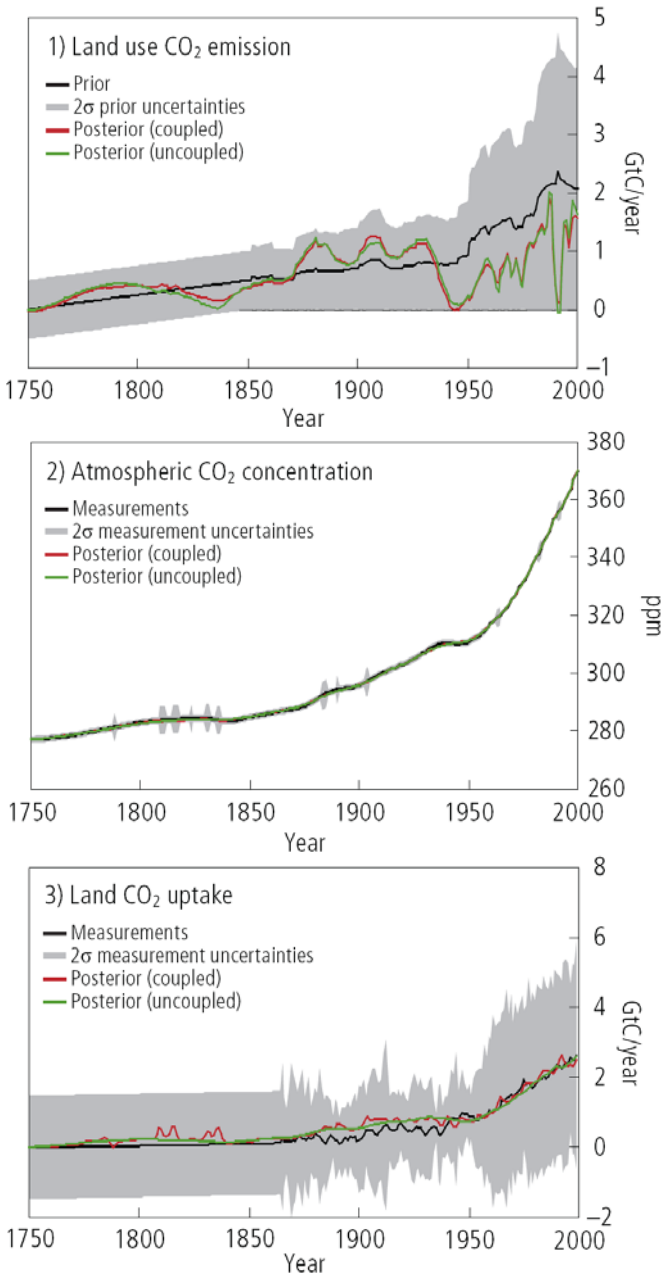

# SUPPLEMENTARY INFORMATION

## S1. INTRODUCTION AND SUMMARY

This Supplementary Information section provides in-depth analyses to support our inversion methodology and conclusions in the main article. First, we show the validity of the ACC2 inversion results based on their qualitative interpretation. Second, we demonstrate that the conclusions in the main article hold under various assumptions.

Two conclusions in the main article are the followings: 1) It is of paramount importance to reconsider how to deal with forcing uncertainty in inversion-based climate sensitivity estimation. 2) Even when the carbon cycle feedback is provided in the inversion, the uncertainty in the historical carbon budget makes it difficult to produce a tighter constraint on climate sensitivity estimation.

The conclusions above rest on several assumptions. Assumptions that we explicitly look at are as follows. First, the prior missing forcing uncertainty presumed in the ACC2 inversion is assumed based on the early 20th-century warming and the natural variability of a GCM control run (Doney et al., 2006), but uncertainty ranges in various radiative forcings are not yet well-established (IPCC, 2007, p.4). Second, we assume that the prior uncertainty range for land use $CO_2$ emission is twice as large as the corresponding estimate of Houghton (2003) because the estimate of land use $CO_2$ emission is different depending on the approach (bottom-up vs. inversion) and also influenced by the uncertainty in the global carbon budget (e.g. missing carbon flux such as soil erosion (Lal, 2005)). Third, ACC2 employs the volcanic forcing of Ammann et al. (2003) among others (e.g. Bertrand et al., 2002; Crowley et al., 2003). The estimate of volcanic forcing depends on the ice cores used, interpretation of the records, and estimation methodology (e.g. scaling from aerosol optimal depth to radiative forcing). Fourth, all the parameters and data are assumed to be independent – autocorrelations are not taken into account in our inversion setup.

Furthermore, there are statements in the main article that can be checked with additional analyses. Regarding the composition of missing forcing, relevant sensitivity analyses provide some insight. Also, further sensitivity analyses can substantiate our claim that the cost function curves are qualitatively comparable with PDFs.

This Supplementary Information section is organized as follows. In Section S2, we discuss the main ACC2 inversion results in more detail. Section S3 aims to strengthen the first main conclusion by looking at the influence of prior forcing uncertainty to the inversion results. Section

S4 is to support the second main conclusion by investigating how the inversion results are affected by the presupposed prior land use $CO_2$ emission range and volcanic forcing. In Section S5, we discuss the implications of other key assumptions to the main conclusions: namely, presupposed ocean diffusivity and prior climate sensitivity. In Section S6, a brief discussion on the posterior missing forcing is provided. Then we look at how the missing forcing is affected by prescribed aerosol forcing, prescribed volcanic forcing, and ENSO-driven temperature variability. Section S7 aims to show the relevancy of our cost function curves to PDFs on the basis of the sensitivity of the cost function value to major parameters (beta, Q10, and forcing scaling factor). Lastly in Section S8, we analyze the implications of the independence assumption of the residuals – specifically, our analysis investigate how the autocorrelations in temperature residuals influences the first main conclusion.

## S2. Full Results of the Main ACC2 Inversions

In this section, full results of the main ACC2 inversions are shown. We demonstrate that the inversion results can be meaningfully interpreted, supporting the validity of the inversion results. We begin with overall discussion of the inversion results (Section S2.1) and discuss problems for statistical tests (Section S2.2). This is followed by detailed accounts for the land use $CO_2$ emission in the late 20th century (Section S2.3), global estimate of Q10 (Section S2.4), temporal suspension of the atmospheric $CO_2$ concentration rise in the mid 20th century (Section S2.5), terrestrial biosphere response to volcanic eruptions (Section S2.6), and optimal climate sensitivity (Section S2.7).

### S2.1. Overall Discussion

Visual inspection of the time series (Figure S1) indicates that in the coupled and uncoupled inversion results, the overall fits to the observations are fairly good in comparison to the associated prior uncertainty ranges. All the posterior parameter estimates (Table S4) do not substantially depart from their prior estimates, supporting the validity of the inversion results. Exceptions are the land use $CO_2$ emission around 1991 and Q10, which are discussed in Sections S2.3 and S2.4, respectively. It had also been demonstrated that the fits for various time series has been drastically improved, compared to the results of forward simulation in which all the parameters are fixed at their prior estimates (Tanaka, 2008, Figure 4.1).

The final values of the cost function are nearly the same in the coupled and uncoupled inversions (371.1 and 365.1, respectively (Table S3)) – however, it is substantially larger in the forcing scaling-based inversion (607.0 (Table S3)). Such a large cost function value stems from the temperature misfit, in particular the short-term changes due to the natural variability and volcanic cooling (Figure S2). In the forcing scaling-based inversion, the squared weighted residuals for

temperature account for nearly 70% of the cost function. The result here indicates that the forcing scaling approach is not sufficient to explain the observed temperature change.

### S2.2. Problems with Statistical Tests

Validation for the ACC2 inversion results relies only on qualitative examinations. A $\chi^2$ test, which is designed to evaluate the size of residuals, is not a proper statistical validation for our problem due to the following two reasons:

First, a $\chi^2$ test can be used only for a linear model. Our model ACC2 is moderately nonlinear as a whole, as a result of the combined effect of several nonlinear processes such as $CO_2$ fertilization, temperature feedback to the ocean and land $CO_2$ uptake, concentration-radiative forcing relationships for $CO_2$, $CH_4$, and $N_2O$, and ocean heat uptake. While $CO_2$ fertilization dampens the rising atmospheric $CO_2$ concentration, the temperature feedback to the ocean and land $CO_2$ uptake further amplifies it. The $CO_2$ concentration-radiative forcing relationship has a damping effect for $CO_2$-induced warming as relevant absorption bands are filled with rising $CO_2$ concentration. Ocean heat uptake delays the warming (Figure S5) – the entire warming effect emerges after several hundred years.

Second, a large number of correlations among the residuals (inserts for Figures S1 and S2; Figure S3) is a problem to get a meaningful result from a $\chi^2$ test. All the parameters and data are assumed to be independent in the ACC2 inversions.

### S2.3. Land Use $CO_2$ Emission in the Late 20th Century

To reproduce the observed atmospheric $CO_2$ concentration in the late 20th century, the posterior estimates of the land use $CO_2$ emission (Houghton, 2003) are substantially smaller than the prior even with strong terrestrial biospheric uptake. The posterior land use $CO_2$ emission (Figure S1.2) is lower than the corresponding prior for the last 60 years. The posterior estimate of the beta factor is 0.59, which is high in the prior range between 0.1 and 0.7. The high beta factor is in line with Friedlingstein et al. (2006) showing strong $CO_2$ fertilization in most process-based terrestrial biosphere models.

It is important to point out that such inversion results should not be regarded merely as an indication for low land use $CO_2$ emission – they should rather be taken as an overall uncertainty in the historical carbon budget. Structural uncertainty in the carbon cycle is reflected to the posterior land use $CO_2$ emission because of its relatively large prior uncertainty range.

It should be noted that the prior uncertainty range of the land use $CO_2$ emission is assumed to be twice as large as the range suggested in Houghton (2003). Without such an adjustment, the inversion produces large residuals (beyond the $2\sigma$ prior uncertainty ranges) for land use $CO_2$ emission around 1991 (Figure S7.2a) and for the atmospheric $CO_2$ concentration between 1930 and 1940 (Figure S7.3a). The reasons for such an adjustment are three-fold: 1) Previous inversion studies (e.g. Gurney et al., 2002) indicate smaller estimates of land use $CO_2$ emission than Houghton's

estimates. 2) In the inversion results, the land use $CO_2$ emission reflects the imbalance of the carbon budget due to the missing carbon cycle processes such as soil erosion, which is estimated to be -1.5 to +1.0 GtC/year (Lal, 2005). 3) Processes related to water cycle are not described in ACC2 (Section S2.4).

### S2.4. Global Estimate of Q10

The posterior estimate of Q10 is 1.18, lying outside of the 2σ prior uncertainty range between 1.5 and 2.5 (Table S2), which is based on the compilation of field measurements (Table 2 in Tjoelker et al. (2003)) and the observational constraint for GCM (Jones and Cox, 2001). It is also significantly lower than 2.0, which is typically assumed in biosphere models.

The low Q10 points to structural uncertainty – the low Q10 reflects the biospheric response not only to the temperature change but also to the soil moisture change, which is not described in ACC2. With global warming, the contrast between wet and dry regions will increase as all GCMs demonstrate (Wang, 2005). Precipitation and probably also soil moisture will increase in most of the presently wet regions and decrease in the subtropical regions. More water in presently wet soils will decrease heterotrophic respiration because of the oxygen limitation while less water in presently dry soils will also reduce heterotrophic respiration because of the water limitation. Thus, the temperature effect and the soil moisture effect on the heterotrophic respiration cancel out each other, resulting in the low Q10.

### S2.5. Temporal Suspension of the Atmospheric $CO_2$ Concentration Rise

The influence of decadal variability shows up in the residuals for the atmospheric $CO_2$ concentration. An example is the plateau between 1940 and 1960. During this period and thereafter, the temperature rise also stalls. Mechanisms that led to this phenomenon are in dispute. An inversion study (Trudinger et al., 2002) shows that the slowdown of the atmospheric $CO_2$ concentration rise is caused by the change in the large-scale ocean circulation. However, such a halt does not appear in the prior ocean $CO_2$ uptake based on $C^4$MIP runs (Figure S1.4).

### S2.6. Terrestrial Biosphere Response to Volcanic Eruptions

Several strong volcanic forcing between 1750 and 1850 are offset by positive missing forcing when the corresponding temperature drops in reconstruction are relatively small (Figures S1.10 to S1.12). The mismatch between the volcanic forcing and reconstructed temperature is explained by the diffuse radiation hypothesis (Robock, 2005): Photosynthesis is enhanced by diffuse radiation produced from the forward scattering of the solar radiation due to stratospheric sulfate aerosols. However, evidences for the diffuse radiation hypothesis are not yet conclusive as there are large discrepancies among different volcanic forcings (Section S4.2) and temperature reconstructions (Jones and Mann, 2004, Figures 7 and 8).

We briefly discuss two examples below. After the Tambora eruption in 1815, no

temperature drop appears in the reconstruction. If the diffuse radiation hypothesis is true, tree ring proxies used for the temperature reconstruction would be biased by the plant growth enhanced by the diffuse radiation. Then, the temperature would have actually been lower after the eruption than what is directly indicated by the proxies.

Following the Pinatubo eruption in 1991, the growth of the atmospheric $CO_2$ concentration slowed down. Our inversion results indicate that the suppression of the heterotrophic respiration due to the cooling was not sufficient to explain the observed $CO_2$ concentration trend, resulting in a drastic reduction in the land use $CO_2$ emission (Figure S1.2). If the diffuse radiation hypothesis is true, the unusually low land use $CO_2$ emission can be attributed to the photosynthesis enhancement due to increased diffuse radiation (Gu et al., 2003).

### S2.7. Optimal Climate Sensitivity

Differences in the optimal climate sensitivity obtained from different approaches can be explained by looking at residuals.

The best estimate of climate sensitivity is larger in the coupled inversion (4.04°C) than in the uncoupled inversion (3.37°C). The higher optimal climate sensitivity in the coupled inversion is due to the declining trend in the residuals for land use $CO_2$ emission toward high climate sensitivity (Figure 3 of the main article and the associated discussion).

The optimal climate sensitivity is higher in the forcing scaling-based inversion (3.77°C) than in the missing forcing-based inversion (3.37°C). Figure S4 shows that this is primarily caused by the residual curve for the surface air temperature change, which dominates the change in the cost function. The temperature residual curve for the forcing scaling-based inversion has a distinct minimum at climate sensitivity of 3.5–4.0°C.

## S3. Assumptions for Prior Forcing Uncertainty

The prior uncertainty of radiative forcing is uncertain (a problem of uncertainty's uncertainty). In this section, we first discuss numerical simulations that are used to derive the standard prior uncertainty range for missing forcing. And then we look at the sensitivity of the inversion results to the prior uncertainty range of missing forcing.

The prior forcing uncertainty range assumed in the ACC2 inversion can be supported by model calculations. The 2σ prior missing forcing range of 0.5 $W/m^2$ is assumed before 1900 in order to account for the temperature variability of 0.5°C under various climate sensitivity (up to 6.5°C as in its 2σ prior range). Such temperature variability is indicated from the early 20th-century warming and the natural variability of a GCM control run (Doney et al., 2006). Figure S5 shows that, if the climate sensitivity is 6.5°C, a sustained perturbation of 0.5 $W/m^2$ leads to a warming of about 0.5°C

over 50 years.

Cost function curves are sensitive to the prior range for missing forcing (Figure S6). If we reduce the prior missing forcing range by 50%, the cost function curve is not only shifted up over the entire range of climate sensitivity, but also tilted up toward high climate sensitivity (Figure S6.1). The temperature time series (Figure S6.3) show that such a tilt stems mainly from the growing misfit for the temperature after volcanic eruptions in the early 19th century. The slope toward high climate sensitivity is coincidentally similar to those for the forcing scaling approach. With smaller prior forcing uncertainty range, the slope eventually converges to that for no forcing uncertainty. The cost function curve for the forcing scaling approach is not sensitive to the prior uncertainty range for the forcing scaling factor, indicating that the single parameter of forcing scaling factor does not have a significant impact on the cost function.

## S4. Assumptions related to Carbon Cycle Feedback

The second main conclusion on carbon cycle feedback rests on the prior assumptions for the land use $CO_2$ emission and also on the prescribed volcanic forcing selected among others. Volcanic eruptions have a non-negligible perturbation to the global carbon cycle. In this section, we demonstrate that the inversion results are influenced by the prior land use $CO_2$ emission – nonetheless, the second main conclusion remains the same.

### S4.1. Prior Uncertainty in Land Use $CO_2$ Emission

The uncertainty range for land use $CO_2$ emission is uncertain and is assumed twice as large as the uncertainty range suggested by Houghton (2003) (Section S2.3). We discuss the sensitivity of the inversion results to prior uncertainty range for land use $CO_2$ emission.

When a 50% smaller prior range for land use $CO_2$ emission (equivalent to Houghton's estimate) is assumed, the cost function value of the coupled inversion becomes substantially smaller than that of the uncoupled inversion over the entire range of climate sensitivity (Figure S7.1). The larger difference between the coupled and uncoupled results stems from the carbon cycle in the early 19th century. The cessation of the $CO_2$ concentration rise during the period 1800-1850 is explained by the suppression of soil respiration during the cooling periods following large volcanic eruptions. Without the climate-carbon cycle feedback, the slump of the $CO_2$ concentration rise is reproduced by the reduction in the land use $CO_2$ emission. This results in a larger penalty in the cost function particularly when the prior range of the land use $CO_2$ emission is assumed 50% smaller than the standard (Figure S7.2a). The opposite but less pronounced results are found when the prior uncertainty of land use $CO_2$ emission is assumed 50% larger than the standard (Figure S7.2c).

Using 50% smaller prior range for land use $CO_2$ emission is problematic. This is indicated

from the large residuals for land use $CO_2$ emission around 1991 (Figure S7.2a) and for the atmospheric $CO_2$ concentration between 1930 and 1940 (Figure S7.3a). Under such an assumption, the inversion is forced to resolve prior information in conflict. In light of the overall uncertainty in the global carbon budget (Section S2.3), it is fair to assume the standard prior range (twice as large as the Houghton's range).

It is worth noting that in the uncoupled inversion results the best estimate of the climate sensitivity is nearly unaffected from the change in the prior uncertainty range for land use $CO_2$ emission. The inversion in the carbon cycle component hardly influences the inversion in the climate component in the absence of the climate-carbon cycle feedback. This result itself is interesting as it suggests that uncertainty in the carbon cycle system can hardly be seen as a problem from the climate system – the uncertainties in radiative forcing and climate sensitivity dwarfs the uncertainties in the carbon cycle. This is so unless a feedback from climate to carbon cycle is provided.

### S4.2. Volcanic Forcing

Estimates of volcanic forcing depend on the ice cores used, interpretation of the records, and estimation methodology (e.g. scaling from aerosol optimal depth to radiative forcing) as indicated by the inconsistency among different volcanic forcing estimates (e.g. Ammann et al., 2003; Bertrand et al., 2002; Crowley et al., 2003). We investigate whether our finding based on Ammann's volcanic forcing is still valid when different volcanic forcing is used.

Inversion results based on the three different volcanic forcings are compared in Figure S8. Missing forcing shows marked differences before 1930 (Figures S8.5 and S8.6), but this does not affect our conclusions on forcing uncertainty. Similar results can be seen in the carbon cycle (Figures S8.2 to S8.4), supporting our conclusion on carbon cycle feedback. The trend of the cost function curve is similar among all the inversion results (Figure S8.1). The climate sensitivity is estimated higher for the coupled inversion in all the three cases. The best guess of climate sensitivity is diverse in particular in the coupled cases, ranging from 3.37°C to 4.44°C.

## S5. Other Key Assumptions in the ACC2 Inversion

In the previous sections we have analyzed how the inversion results are influenced by the prior missing forcing range, the prior land use $CO_2$ emission range, and the prescribed volcanic forcing. In this section, we discuss the influences from remaining key assumptions: namely, the presupposed ocean diffusivity and the prior climate sensitivity.

### S5.1. Ocean Diffusivity

Ocean diffusivity is a major uncertainty in the climate system. However, we assume a fixed estimate

for ocean diffusivity (0.55 $cm^2/s$) based on Kriegler (2005, Figure 2.8) because ocean diffusivity cannot be well-constrained simultaneously with climate sensitivity in our inversion setup, which does not utilize ocean heat distribution data (Levitus et al., 2000). We look into how our results are affected when assuming different ocean diffusivity (1.0 $cm^2/s$ and 2.0 $cm^2/s$).

The results of such a sensitivity analysis are shown in Figure S9. The influence of the ocean diffusivity to the inversion results is systematic and small (Figure S9.1). Time series in Figures S9.2 and S9.3 are nearly the same. Thus, our main findings are not affected by the treatment of ocean diffusivity.

### S5.2. Prior Climate Sensitivity

It has been argued that prior assumptions highly influence inversion results (Tol and de Vos, 1998; Frame et al., 2005). We investigate the sensitivity of the inversion results to different prior assumptions for climate sensitivity. The prior 2σ uncertainty range adopted in the standard inversion is 0.5°C–6.5°C. The prior mean is 3.5°C as normal distributions are assumed for all the parameters and data in the ACC2 inversion. We try our inversion for the 2σ uncertainty range of 1.5°C–4.5°C, a conventional range indicated by GCMs (IPCC, 2001, Chapter 9). The 2σ uncertainty range of 0.5°C–10.5°C is also tested, a conservative range emphasizing the long tail indicated by PDFs for climate sensitivity (e.g. IPCC, 2007, pp.798-799).

The resulting change in the best estimate of climate sensitivity is, however, not substantial (Figure S10). One reason is that in our approach the time-variant parameters are dominant in the cost function over constant parameter such as climate sensitivity. The analysis here suggests that our main conclusions are not significantly influenced by the prior climate sensitivity.

## S6. MISSING FORCING

Missing forcing is "catch-all" forcing, comprising mainly three elements as discussed in the main article. First, we provide a brief discussion on the posterior missing forcing. Then we investigate how the missing forcing is influenced by aerosol forcing, volcanic forcing, ENSO-induced temperature variability to get an insight into the composition of missing forcing.

### S6.1. Posterior Missing Forcing

The missing forcing is punctuated by large spikes corresponding to volcanic eruptions. Most of these spikes are positive and some others negative, depending on how are the mismatches between the volcanic forcing and the reconstructed temperature. The missing forcing after 1900 is highly variable, reflecting the interannual variability of the temperature records. The fluctuation becomes larger toward present as the prior temperature uncertainty gets smaller with extensive observation network

put into place and also as the prior uncertainty of the missing forcing becomes larger to reflect aerosol forcing uncertainty. The average missing forcing over the last 50 years is about -0.12 W/m$^2$, an indication that the aerosol forcing used in ACC2 is slightly underestimated in magnitude.

### S6.2. Influence from Aerosol Forcing

We look at how the uncertainty in aerosol forcing is reflected to missing forcing. The aerosol forcing is a major uncertainty in the climate system (IPCC, 2007, p.32). In ACC2, the aerosol forcing is represented by the following three types: sulfate aerosol forcing (direct effect), carbonaceous aerosol forcing (direct effect), and all aerosol forcing (indirect effect) (Table 2.1 of Tanaka (2008)). The direct sulfate aerosol forcing and indirect aerosol forcing are calculated based on the respective parameterizations given as a function of $SO_2$ emission. The carbonaceous aerosol forcing is given as a function of CO emission. These three types of aerosol forcings are summed up to 1.3 W/m$^2$ in year 2000. We perform a sensitivity analysis of the inversion results by assuming 50% weaker total aerosol forcing over the entire period and also by assuming 50% stronger total aerosol forcing.

The results of such a sensitivity analysis are in Figure S11, showing that the missing forcing acts to cancel out the hypothesized change in the magnitude of aerosol forcing. The offset between the aerosol forcing and the missing forcing is only partial – there are large differences in the posterior estimates of climate sensitivity (1.95°C for 50% weaker aerosol forcing; 3.37°C for standard aerosol forcing; and 6.71°C for 50% stronger aerosol forcing). Final values of the cost function are, however, similar (368.8 for 50% weaker aerosol forcing; 371.7 for standard aerosol forcing; and 386.9 for 50% stronger aerosol forcing).

### S6.3. Influence from Volcanic Forcing

We check how the uncertainty in volcanic forcing (Section S4.2) is reflected to the missing forcing. We perform a sensitivity analysis of the inversion results to volcanic forcing (Ammann et al., 2003; Bertrand et al., 2002; Crowley et al., 2003).

The results of the sensitivity analysis are in Figure S12. It is demonstrated that the missing forcing is highly influenced by the volcanic forcing. It is evident in particular before 1900, but for the last 100 years it is less explicit as it is superimposed by the influence from the interannual variability in the temperature records. Mostly missing forcing turns strongly positive, contemporaneous with volcanic eruptions, which can be interpreted as corrections for the volcanic forcing to reproduce the reconstructed temperature. Note that such corrections are not always positive (e.g. 1890 in Ammann's volcanic forcing). The insert of Figure S12.1 shows that the missing forcing is all contained within the 2σ prior boundary, except for the period influenced by the Tambora eruption in 1815 in Crowley's volcanic forcing.

### S6.4. Influence from ENSO-driven Temperature Variability

We look into how the missing forcing is influenced by interannual variability in the temperature data.

In the standard ACC2 inversion setup, the ENSO-induced interannual variability in the temperature records is removed by using a linear regression as a function of an annualized Southern Oscillation Index (SOI) (Tanaka, 2008, Section 3.5.1). The annualization includes a 4-month lead because the temperature variability is statistically best explained by SOI with 4-month lead (Kriegler, 2005, Figure 2.4; our pre-analysis). The ENSO-related correction on the temperature records is applied only after 1930 due to the credibility of the index. We perform an inversion without using the ENSO-related correction on the temperature records and compare it with the standard results.

The two inversion results are compared in Figure S13, showing that the missing forcing reflects the interannual variability of the temperature records. The insert of Figure S13.2 demonstrates that, when a strong El Niño or La Niña event occurs, the temperature fit is better with the correction for ENSO-induced temperature variability. Without the ENSO-related correction, the missing forcing is adjusted such that it artificially produces the ENSO-induced temperature variability (insert of Figure S13.1).

## S7. COST FUNCTION CURVE VS PDF

In the main article, we argue that the cost function curves for climate sensitivity (consisting of different optimization results) are qualitatively indicative of PDFs for climate sensitivity in literature because the cost function changes monotonically with parameters and it does not show other local optima or extreme irregularity. We now demonstrate this by a sensitivity analysis of the cost function curves with respect to major influential parameters.

The results in Figures S14.1 to S14.4 show that the changes in the cost function curves are not so drastic or irregular for middle to high climate sensitivity. These results suggest that cost function curves are comparable to PDFs for middle to high climate sensitivity. Although rigorous proofs for the statements above require extensive parameter sampling and mathematical derivations, our sensitivity analysis provides a first-order indication that the cost function curves are qualitatively comparable to PDFs for climate sensitivity.

## S8. AUTOCORRELATIONS

The residuals for the data and parameters in the ACC2 inversion are assumed to be independent without accounting for their autocorrelations. Although such an assumption implies that fits for time series having strong autocorrelations are over-emphasized, the autocorrelations are neglected altogether in the ACC2 inversion because of the difficulty in fully estimating them. However,

Ricciuto et al. (2008) demonstrate that neglecting autocorrelations result in overconfidence in parameter estimation by using an inversion setup for a simple global carbon cycle and climate model. It is also statistically known that the ignorance of autocorrelations biases the estimation (e.g. Zellner and Tiao, 1964). Thus, in this section, we quantitatively assess how the solutions of the ACC2 inversions are influenced from the ignorance of autocorrelations. Our analysis focuses on the autocorrelations in the surface air temperature residuals and their impacts on the cost function curves in Figure 1 of the main article.

### S8.1. Implementing AR(1) Model in the Cost Function

The following explains how the autocorrelations in temperature residuals can be taken into account in the ACC2 inversion. The solution of the ACC2 inversion corresponds to the minimum of the cost function $S(\mathbf{m})$ (equivalent to equation (1) of the main article):

$$S(\mathbf{m}) = \frac{1}{2}\left( \sum_{i=1}^{a} \left( \frac{g_i(\mathbf{m}) - d_{mes,i}}{\sigma_{d,i}} \right)^2 + \sum_{j=1}^{b} \left( \frac{m_j - m_{prior,j}}{\sigma_{m,j}} \right)^2 \right). \qquad \text{(S1)}$$

$g_i(\mathbf{m})$ is the forward model projection for data $i$ based on a set of parameter $\mathbf{m}$. $a$ and $b$ are the total numbers of data and parameters, respectively. $d_{mes,i}$ and $m_{prior,j}$ denote measurement $i$ and prior estimate of parameter $j$, respectively. $\sigma_{d,i}$ and $\sigma_{m,j}$ are one-sigma uncertainty ranges for measurement $i$ and for prior estimate of parameter $j$, respectively. In terms of "residuals," i.e. the differences between prior and posterior values, equation (S1) can be expressed as

$$S(\mathbf{m}) = \frac{1}{2}\left( \sum_{i=1}^{a} \left( \frac{r_{d,i}}{\sigma_{d,i}} \right)^2 + \sum_{j=1}^{b} \left( \frac{r_{m,j}}{\sigma_{m,j}} \right)^2 \right), \qquad \text{(S2)}$$

where $r_{d,i}$ and $r_{m,j}$ are the residuals for data *i* and parameter *j*.

In order to account for the autocorrelations in temperature residuals, we use an AR model of 1st-order (AR(1)), a simplest method to describe an AR process. Collins et al. (2001) demonstrate that the global-mean surface air temperature variability of the 1000-year control run of HadCM3 can be described as an AR(1) process. Kriegler (2005, p.43) concludes that based on several statistical tests, an AR(1) model is sufficient to describe the weather-driven variability of SST residuals during the period 1870-2002 except for ENSO. However, it is not clear how the decadal variability appeared in the residuals can be explained just with an AR(1) model. Eden et al. (2002) demonstrate that AR(5) provides a best fit to explain the variability in the mix layer temperature of the North Atlantic. Nevertheless, we use the AR(1) representation as a first cut and check the residual spectrums to see whether the AR(1) model removes the autocorrelations in temperature residuals.

An AR(1) model (e.g. Box and Jenkins, 1970, pp.56-58; von Storch and Zwiers, 1999, p.204) between temperature residuals can be described as

$$r_{d,k+1} = \alpha \cdot r_{d,k} + \beta + \varepsilon_{d,k}\ ,\quad k = 1,2,\cdots,250 \tag{S3}$$

where $\alpha$ and $\beta$ are the propagator and constant, respectively. $r_{d,k}$ and $r_{d,k+1}$ are temperature residuals. Index numbers 1-251 are assigned to temperature residuals in years 1750–2000. $\varepsilon_{d,k}$ is Independently and Identically Distributed (IID) (thus, white noise) and follows a normal distribution with a mean of zero and a standard deviation of $\sigma_\varepsilon$. By further assuming $\beta = 0$, the AR(1) model is simplified to

$$r_{d,k+1} = \alpha \cdot r_{d,k} + \varepsilon_{d,k}\ . \tag{S4}$$

The AR(1) model is implemented to the cost function $S(\mathbf{m})$ as follows:

$$S(\mathbf{m}) = \frac{1}{2}\left(\left(\frac{r_{d,1}}{\sigma_\varepsilon}\right)^2 + \sum_{i=1}^{250}\left(\frac{r_{d,i+1} - \alpha \cdot r_{d,i}}{\sigma_\varepsilon}\right)^2 + \sum_{l=251}^{a}\left(\frac{r_{d,l}}{\sigma_{d,l}}\right)^2 + \sum_{j=1}^{b}\left(\frac{r_{m,j}}{\sigma_{m,j}}\right)^2 + \left(\frac{r_{m,b+1}}{\sigma_{m,b+1}}\right)^2\right). \tag{S5}$$

The first term on the right side of equation (S5) account for the squared weighted residual for the temperature residual in 1750. The autocorrelation for this start year is not considered, but this does not significantly affect the results because the time series are relatively long in our inversion. For the temperature residuals from 1751 onward, autocorrelations are taken into account (second term in equation (S5)). The standard deviation $\sigma_\varepsilon$ is used for all the temperature residuals instead of the prior uncertainty for temperature change, $\sigma_{d,k}$. Residual terms of the other data and parameters are unchanged (third and fourth terms). The last term on the right side of equation (S5) is introduced for the new parameter $\alpha$. The implementation here is similar to the form of the likelihood function for an AR(1) process (e.g. Box and Jenkins, 1970, pp.274-284; von Storch and Zwiers, 1999, pp.257-258).

### S8.2. Estimation of AR(1) Propagator

This section discusses the estimation problem of the propagator $\alpha$ and the standard deviation $\sigma_\varepsilon$ in equation (S4). For our exercise in this section, we assume a fixed value of 0.45 for propagator $\alpha$, the maximum likelihood estimate for the SST residuals (except for ENSO) during the period 1870-2002 (Kriegler, 2005, p.40). We also assume a value of 0.078°C for the standard deviation $\sigma_\varepsilon$ (Kriegler, 2005, p.36). This set of estimates is assumed for all the ACC2 inversion cases when the AR(1) model is introduced. As a result of such an assumption, the propagator $\alpha$ is no longer considered as a new parameter in the inversion. Thus, the last term in equation (S5) is dropped and the cost function including the AR(1) model can be rewritten as

$$S(\mathbf{m}) = \frac{1}{2}\left(\left(\frac{r_{d,1}}{\sigma_\varepsilon}\right)^2 + \sum_{i=1}^{250}\left(\frac{r_{d,i+1} - \alpha \cdot r_{d,i}}{\sigma_\varepsilon}\right)^2 + \sum_{l=251}^{a}\left(\frac{r_{d,l}}{\sigma_{d,l}}\right)^2 + \sum_{j=1}^{b}\left(\frac{r_{m,j}}{\sigma_{m,j}}\right)^2\right). \tag{S6}$$

Our approach stated above is in contrast to other studies in which the propagator for the AR(1)

model is treated similar to other parameters and optimized in the inversion (e.g. Ricciuto et al., 2008). The value of propagator is indeed specific to the inversion result. However, we dare to take this approach due to a problem for interpretation as discussed below.

To interpret the implemented AR(1) model from the perspective of inverse estimation, equation (S5) is reformulated as follows:

$$S(\mathbf{m}) = \frac{1}{2}\left( \cdots + \left( \frac{r_{d,k}}{\sigma_\varepsilon / \sqrt{1+\alpha^2}} \right)^2 - \frac{1}{\sigma_\varepsilon / 2\alpha} r_{d,k-1} \cdot r_{d,k} - \frac{1}{\sigma_\varepsilon / 2\alpha} r_{d,k} \cdot r_{d,k+1} + \cdots \right)^2 . \quad \text{(S7)}$$

Only the changes related to temperature residual $r_{d,k}$ are explicitly shown in equation (S7). In all the three terms on the right side of equation (S7), the propagator $\alpha$ appears. If the propagator $\alpha$ is optimized in the inversion similar to other studies, equation (S7) indicates that the prior uncertainty for $r_{d,k}$ (and also the associated covariances), which must be fixed before the inversion, is optimized to minimize the cost function. Optimizing a prior uncertainty in the inversion is not compatible with the inverse estimation theory (e.g. Tarantola, 2005) even though numerical computation is feasible.

### S8.3. Experimental Design

By using the AR(1) model discussed above, we re-calculate the three cost function curves in Figure 1 of the main article: namely, the missing forcing-based inversion, the forcing scaling-based inversion, and the inversion assuming no forcing uncertainty. Similar to other sensitivity analyses, the relationship between the value of the cost function and the value of climate sensitivity is calculated by performing a series of inversions by which the climate sensitivity is fixed at values between 1°C and 10°C at intervals of 0.25°C. By comparing with the original inversion results without the AR(1) model, we investigate if the conclusion of the importance of forcing uncertainty can still be drawn.

Except for the AR(1) model implementation, other parts of the model and the inversion setup are kept the same. Some detailed notes for the methodology follow. The standard deviation $\sigma_\varepsilon$ is assumed to be larger by a factor of 4 when volcanic forcing is stronger than -0.5 W/m$^2$ similar to the treatment for the original prior uncertainty of temperature change (Tanaka, 2008, Section 3.5.2). The ENSO-driven temperature variability is also statistically considered as in the standard inversion without the AR(1) model (Tanaka, 2008, Section 3.5.1). The Kriegler's estimate of $\sigma_\varepsilon$ is obtained for the period of instrumental temperature, but the same estimate is assumed for all the period in our exercise. Autocorrelations for the missing forcing are still neglected because the estimates of the associated propagator and standard deviation are not available. Autocorrelations for the atmospheric $CO_2$ concentration is also not included in our analysis.

### S8.4. Results and Discussion

In Figure S15.1, the cost function curves for the inversions including the AR(1) model are compared

with those without the AR(1) model. The associated residuals in several selected time series are shown in Figure S15.2. In more detail, Figures S15.3 to S15.6 show the radiative forcing and temperature change with the climate sensitivity fixed at 1, 3, 5, and 10°C. Histograms and spectrums of the temperature residuals are shown in Figure S16.

First of all, visual inspection of the spectrums in Figure S16 indicates that in all the cases the residuals appear as white noise when the AR(1) is implemented.

Visual inspection of the cost function curves in Figure S15.1 suggests that on the whole, the cost function curves based on the inversions including the AR(1) model are wider than those based on the standard inversions without the AR(1) model. This result suggests that the ignorance of autocorrelations leads to an overconfidence of climate sensitivity estimation, which is in line with the result of the analysis for carbon cycle (Ricciuto et al., 2008).

Looking into this result in more details, the influence of the AR(1) model to the cost function curves is different for low and high climate sensitivity. Toward high climate sensitivity, the slopes of the cost function curves are hardly influenced by the inclusion of the AR(1) model in all the three inversion cases. This result suggests that our conclusion on the importance of forcing uncertainty is unaffected even if the autocorrelations in temperature residuals are neglected.

On the contrary, in low climate sensitivity, the slopes of the cost function curves become much flatter by the inclusion of the AR(1) model. This is particularly so in the forcing scaling case. The flatter curve for the forcing scaling case stems from the trend in the temperature residuals (right panel of Figure S15.2). Figure S15.6 furthermore shows this is caused by the temperature residuals during the period 1940-1950 and 1980-2000, which are less penalized than in the case without the AR(1) model. But these results are highly influenced by the assumption for the value of standard deviation $\sigma_\varepsilon$.

The best estimate of climate sensitivity for the missing forcing approach is slightly lowered from 3.37°C to 3.06°C when the AR(1) model is considered (Figure S15.1). This is primarily caused by the change in the shape of missing forcing residual curve (left panel of Figure S15.2). Figure S15.3 shows that the missing forcing becomes substantially smaller during the last 50 years of the inversion with climate sensitivity fixed at 1°C. The smaller missing forcing in combination of small climate sensitivity results in an apparent systematic underestimation of the recent temperature (Figure S15.4). However, this turns out to be the 'best estimates' because the systematic errors are partly explained as autocorrelations. This result points to the need for careful interpretation of the inversion results because considering autocorrelations can mask wrong results.

The other noteworthy result is that the cost function curve for the missing forcing approach in Figure S15.1 is lifted up by the inclusion of the AR(1) model whereas those for the other two approaches are lowered. The left panel of Figure S15.2 indicates that the increase in the cost function values for the missing forcing approach is primarily due to the increase in the temperature residuals over the entire range of climate sensitivity. Furthermore, Figure S15.6 shows that the temperature

residuals before 1850 are more penalized due to the smaller standard deviation, which also depends on the presupposed value of standard deviation $\sigma_\varepsilon$.

In conclusion, our analysis confirms the fact that the ignorance of autocorrelations leads to an overconfidence of parameter estimation (e.g. Zellner and Tiao, 1964; Ricciuto et al., 2008). In our results, however, this does apply to low climate sensitivity but not high climate sensitivity. By neglecting the autocorrelations in temperature residuals, the confirmation of ruling out the low climate sensitivity becomes overstated. On the contrary, the main conclusion on the importance of forcing uncertainty holds irrespective of the treatment of the autocorrelations.

The analysis presented here considers only the autocorrelations in temperature residuals described as the AR(1) model, leaving out all the other autocorrelations including those remaining in the residuals of temperature and those in other parameters and data. Furthermore, using AR models would only partially account for the autocorrelations because of the complexity of correlation structure. A full solution would be to introduce stochasticity to the model as model errors (Houtekamer et al., 1996) and the ensemble results can be used to estimate the off-diagonal elements of the covariance matrices.

**Table S1.** Data in the ACC2 coupled inversion (after Table 3.1 of Tanaka (2008))

* Four times larger uncertainty ranges are assumed when volcanic forcing is stronger than -0.5 W/m$^2$ (Tanaka, 2008, Section 3.5.2). The total number of degrees of freedom for data is 1,498.

| Names (degrees of freedom) | Periods | Measurement types | Temporal resolutions | 2σ measurement uncertainties | Data sources |
|---|---|---|---|---|---|
| Ocean $CO_2$ uptake (df=250) | 1750-1860 | N/A | Linear extrapolation to the origin from 1860 to 1750 | Average uncertainties between 1865 and 2000 | N/A |
| | 1861-2000 | C$^4$MIP GCMs/EMIC | 10-year moving average | Maxima and minima of GCMs runs (=1σ) | Friedlingstein et al. (2006) |
| Land $CO_2$ uptake (df=250) | 1750-1860 | N/A | Linear extrapolation to the origin from 1860 to 1750 | Average uncertainties between 1865 and 2000 | N/A |
| | 1861-2000 | C$^4$MIP GCMs/EMIC | 10-year moving average | Maxima and minima of GCMs runs (=1σ) | Friedlingstein et al. (2006) |
| Atmospheric $CO_2$ concentration (df=250) | 1750-1968 | Ice core sampling (Law Dome, Antarctica) | 75-year cutoff spline fit with 5-year intervals (1750-1830)<br>25-year cutoff spline fit with 1-year intervals (1832-1968)<br>Linear interpolations between the data points | *1.2 ppm | Etheridge et al. (1996) |
| | 1969-2000 | Station measurements (Mauna Loa, Hawaii) | Annual fit | *0.8 ppm<br>(0.2 ppm in the literature) | Keeling et al. (2005) |
| Atmospheric $CH_4$ concentration (df=249) | 1750-1850 | Ice core sampling (Law Dome, Antarctica; Summit, Greenland) | 75-year cutoff spline fit with 10-year intervals (1750-1900)<br>12.5-year cutoff spline fit with 2-year intervals (1900-1984)<br>Linear interpolations between the data points | *5 ppb | Etheridge et al. (1998) |
| | 1851-1983 | | | | Etheridge data compiled by Hansen and Sato (2004)<br>Etheridge et al. (1998) |
| | 1984-2000 | Station measurements (CMDL global air sampling network) | Annual fit | *12 ppb<br>(3 ppb in the literature) | Dlugokencky data compiled by Hansen and Sato (2004) for mean estimates<br>Masarie et al. (2001, Table 1) for uncertainties |
| Atmospheric $N_2O$ concentration (df=249) | 1750-1961 | Ice core sampling (Summit, Greenland) | 300-year cutoff spline fit with 1-year intervals | *Time variant | Flueckiger (personal communication) |
| | 1962-1977 | | | *Interpolation | Hansen and Sato (2004) |
| | 1978-2000 | Station measurements (CMDL global air sampling network) | Annual fit | *2.0 ppb<br>(0.5 ppb in the literature) | Hansen and Sato (2004) for mean estimates<br>Masarie et al. (2001, Table 1) for uncertainties |
| Surface air temperature change (df=250) | 1750-1855 | Multi-proxy | 1-year intervals | *0.36°C | Jones et al. (1998) for mean estimates<br>Mann and Jones (2003) for uncertainties |
| | 1856-2000 | Instrumental measurements | Annual fit | *0.20°C (1856-1860)<br>*0.05°C (2000)<br>*Linear interpolation between the periods | Jones et al. (2006) |

**Table S2.** Parameters in the ACC2 coupled inversion (after Table 3.2 of Tanaka (2008))

* Four times larger uncertainty ranges are assumed when volcanic forcing is stronger than -0.5 $W/m^2$ (Tanaka, 2008, Section 3.5.2). The total number of degrees of freedom for parameters is 1,266.

| Names (degrees of freedom) | Prior estimates | 2σ prior uncertainties |
|---|---|---|
| Anthropogenic $CO_2$ emission due to fossil fuel combustion (df=251) | Marland et al. (2006) between 1750 and 2000 | ±8% of the prior mean (Marland et al., 2006) |
| Anthropogenic $CO_2$ emission due to land use change (df=251) | Houghton (2003) between 1850 and 2000<br>Linear extrapolation between 1750 and 1849<br>Zero emission in 1750 | ±100% of the prior mean<br>(±50% in Houghton (2003)) |
| Anthropogenic $CH_4$ emission (df=251) | van Aardenne et al. (2001) between 1890 and 2000<br>Nonlinear extrapolation between 1750 and 1890<br>Zero emission in 1750 | ±50% in 2000, ±100% in 1970<br>±150% between 1890 and 1950<br>Linear interpolations between the periods<br>Absolute uncertainty ranges assumed constant before 1890<br>(John van Aardenne, personal communication) |
| Anthropogenic $N_2O$ emission (df=251) | van Aardenne et al. (2001) between 1890 and 2000<br>Linear extrapolation between 1750 and 1890<br>Zero emission in 1750 | ±50% in 2000, ±100% in 1970<br>±150% between 1890 and 1950<br>Linear interpolations between the periods<br>Absolute uncertain ranges assumed constant before 1890<br>(John van Aardenne, personal communication) |
| Missing forcing (df=251) | Zero forcing between 1750 and 2000 | *±0.5 $W/m^2$ between 1750 and 1900<br>*±1.0 $W/m^2$ in 2000<br>*Linear interpolation between 1900 and 2000 |
| Preindustrial mixed layer temperature (df=1) | 19.59°C (Hoffert et al., 1981, pp.290-291; Sundquist and Plummer, 1981, p.267) | Between 13.59 and 25.59°C |
| Atmosphere-mixed layer temperature scaling factor (df=1) | 0.5 | Between 0.0 and 1.0 |
| Beta factor for $CO_2$ fertilization (df=1) | 0.4<br>(0.287 (Meyer et al., 1999; Kicklighter et al., 1999), 0.4 (Gitz and Ciais, 2003), 0.45 (Brovkin et al., 1997), and 0.15 to 0.6 (Kohlmaier et al., 1987)) | Between 0.1 and 0.7 (references in left column) |
| Q10 for heterotrophic respiration (df=1) | 2.0 (Jones and Cox, 2001; Tjoelker et al., 2001) | Between 1.5 and 2.5 (references in left column) |
| Preindustrial ocean $CO_2$ uptake (df=1) | -0.24 GtC/year (net degassing)<br>(-0.48 GtC/year in Mackenzie and Lerman (2006)) | Between -0.48 and 0.0 GtC/year |
| Preindustrial land $CO_2$ uptake (df=1) | 0.30 GtC/year (net uptake)<br>(0.36 - 0.6 GtC/year in Mackenzie and Lerman (2006)) | Between 0.0 and 0.60 GtC/year |
| Natural $CH_4$ emission (df=1) | 210 Mt($CH_4$)/year (IPCC, 2001, Table 4.2) | Between -30 and 450 Mt($CH_4$)/year (IPCC, 2001, Table 4.2) |
| Natural $N_2O$ emission (df=1) | 10.2 Mt(N)/year (IPCC, 2001, Table 4.4) | Between 7.8 and 12.6 Mt(N)/year (IPCC, 2001, Table 4.4) |
| $CH_4$ lifetime with respect to OH depletion (df=1) | 9.6 year (IPCC, 2001, Table 4.3) | Between 5.4 and 13.8 year (IPCC, 2001, Table 4.3) |
| $N_2O$ lifetime (df=1) | 110 year (IPCC, 2001, Table 4.5) | Between 83 and 137 year (IPCC, 2001, Table 4.5) |
| Climate sensitivity (df=1) | 3.5°C (Forest et al., 2002; Gregory et al., 2002; Knutti et al., 2002; IPCC, 2004; Kriegler, 2005; Stainforth et al., 2005; Forest et al., 2006; Hegerl et al., 2006; IPCC, 2007; Räisänen, 2007) | Between 0.5 and 6.5°C (references in left column) |

**Table S3.** Cost function values and squared weighted residuals in the main ACC2 inversions

The final values of the cost function are shown in the top row. Other entries show the contributions to the cost function arising from time-dependent parameters and data and also from constant parameters. These are equivalent to the squares of the residuals weighted by the associated prior uncertainty ranges (σ). Squared weighted residuals from time series are summed up over the time horizon of simulation. Units for all the quantities shown here are 1. Parameters marked with "—" are not included for the corresponding inversion setup. For example, in the uncoupled experiment, the preindustrial mixed layer temperature, the atmosphere-mixed layer temperature scaling factor, and Q10 for heterotrophic respiration are not included in the cost function as carbon cycle processes are not influenced by temperature change.

| | Coupled Missing forcing | Uncoupled Missing forcing | Uncoupled Forcing scaling | Uncoupled No forcing uncertainty |
|---|---|---|---|---|
| Total | 371.1 | 365.1 | 607.0 | 612.5 |
| | | | | |
| Parameters (time series) | | | | |
| Fossil fuel $CO_2$ emission | 1.5 | 1.4 | 1.5 | 1.5 |
| Land use $CO_2$ emission | 87.6 | 96.5 | 98.8 | 98.9 |
| Anthropogenic $CH_4$ emission | 5.8 | 5.8 | 5.8 | 5.8 |
| Anthropogenic $N_2O$ emission | 16.6 | 16.5 | 16.5 | 16.8 |
| Missing forcing | 74.3 | 64.8 | — | — |
| | | | | |
| Parameters (constants) | | | | |
| Preindustrial mixed layer temperature | 0.01 | — | — | — |
| Atmosphere-mixed layer temperature scaling factor | 0.21 | — | — | — |
| Beta factor for $CO_2$ fertilization | 0.83 | 0.35 | 0.35 | 0.34 |
| Q10 for heterotrophic respiration | 5.58 | — | — | — |
| Preindustrial ocean $CO_2$ uptake | 0.46 | 0.39 | 0.39 | 0.39 |
| Preindustrial land $CO_2$ uptake | 0.71 | 0.60 | 0.60 | 0.60 |
| Natural $CH_4$ emission | 0.42 | 0.42 | 0.42 | 0.42 |
| Natural $N_2O$ emission | 0.45 | 0.45 | 0.46 | 0.45 |
| $CH_4$ lifetime | 0.13 | 0.13 | 0.13 | 0.13 |
| $N_2O$ lifetime | 0.05 | 0.05 | 0.05 | 0.05 |
| Forcing scaling factor | — | — | 0.02 | — |
| Climate sensitivity | 0.06 | 0.00 | 0.02 | 0.04 |
| | | | | |
| Data (time series) | | | | |
| Ocean $CO_2$ uptake | 18.8 | 19.4 | 19.4 | 19.5 |
| Land $CO_2$ uptake | 14.6 | 11.7 | 11.8 | 11.8 |
| Atmospheric $CO_2$ concentration | 27.9 | 30.6 | 28.7 | 28.6 |
| Atmospheric $CH_4$ concentration | 0.2 | 0.2 | 0.2 | 0.2 |
| Atmospheric $N_2O$ concentration | 2.7 | 2.7 | 2.9 | 2.8 |
| Surface air temperature change | 112.3 | 113.1 | 418.9 | 424.3 |

**Table S4.** Prior and posterior parameter estimates in the main ACC2 inversions

2σ prior uncertainty ranges are shown in brackets in the column for prior. Parameters marked with "—" are not included in the corresponding inversion setup.

| | Posterior<br>Coupled<br>Missing forcing | Posterior<br>Uncoupled<br>Missing forcing | Posterior<br>Uncoupled<br>Forcing scaling | Posterior<br>Uncoupled<br>No forcing uncertainty | Prior<br>For all cases |
|---|---|---|---|---|---|
| Preindustrial mixed layer temperature (°C) | 19.9 | — | — | — | 19.6 (13.6 ~ 25.6) |
| Atmosphere-mixed layer temperature scaling factor (1) | 0.34 | — | — | — | 0.5 (0.0 ~ 1.0) |
| Beta factor for $CO_2$ fertilization (1) | 0.59 | 0.53 | 0.53 | 0.52 | 0.4 (0.1 ~ 0.8) |
| Q10 for heterotrophic respiration (1) | 1.17 | — | — | — | 2.0 (1.5 ~ 2.5) |
| Preindustrial ocean $CO_2$ uptake (GtC/year) | -0.36 | -0.35 | -0.35 | -0.35 | -0.24 (0 ~ -0.48) |
| Preindustrial land $CO_2$ uptake (GtC/year) | 0.12 | 0.14 | 0.14 | 0.14 | 0.3 (0 ~ 0.6) |
| Natural $CH_4$ emission (Mt($CH_4$)/year) | 320 | 320 | 320 | 320 | 210 (-30 ~ 450) |
| Natural $N_2O$ emission (Mt(N)/year) | 11.3 | 11.3 | 11.3 | 11.3 | 10.2 (7.8 ~ 12.6) |
| $CH_4$ lifetime (year) | 8.54 | 8.54 | 8.54 | 8.54 | 9.6 (5.4 ~ 13.8) |
| $N_2O$ lifetime (year) | 114 | 114 | 114 | 114 | 110 (83 ~ 137) |
| Forcing scaling factor (1) | — | — | 1.106 | — | 1.0 (0.0 ~ 2.0) |
| Climate sensitivity (°C) | 4.04 | 3.37 | 3.77 | 3.10 | 3.5 (0.5 ~ 6.5) |

**Figure S1.** Comparison of the ACC2 coupled and uncoupled inversion results

Shown below are the results of the coupled and uncoupled inversions with optimal climate sensitivity (4.04°C and 3.37°C, respectively). Forcing uncertainty is expressed as missing forcing. Unless noted otherwise, inserts show the "residuals," i.e. the differences between prior and posterior values. For the anthropogenic $CH_4$ and $N_2O$ emissions and atmospheric $CH_4$ and $N_2O$ concentrations in Figures S1.6 to S1.9, the posterior estimates for the coupled inversion are indistinguishable from those for the uncoupled inversion. In Figures S1.10 and S1.11, prior for missing forcing is 0 W/m$^2$ over the entire period. In Figures S1.3 and S1.8 to S1.12, prior uncertainty ranges are assumed four times larger when volcanic forcing is stronger than -0.5 W/m$^2$. In Figures S1.10 and S1.11, individual forcings in the coupled and uncoupled inversions are nearly the same except for the missing forcing and the total forcing. Measurements shown in Figure S1.12 are for the coupled inversion.

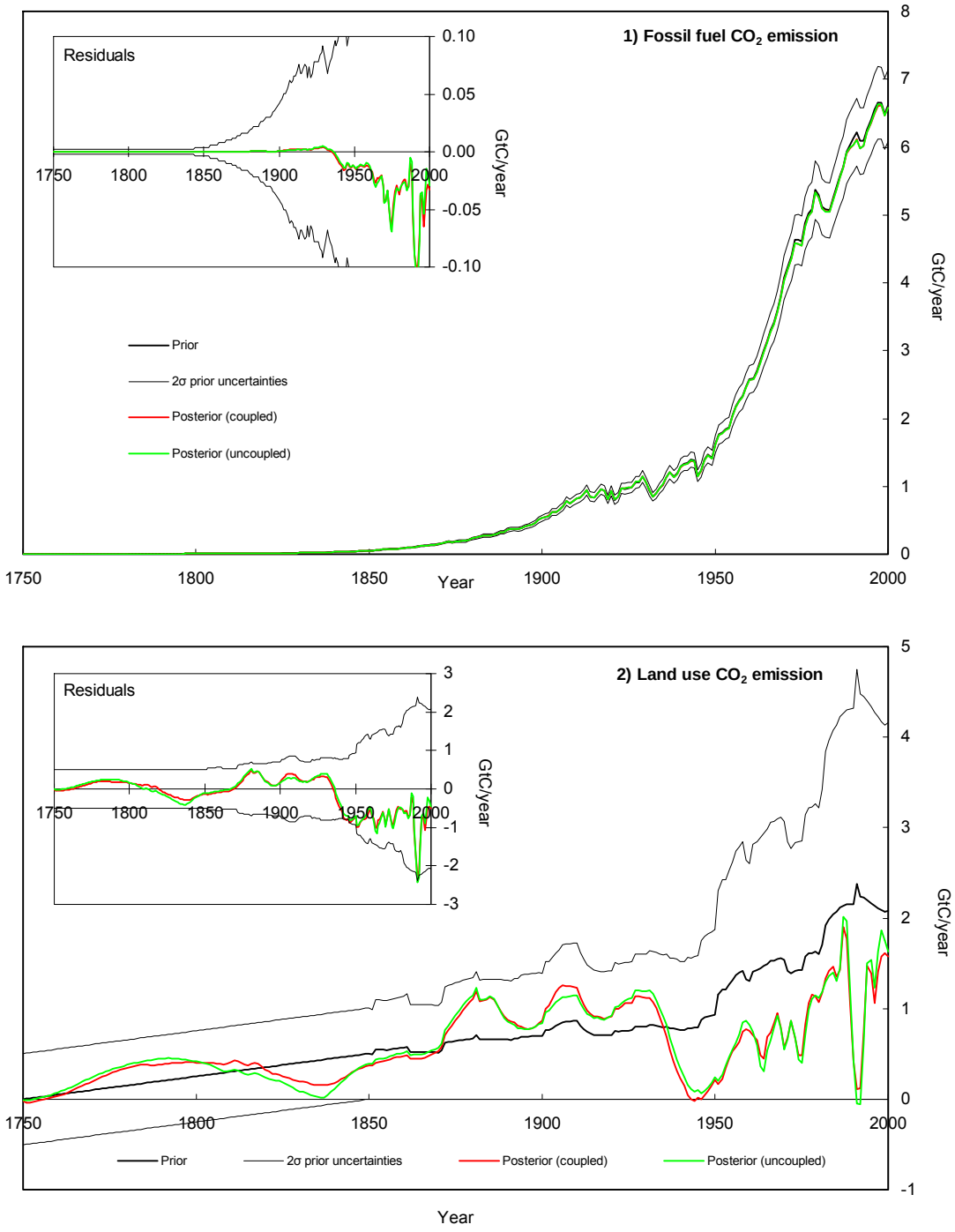

**Figure S1.** (Continued) Time series in the ACC2 coupled and uncoupled inversions

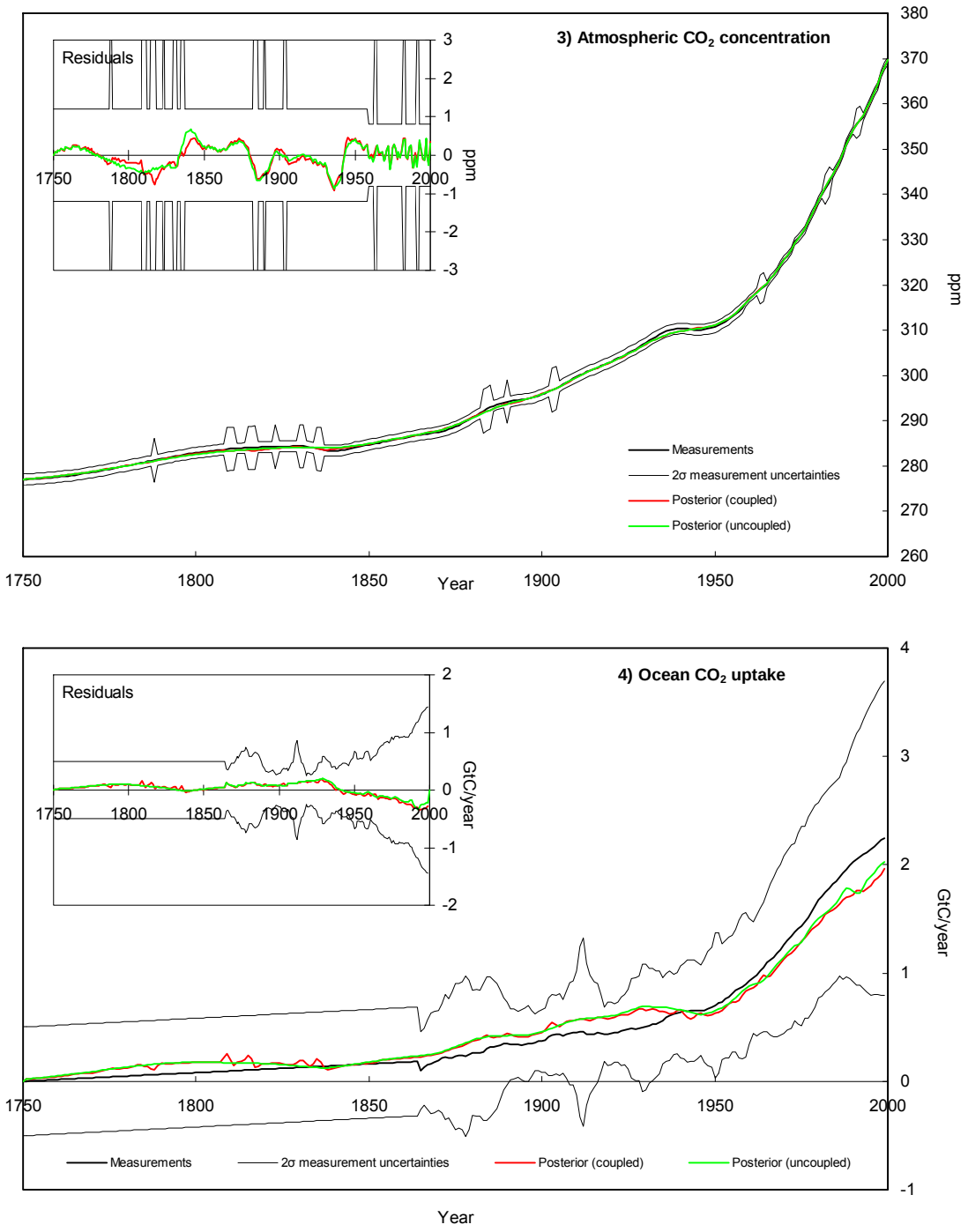

**Figure S1.** (Continued) Time series in the ACC2 coupled and uncoupled inversions

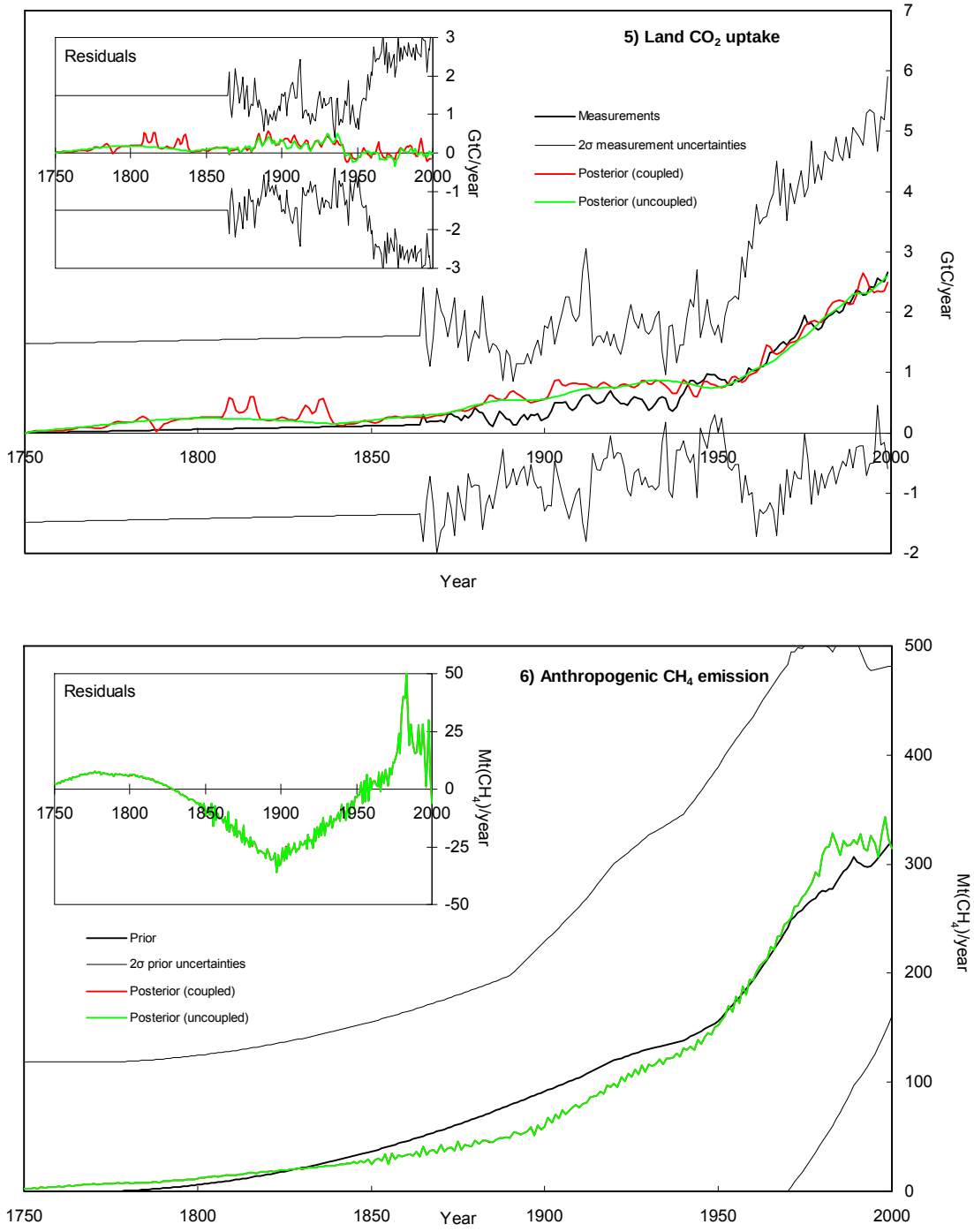

**Figure S1.** (Continued) Time series in the ACC2 coupled and uncoupled inversions

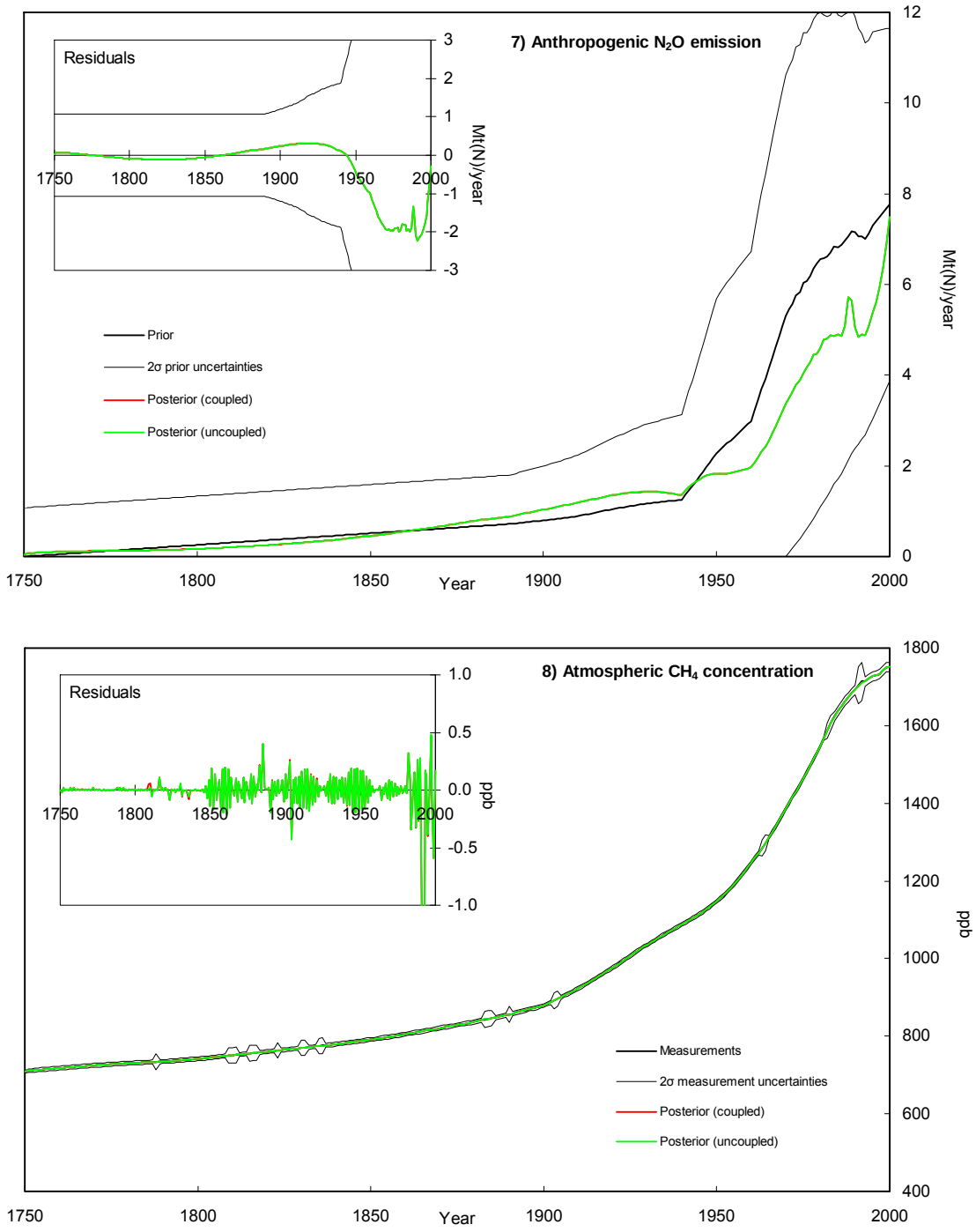

**Figure S1.** (Continued) Time series in the ACC2 coupled and uncoupled inversions

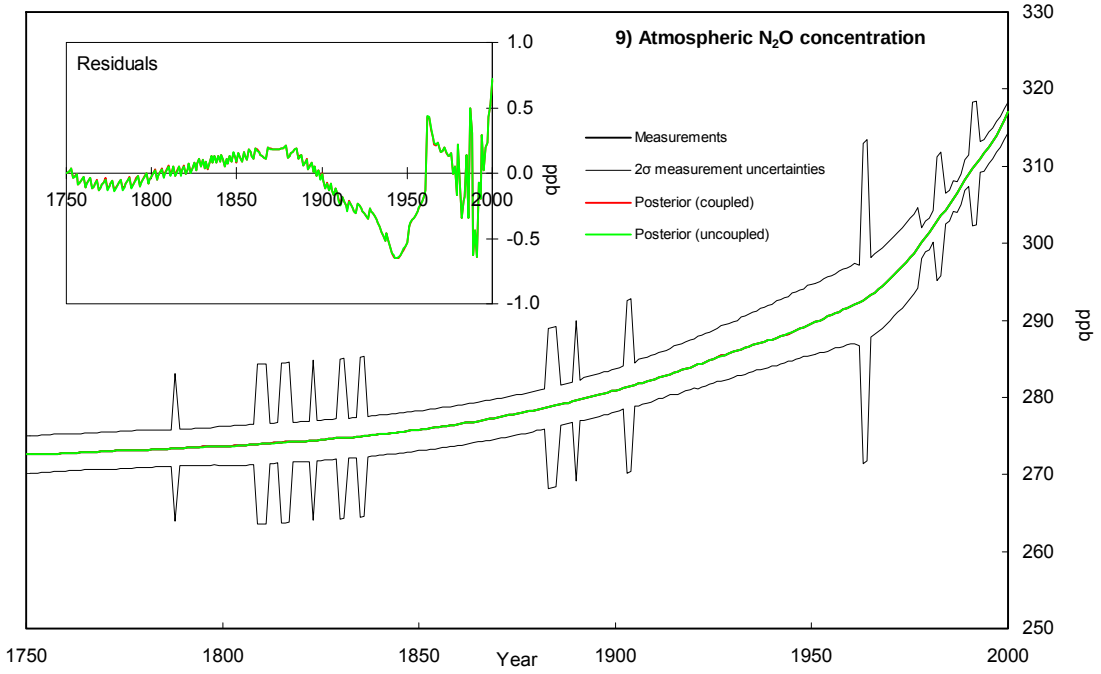


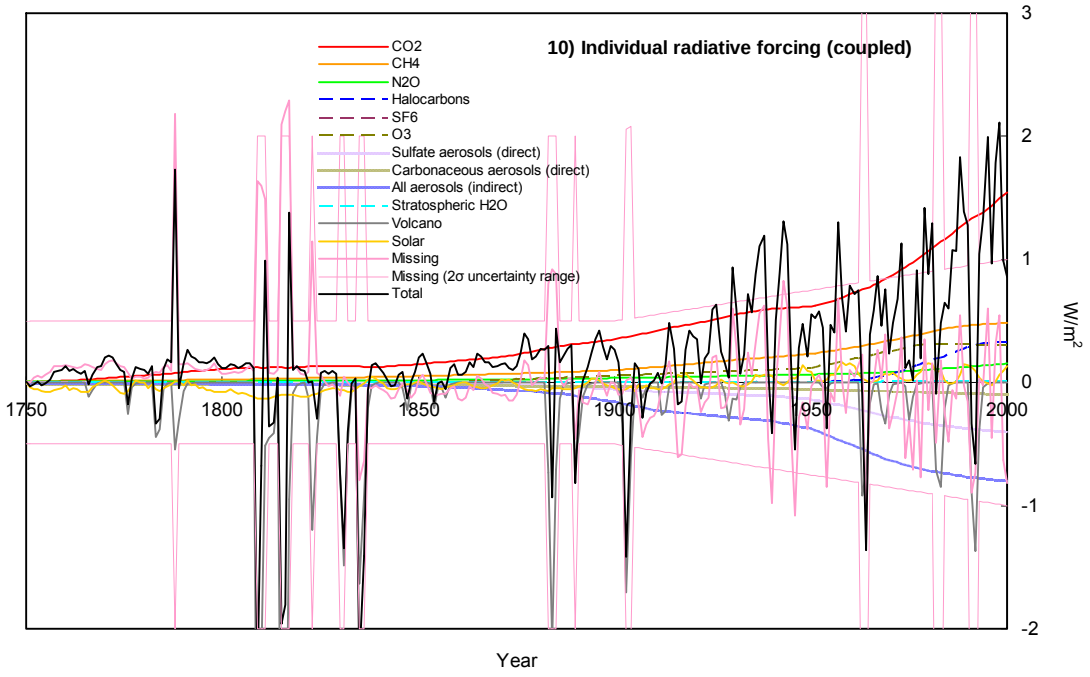

**Figure S1.** (Continued) Time series in the ACC2 coupled and uncoupled inversions

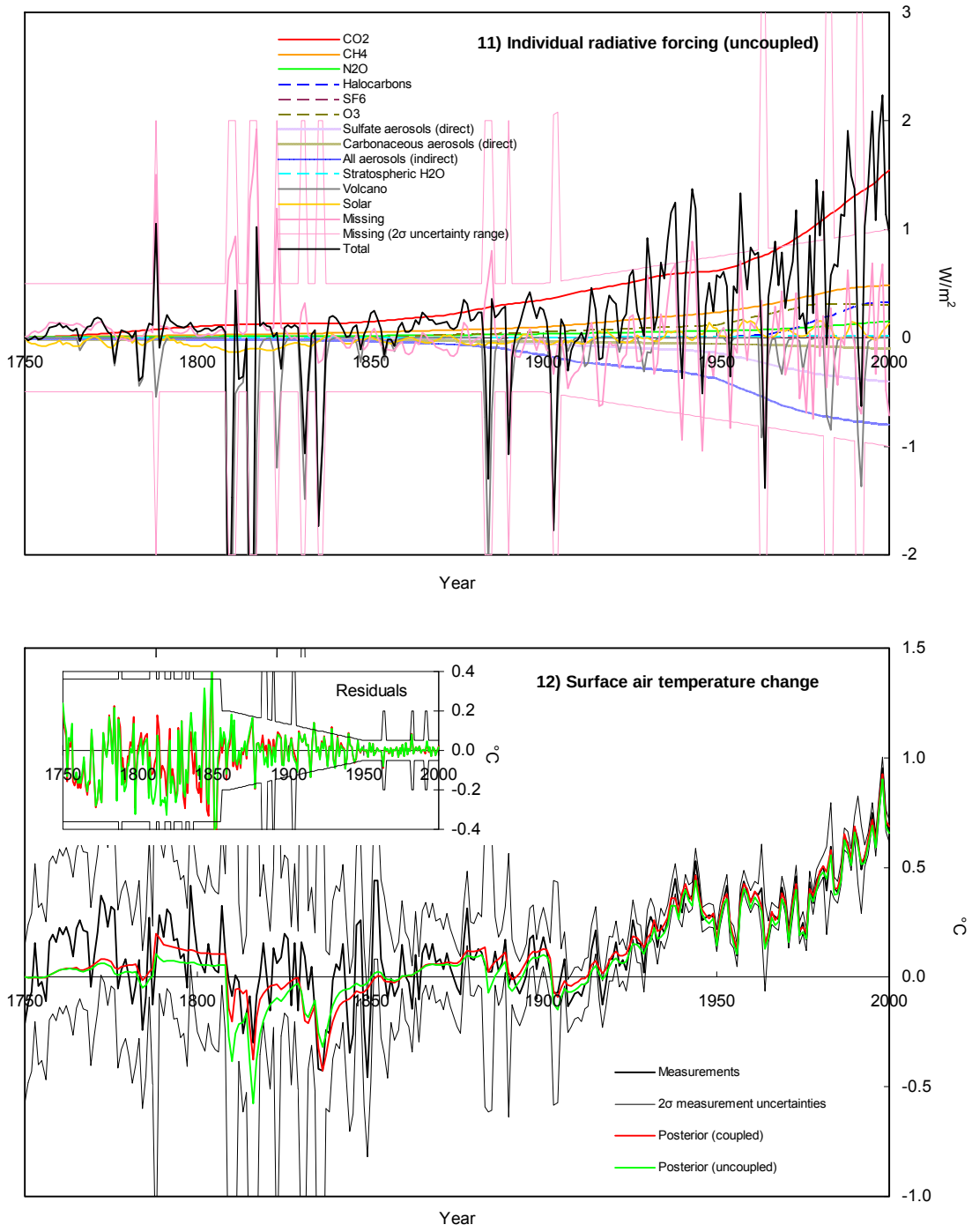

**Figure S2.** Comparison of the results of the ACC2 uncoupled inversions giving different treatments to forcing uncertainty

Only the results for the climate component are shown as the other components are insensitive to the treatment of forcing uncertainty. The main figure of S2.1 shows the total forcing, which is the sum of the GHG, aerosol, volcanic, solar, and missing forcing. Note that in the inversion setup using forcing scaling or assuming no forcing uncertainty, missing forcing is fixed at 0 W/m$^2$ over the entire period. Insert in Figure S2.1 shows missing forcing and "additional forcing by scaling," i.e. additional aerosol forcing that are added by scaling the prescribed total aerosol forcing according to the forcing scaling factor obtained from the inversion (=1.106, that is 10.6% of the prescribed total aerosol forcing). In Figures S2.1 and S2.2, prior uncertainty ranges are assumed four times larger when volcanic forcing is stronger than -0.5 W/m$^2$. Measurements shown in Figure S2.2 are for the inversion using the missing forcing approach. Values in the square brackets are the best estimates of climate sensitivity for the respective inversions.

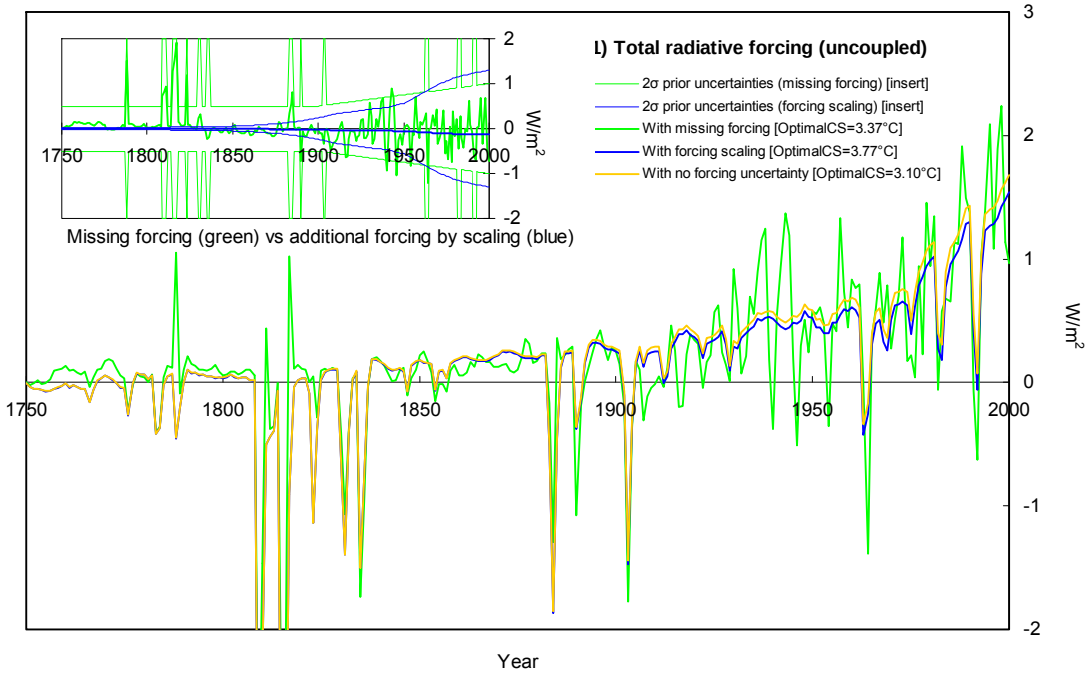


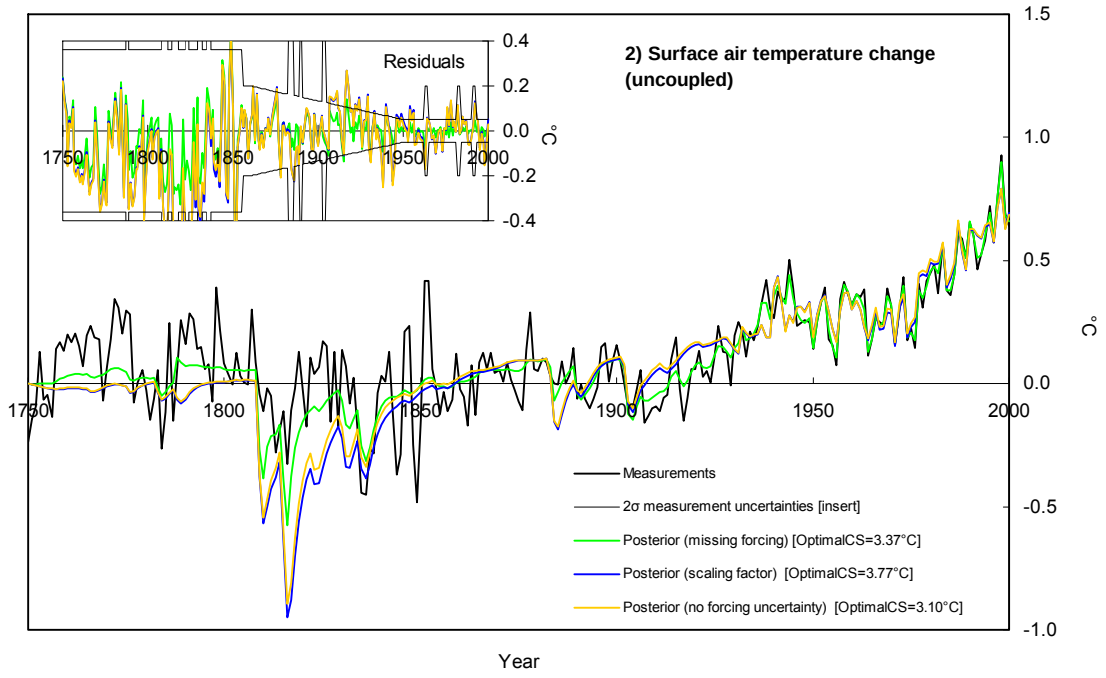

**Figure S3.** Various contributions to the cost functions of the main ACC2 inversions

Shown below are the squares of the residuals weighted by the associated prior uncertainty ranges (σ). Not that they are shown on a logarithmic scale. Explanations for acronyms follow. EMICO2FF: fossil fuel $CO_2$ emission, EMICO2LU: land use $CO_2$ emission, EMICH4ANT: anthropogenic $CH_4$ emission, EMIN2OANT: anthropogenic $N_2O$ emission, MISFOR: missing forcing, UPCO2OCN: ocean $CO_2$ uptake, UPCO2LND: land $CO_2$ uptake, CONCO2: atmospheric $CO_2$ concentration, CONCH4: atmospheric $CH_4$ concentration, CONN2O: atmospheric $N_2O$ concentration, TEMP: surface air temperature change, SUM: sum of the squared weighted residuals for all the time series.

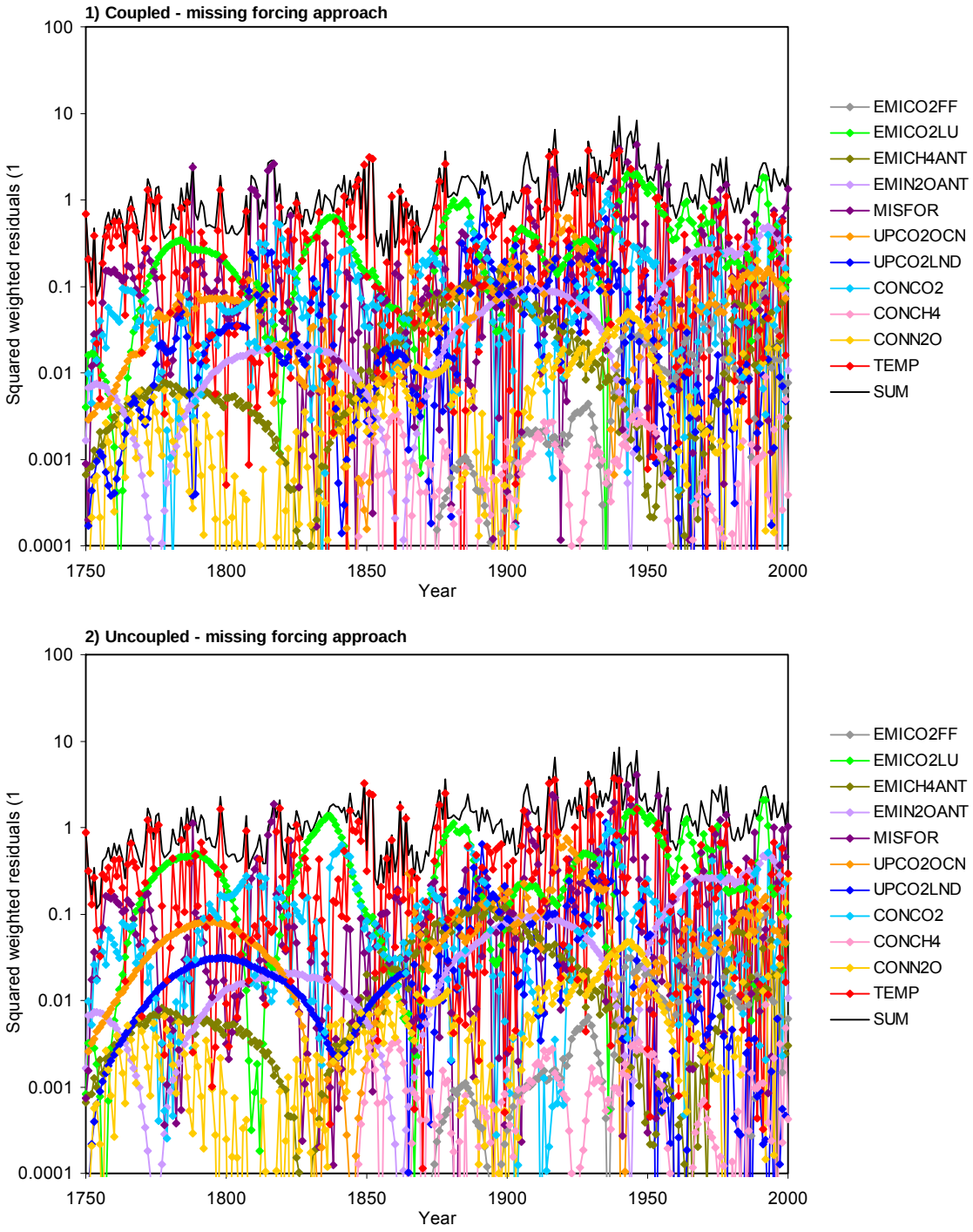

**Figure S3.** (Continued) Squared weighted residuals in time series of the main ACC2 inversions

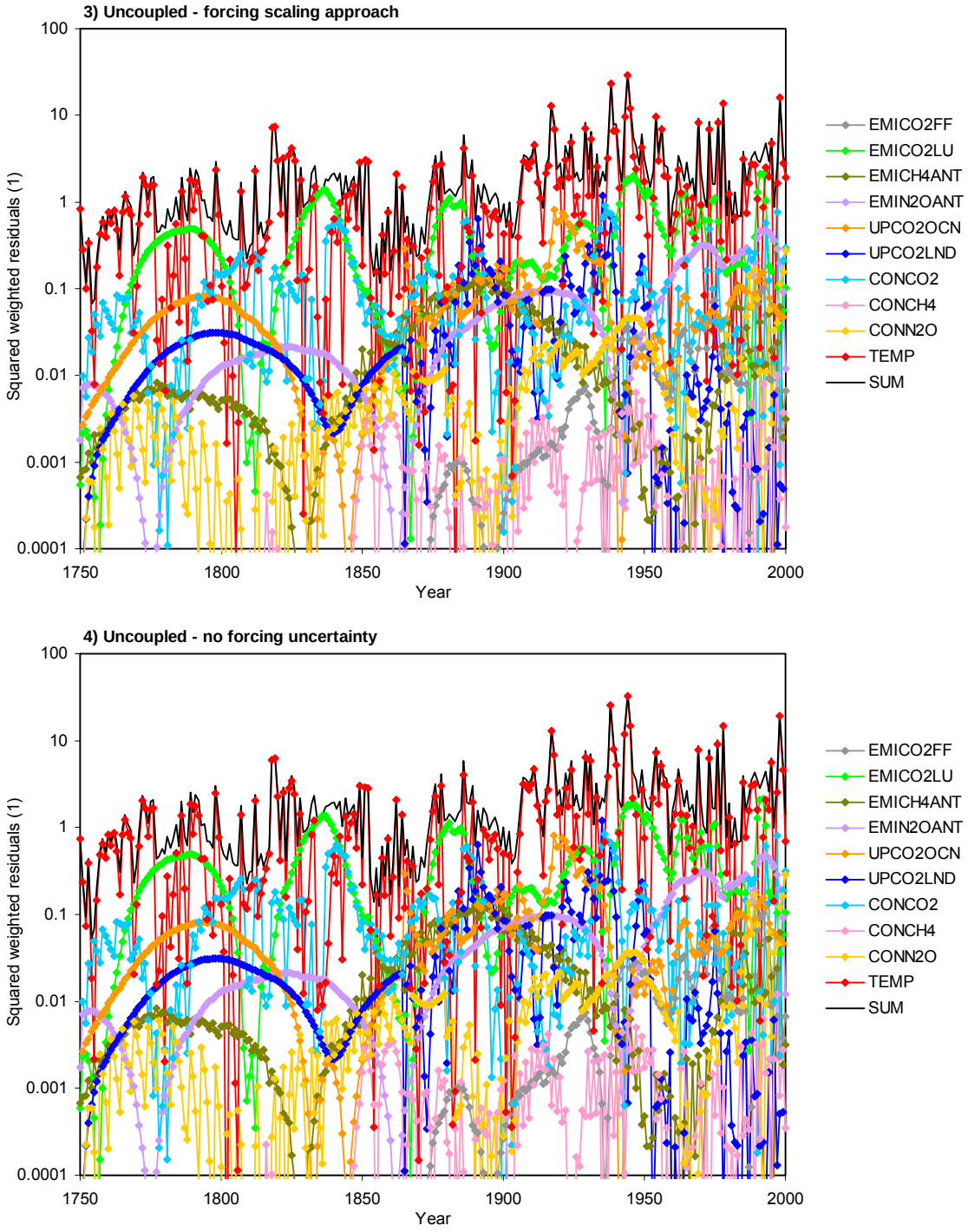

**Figure S4.** Various contributions to the cost function in the ACC2 inversions giving different treatments to forcing uncertainty

Squared weighted residuals summed over the entire time horizon are shown for the missing forcing- and forcing scaling-based uncoupled inversions with climate sensitivity fixed at values between 1°C and 10°C at intervals of 0.25°C. Except for temperature change, squared weighted residuals from the two approaches are hardly distinguishable.

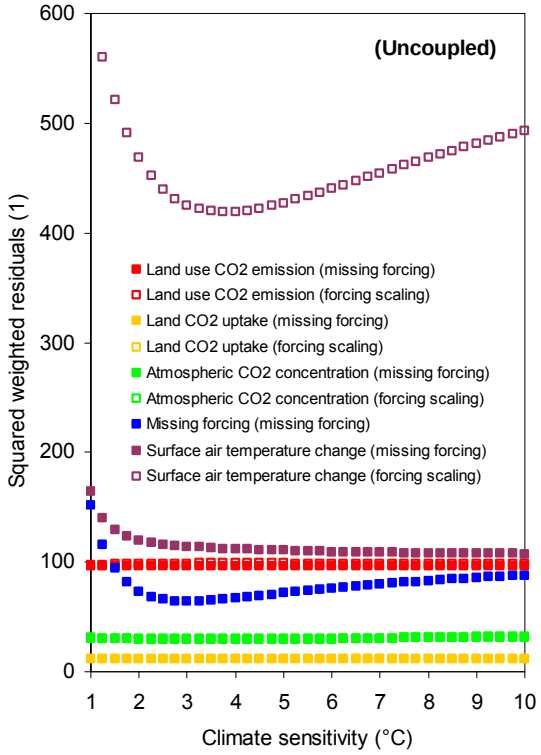

**Figure S5.** Global-mean surface air temperature response to constant radiative forcing perturbation

Temperature response to sustained perturbation in radiative forcing (0.25, 0.50, and 0.75 W/m$^2$) is computed under different assumptions on climate sensitivity (1, 4, 7, and 10°C). The forcing perturbation starts in the year 0. The initial state is equivalent to the preindustrial state assumed for the year 1750. Calculations are performed by using DOECLIM (Kriegler, 2005; Section 2.3 of Tanaka and Kriegler et al. (2007)), the climate component of ACC2. No climate-carbon cycle feedback is provided.

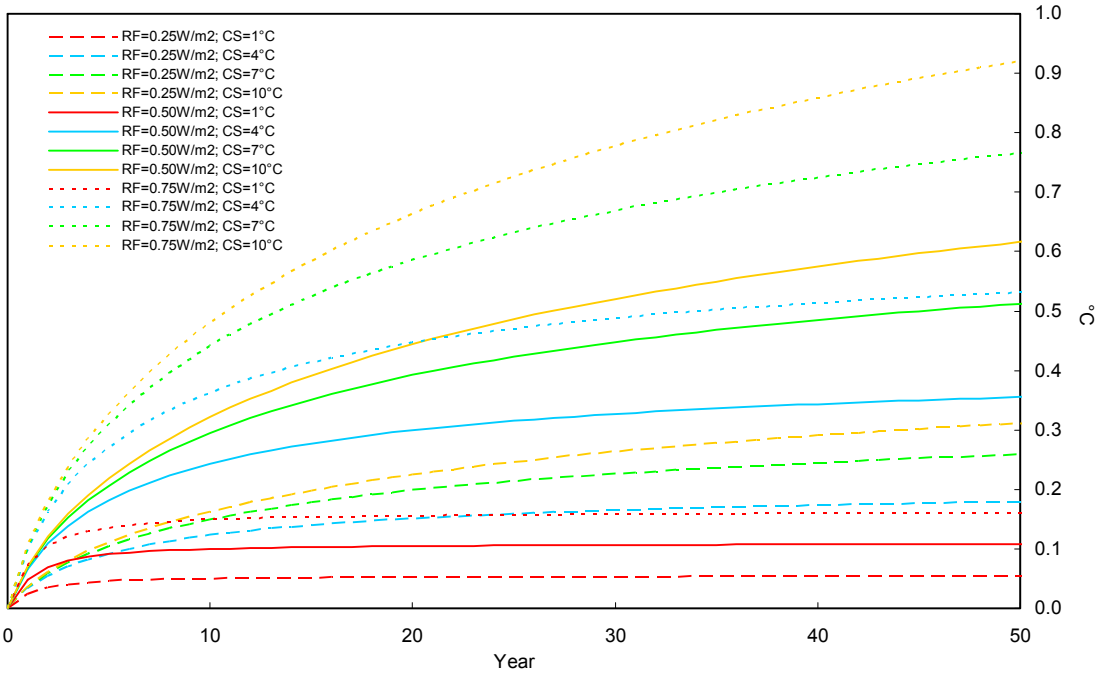

**Figure S6.** Sensitivity of the ACC2 inversion results to the prior forcing uncertainty

Missing forcing- and forcing scaling-based ACC2 uncoupled inversions are performed by assuming 50% smaller, standard, and 50% larger prior uncertainty ranges for missing forcing and forcing scaling factor with climate sensitivity fixed at values between 1°C and 10°C at intervals of 0.25°C. Figure S6.1 shows the changes in the final value of the cost function. Values in the square brackets are the best estimates of climate sensitivity for the respective inversion setups. Cost functions values for the different forcing scaling cases are indistinguishable. In Figures S6.2 and S6.3, forcing residuals (that is, posterior missing forcing and additional forcing by scaling) and temperature residuals are compared for different climate sensitivity (1, 3, 5, and 10°C) and different prior forcing uncertainty (50% smaller, standard, and 50% larger ranges). Thick red and blue lines in Figure S6.2 are the posterior missing forcing and additional forcing by scaling, respectively. Thin lines represent the respective 2σ prior uncertainty ranges. In Figure S6.3, thick red and blue lines represent the temperature residuals for the missing forcing- and forcing scaling-based inversions, respectively. Thin black line is the 2σ prior uncertainty ranges used for both types of inversions.

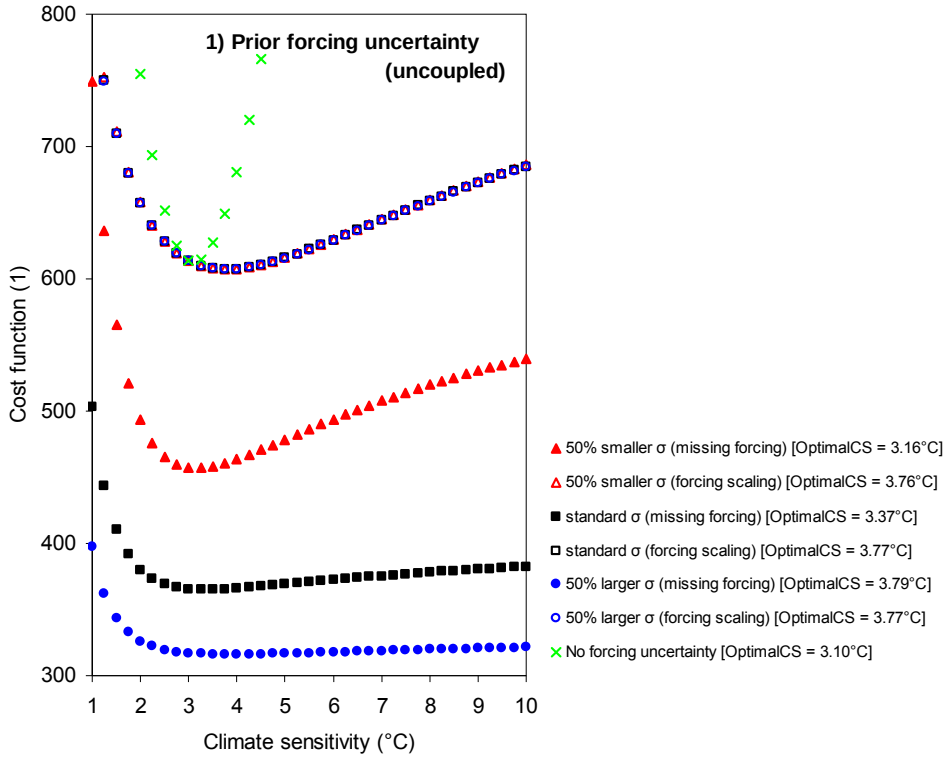

**Figure S6.** (Continued) Sensitivity of the ACC2 inversion results to the prior forcing uncertainty

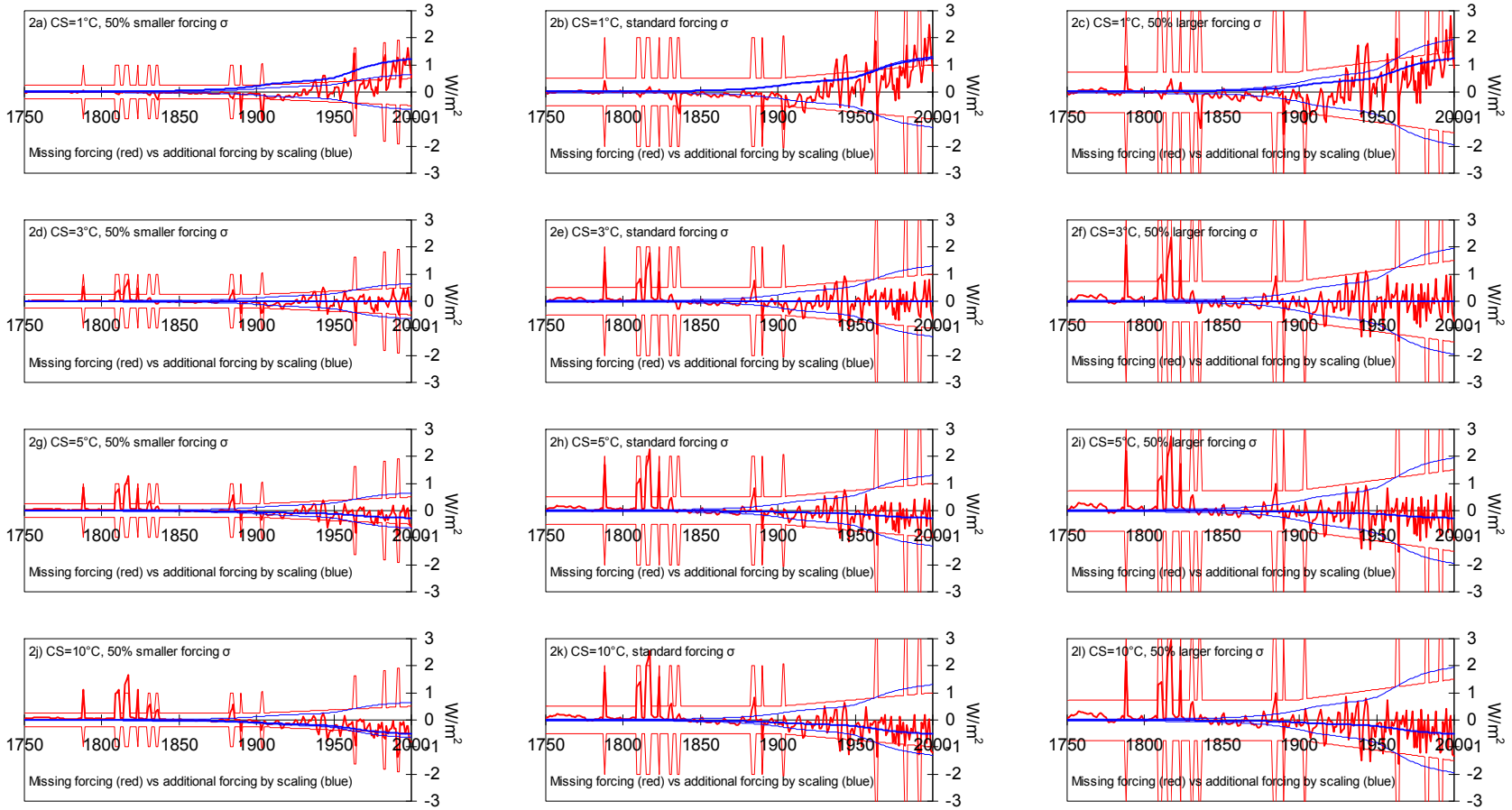

**Figure S6.** (Continued) Sensitivity of the ACC2 inversion results to the prior forcing uncertainty

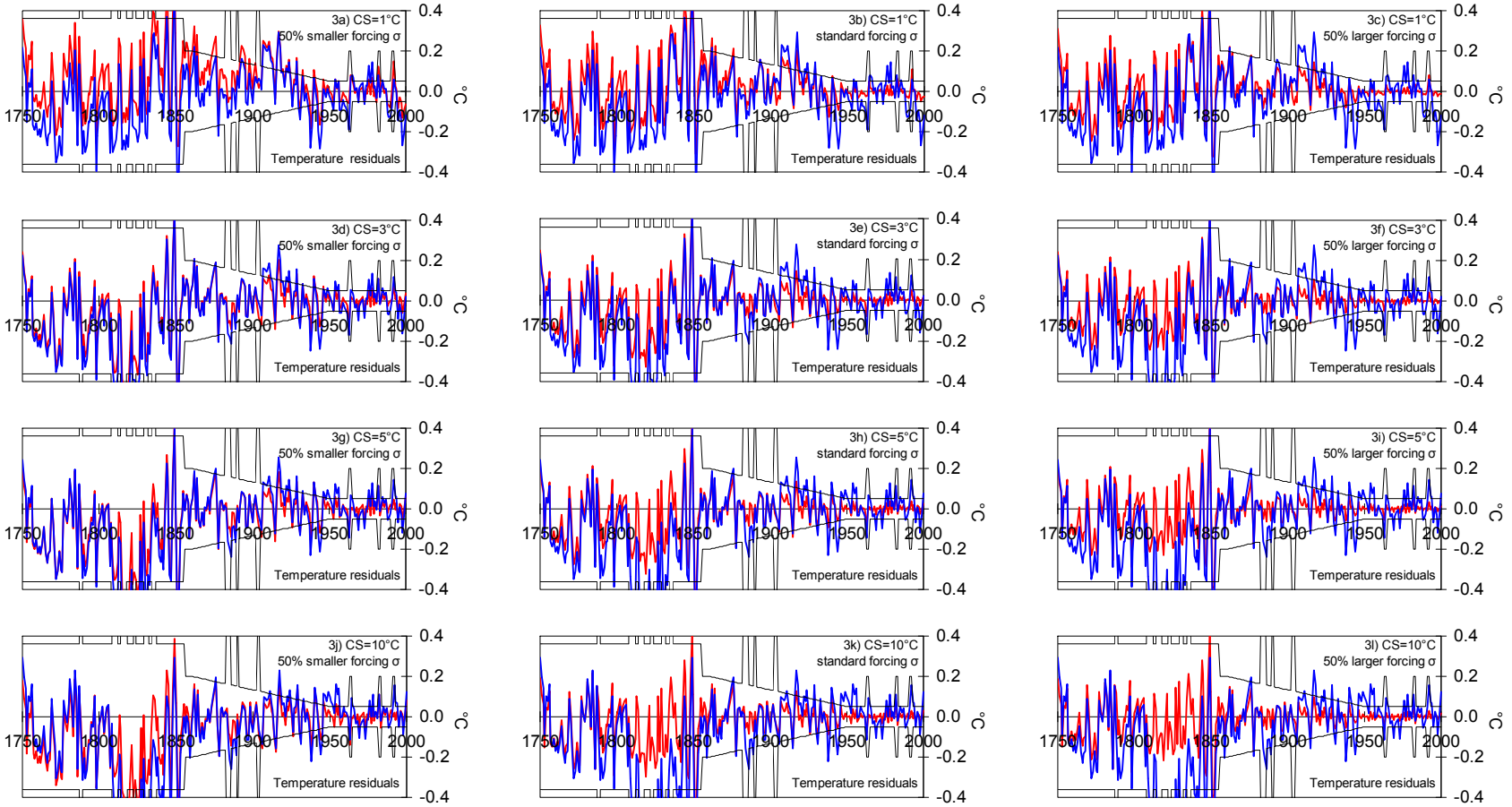

**Figure S7.** Sensitivity of the ACC2 inversion results to prior land use $CO_2$ emission uncertainty

Figure S7.1 shows the changes in the final value of the cost function when the prior uncertainty in land use $CO_2$ emission is assumed to be larger/smaller than the standard by 50%. The ACC2 coupled and inversions are performed with climate sensitivity fixed at values between 1°C and 10°C at intervals of 0.25°C. Black plots are identical with those shown in Figure 1 of the main article. Values in the square brackets are the best estimates of climate sensitivity for the respective inversion setups. Figures S7.2 to S7.4 shows the associated coupled inversion results in the carbon cycle using respective optimal climate sensitivity.

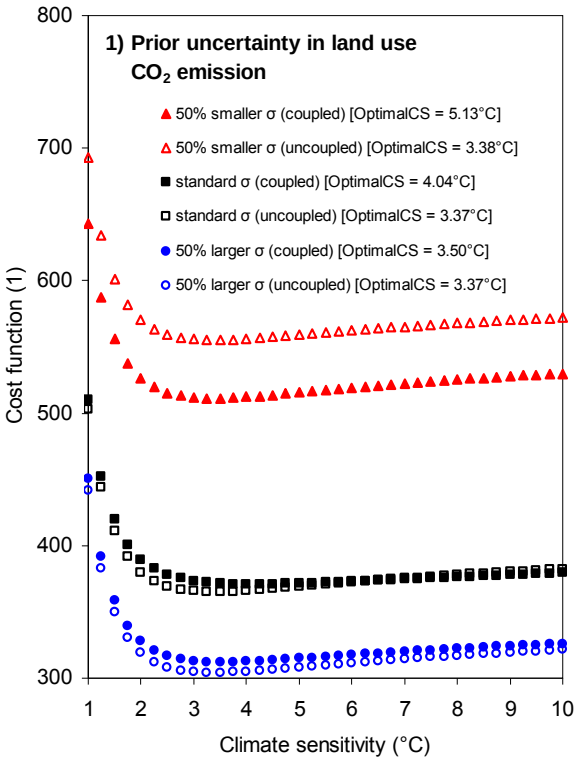

**Figure S7.** (Continued) Sensitivity of the ACC2 inversion results to prior land use $CO_2$ emission uncertainty

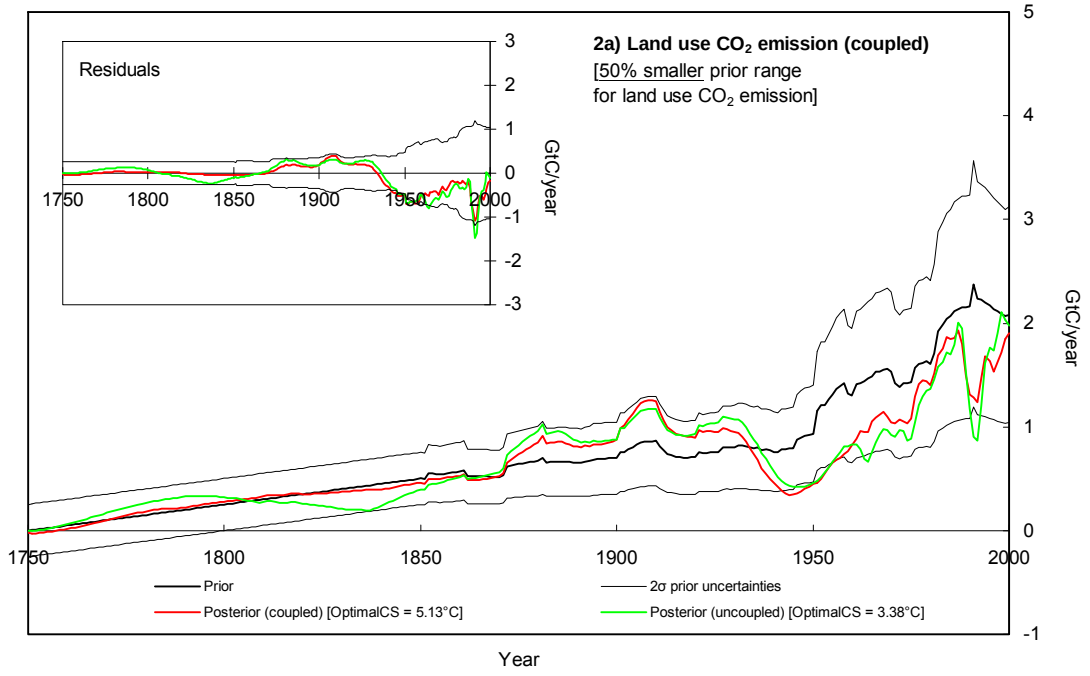


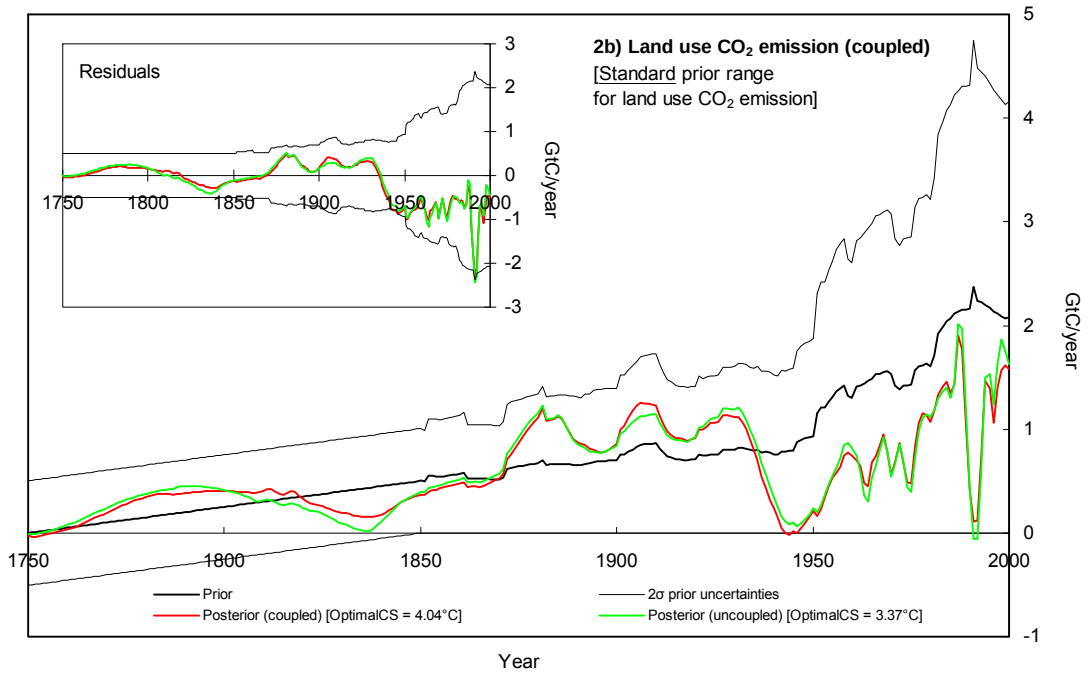

**Figure S7.** (Continued) Sensitivity of the ACC2 inversion results to prior land use $CO_2$ emission uncertainty

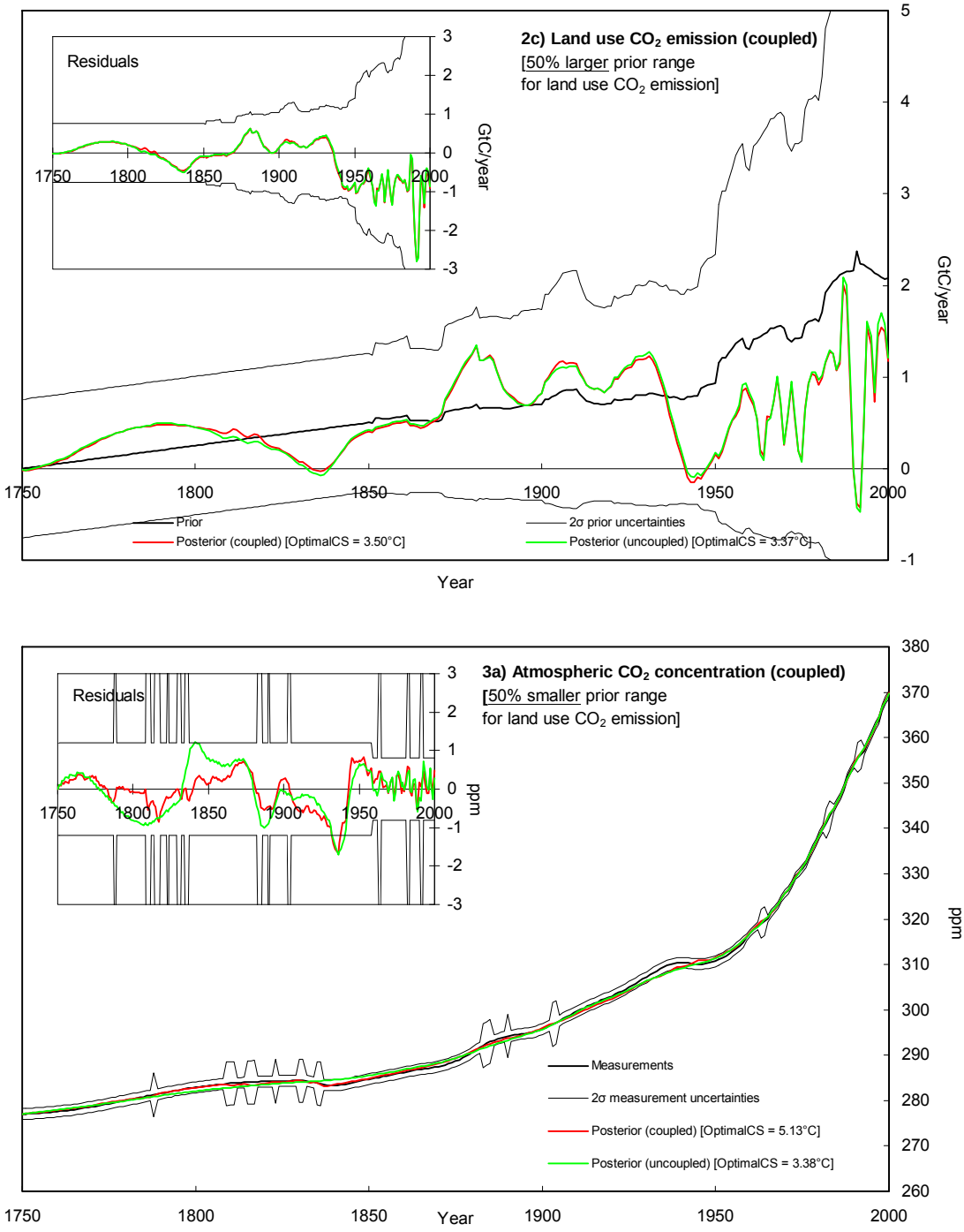

**Figure S7.** (Continued) Sensitivity of the ACC2 inversion results to prior land use $CO_2$ emission uncertainty

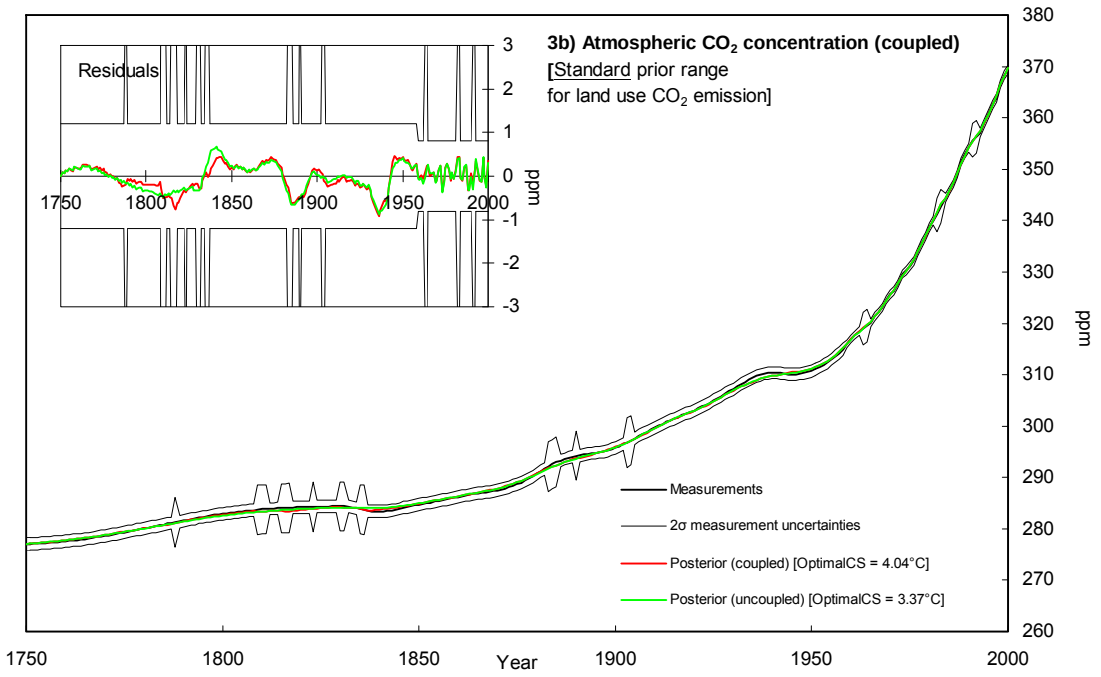


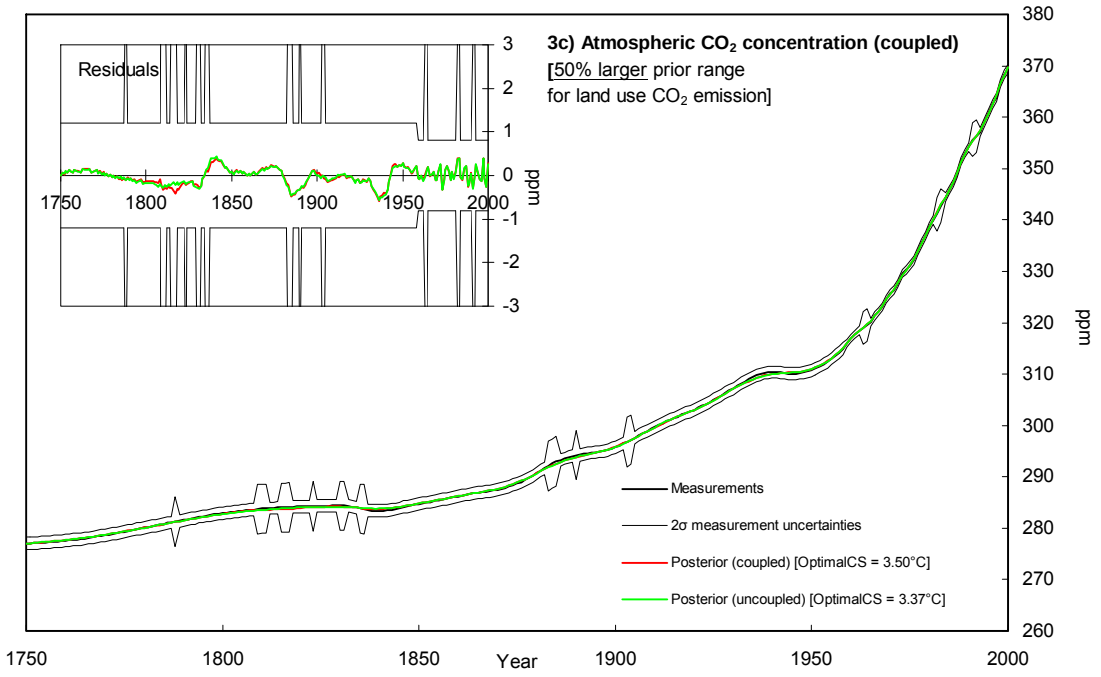

**Figure S7.** (Continued) Sensitivity of the ACC2 inversion results to prior land use $CO_2$ emission uncertainty

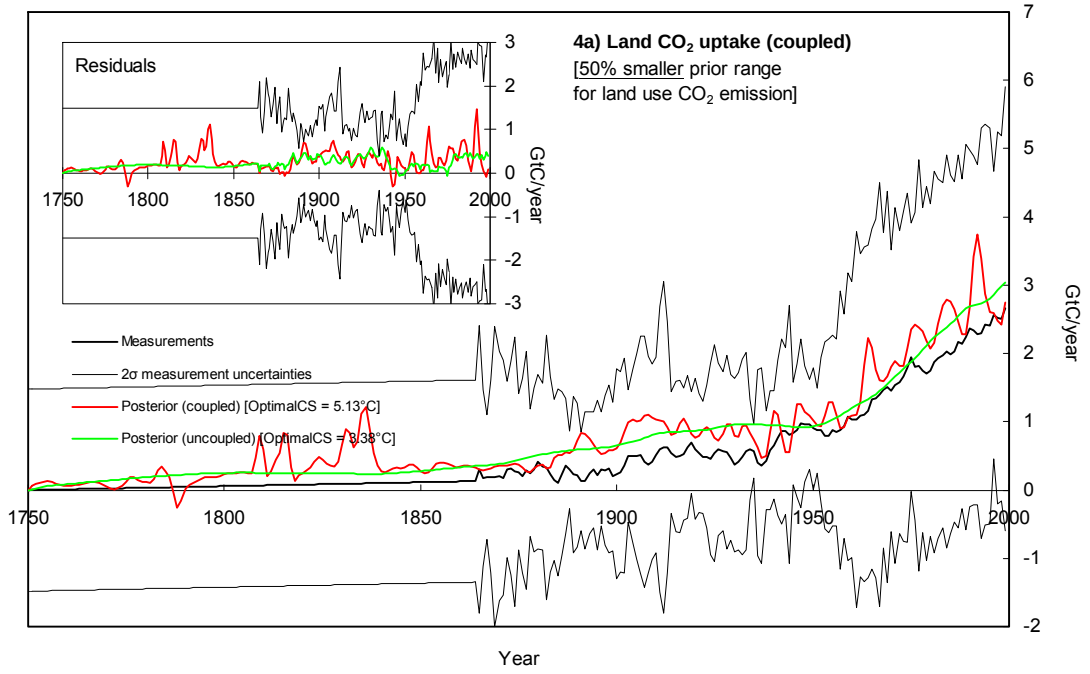


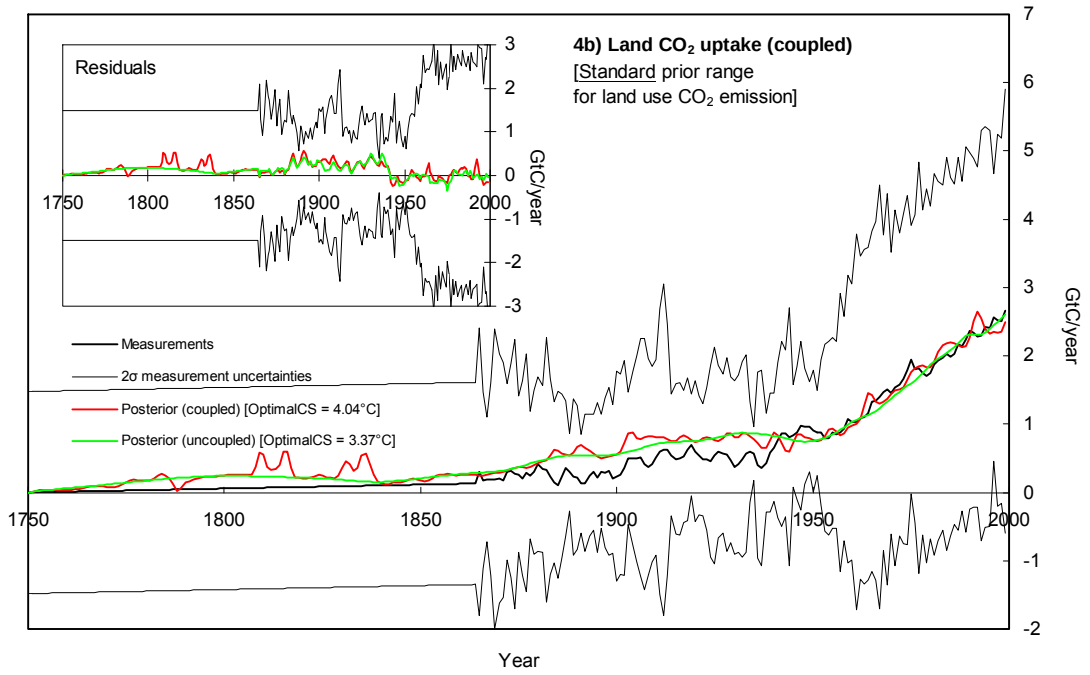

**Figure S7.** (Continued) Sensitivity of the ACC2 inversion results to prior land use $CO_2$ emission uncertainty

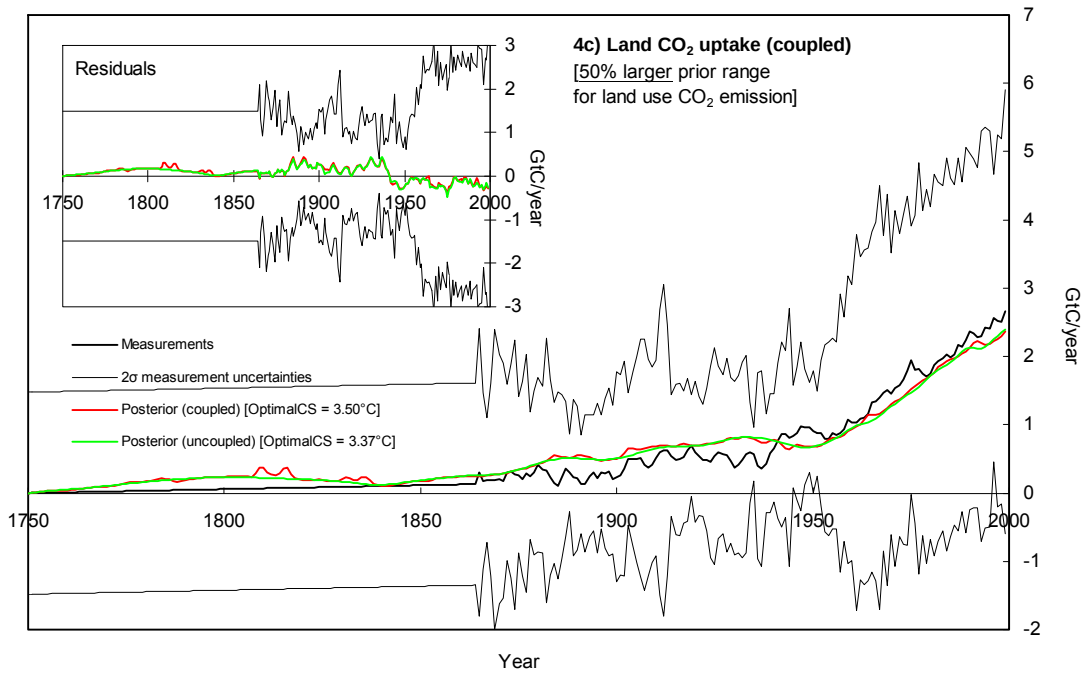

**Figure S8.** Sensitivity of the ACC2 inversion results to volcanic forcing

Figure S8.1 shows the changes in the final value of the cost function when different volcanic forcing is used (Ammann et al., 2003; Bertrand et al., 2002; Crowley et al., 2003). Inversions are performed with climate sensitivity fixed at values between 1°C and 10°C at intervals of 0.25°C. Black plots are identical with those shown in Figure 1 of the main article. Values in the square brackets are the best estimates of climate sensitivity for the respective inversion setups. Figures S8.2 to S8.8 show the associated coupled inversion results with respective optimal climate sensitivity. In Figures S8.3, S8.6, and S8.8, prior uncertainty ranges are assumed four times larger when volcanic forcing is stronger than -0.5 W/m$^2$. Measurements shown in Figure S8.8 are for the coupled inversion using Ammann's volcanic forcing.

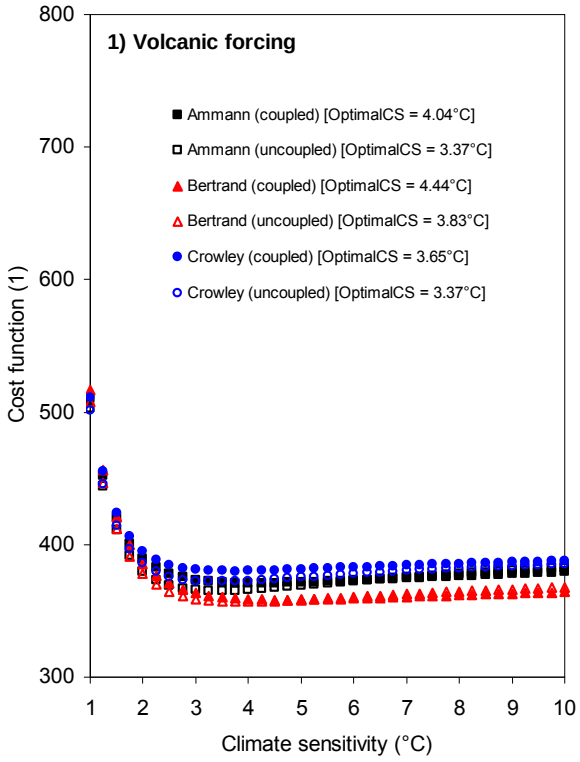

**Figure S8.** (Continued) Sensitivity of the ACC2 inversion results to volcanic forcing

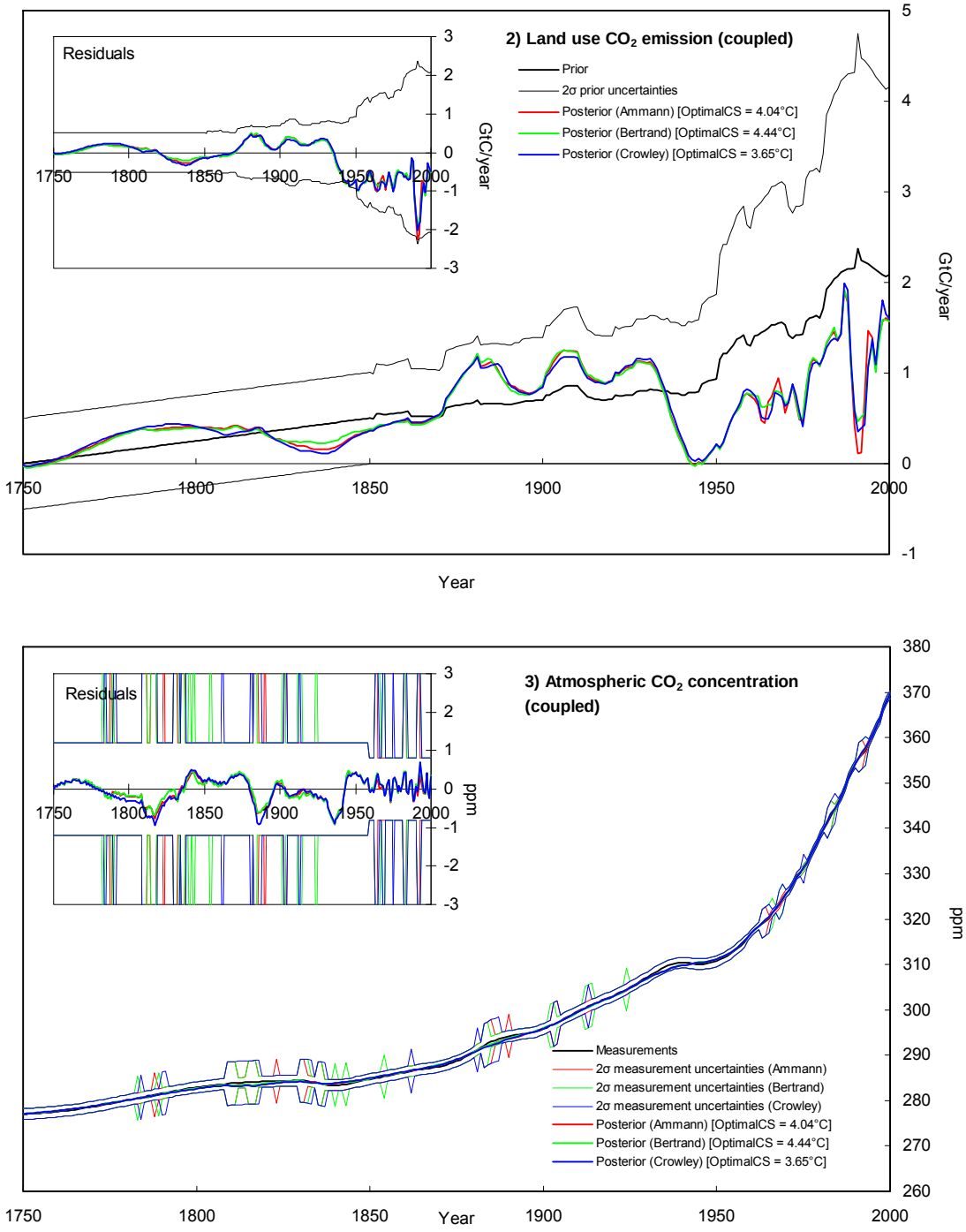

**Figure S8.** (Continued) Sensitivity of the ACC2 inversion results to volcanic forcing

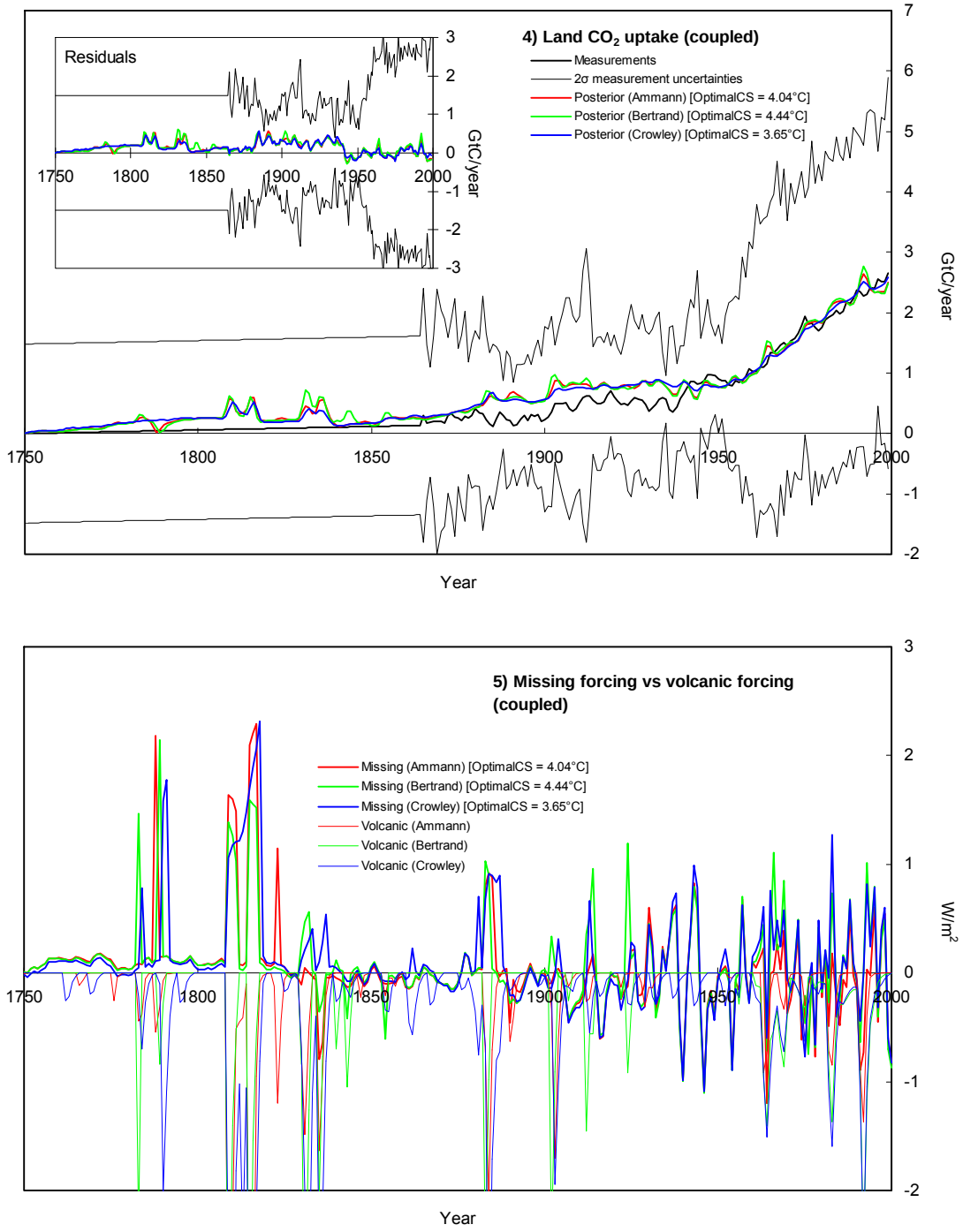

**Figure S8.** (Continued) Sensitivity of the ACC2 inversion results to volcanic forcing

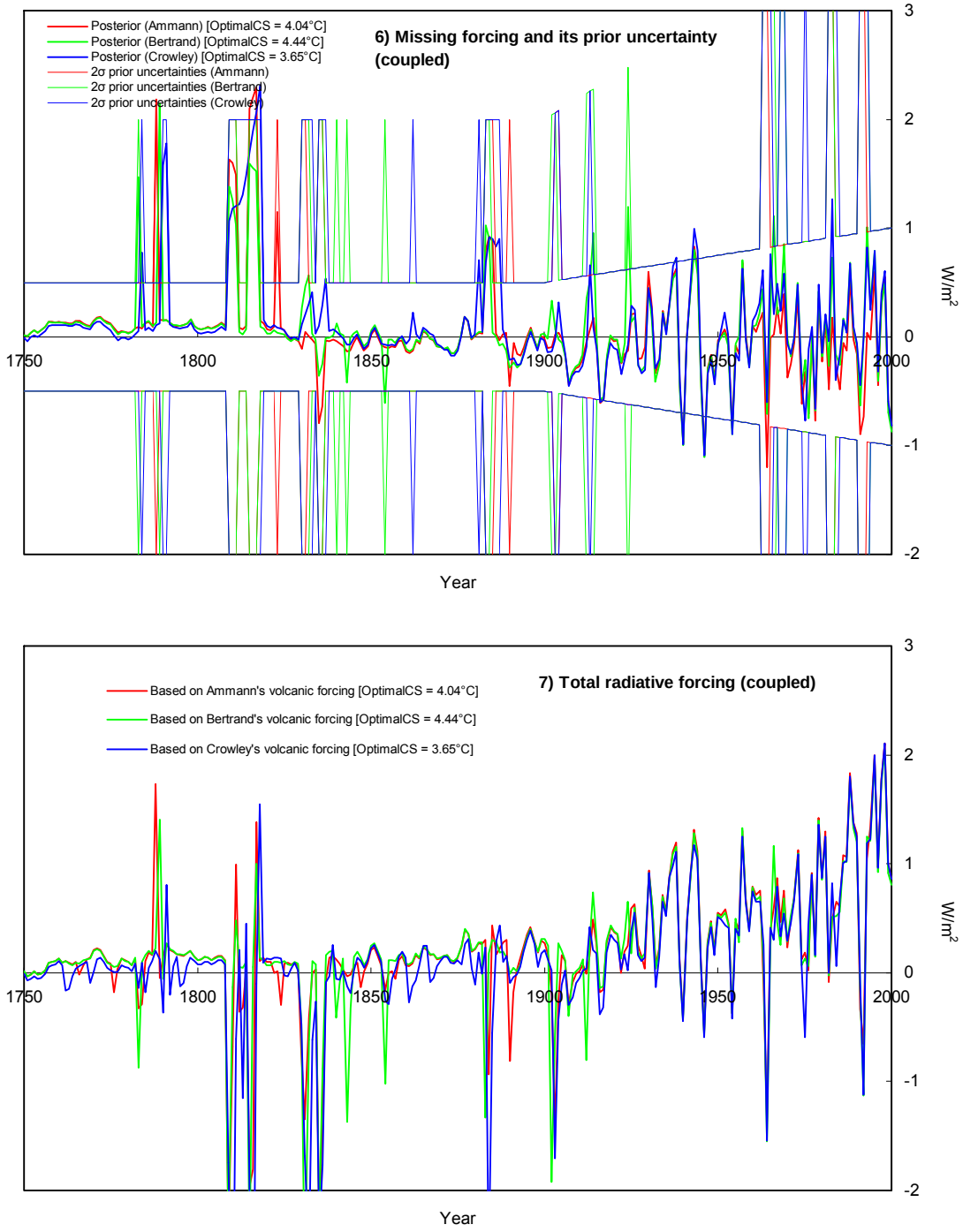

**Figure S8.** (Continued) Sensitivity of the ACC2 inversion results to volcanic forcing

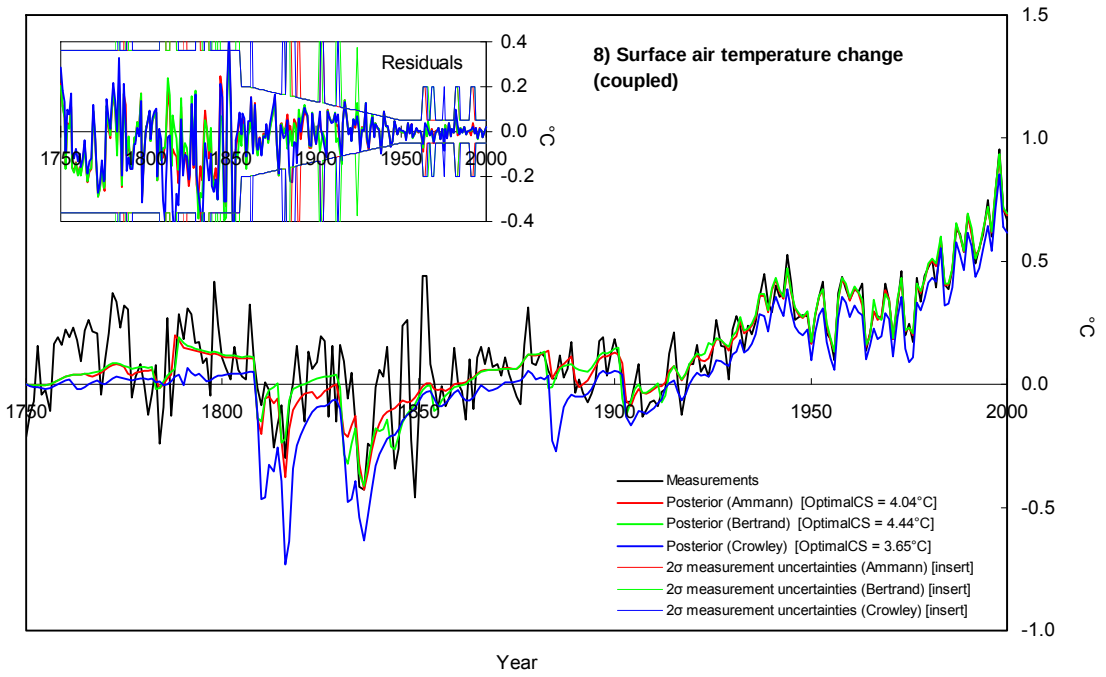

**Figure S9.** Sensitivity of the ACC2 inversion results to ocean diffusivity

Figure S9.1 shows the changes in the final value of the cost function when ocean diffusivity is assumed to be 0.55 $cm^2/s$ (standard), 1 $cm^2/s$, and 2 $cm^2/s$. The uncoupled inversions are performed with climate sensitivity fixed at values between 1°C and 10°C at intervals of 0.25°C. Black plots are identical with those shown in Figure 1 of the main article. Values in the square brackets are the best estimates of climate sensitivity for the respective inversion setups. Figures S9.2 and S9.3 show the associated uncoupled inversion results of radiative forcing and temperature change with respective optimal climate sensitivity indicated in the square brackets. Measurements shown in Figure S9.3 are for the uncoupled inversion with ocean diffusivity of 0.55 $cm^2/s$.

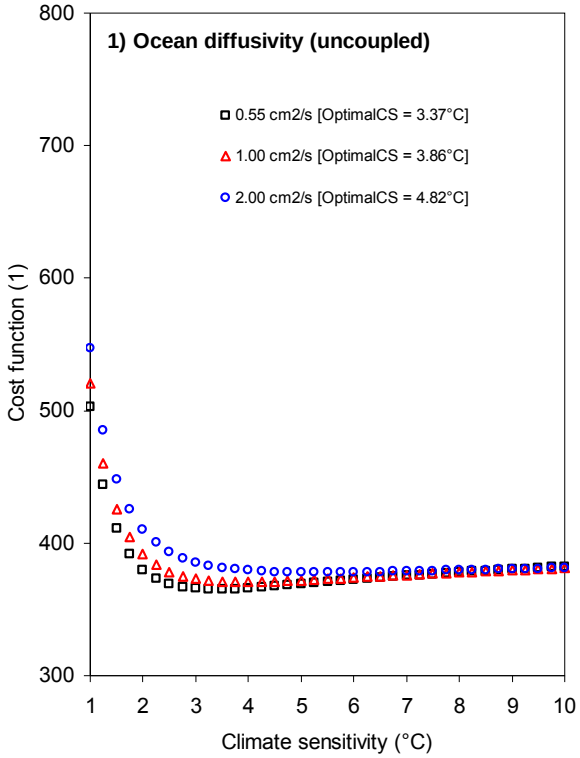

**Figure S9.** (Continued) Sensitivity of the ACC2 inversion results to ocean diffusivity

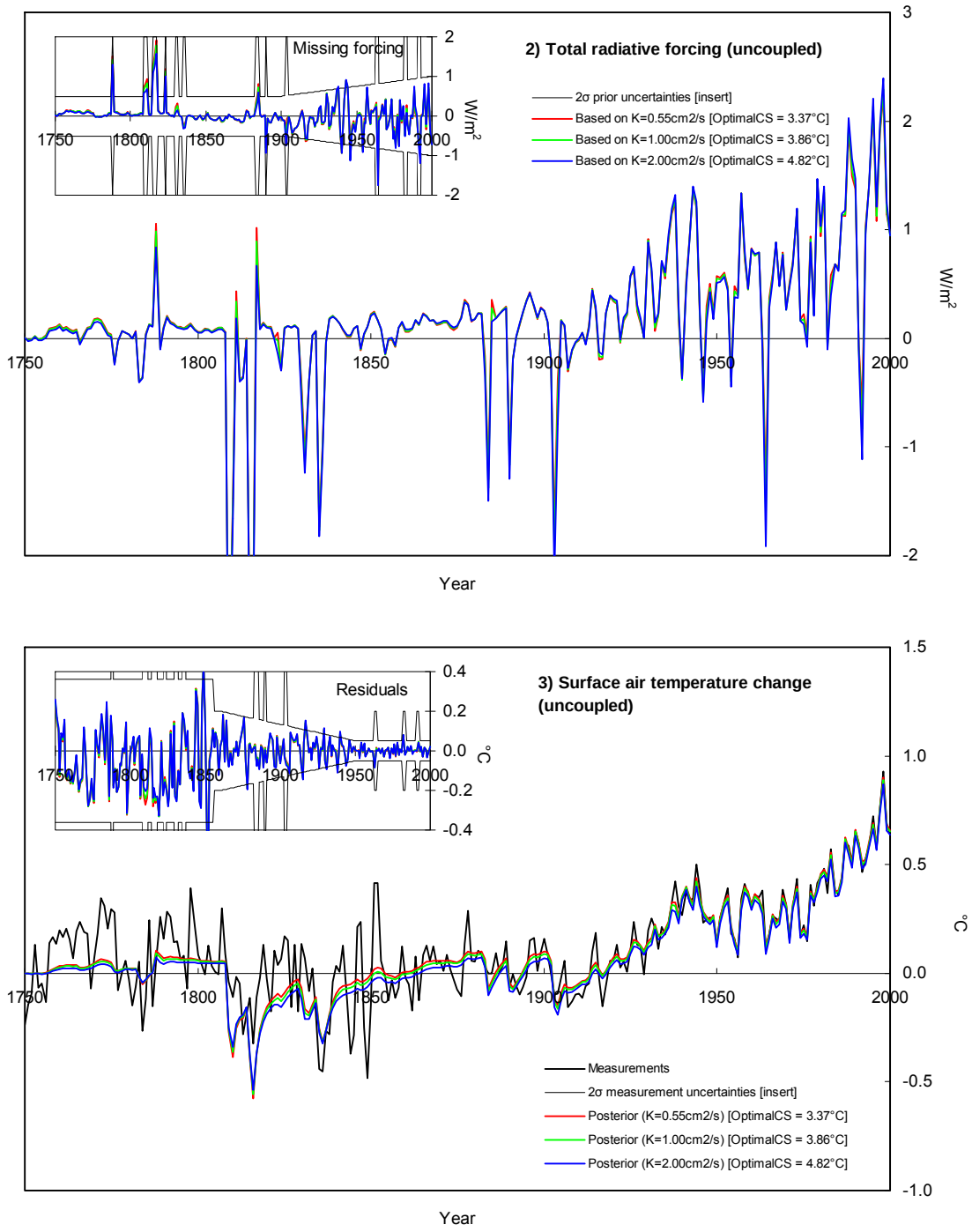

**Figure S10.** Sensitivity of the ACC2 inversion results to prior climate sensitivity

Shown below are the ACC2 uncoupled inversion results for radiative forcing and temperature change under different assumptions on prior climate sensitivity. The 2σ prior range of 0.5°C–6.5°C is the standard assumption adopted in the ACC2 inversion. The 2σ prior range of 1.5°C–4.5°C (IPCC, 2001, Chapter 9) is a conventional range. The 2σ prior range of 0.5°C–10.5°C is a conservative range (e.g. IPCC, 2007, pp.798-799). The inversion results are nearly indistinguishable each other. Values in the square brackets are the best estimates of climate sensitivity for the respective inversion setups. Measurements shown in Figure S10.2 are for the uncoupled inversion with the standard prior range for climate sensitivity.

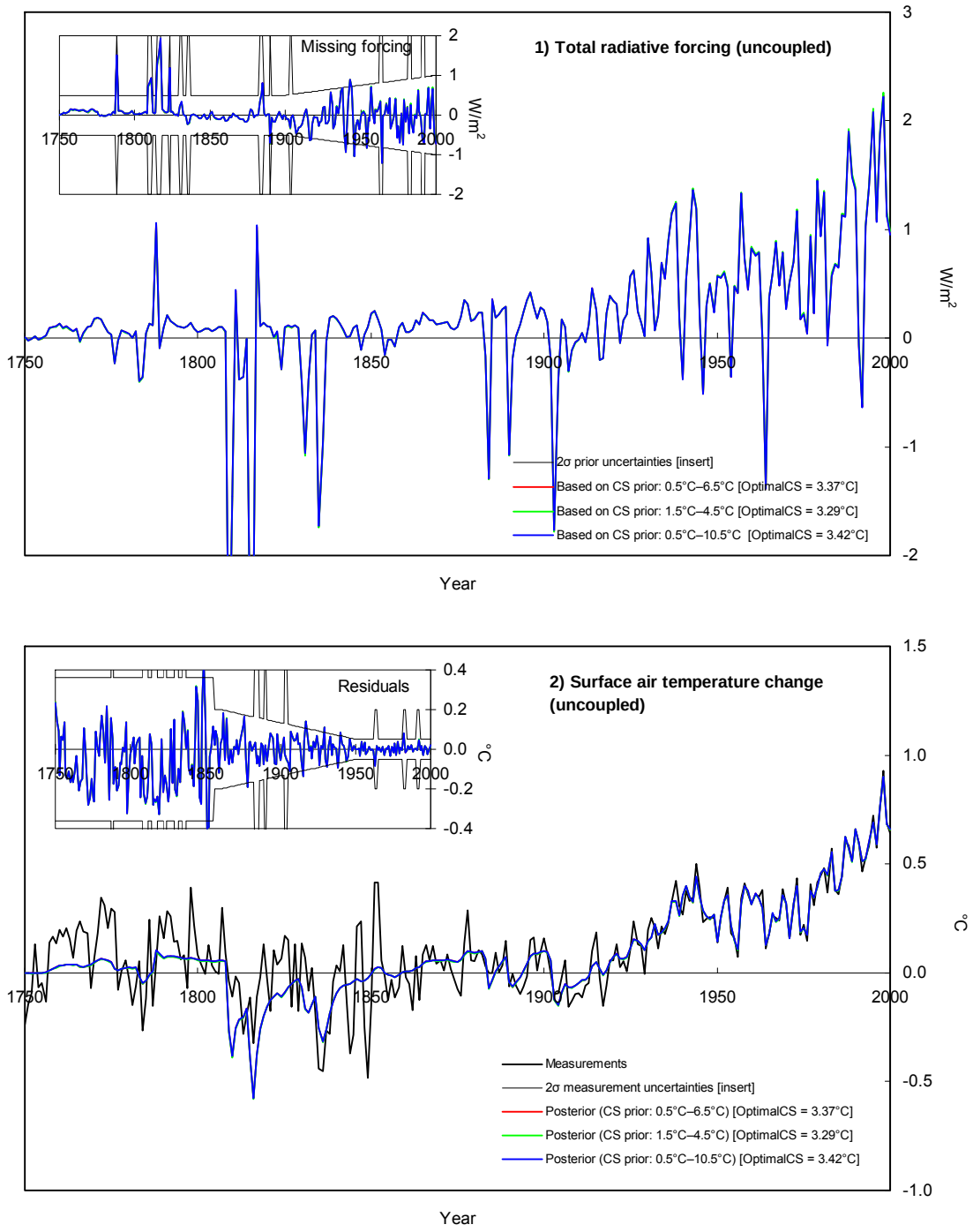

**Figure S11.** Influence of prescribed aerosol forcing to missing forcing

Shown below are the results of ACC2 uncoupled inversions when 50% smaller, standard, and 50% larger total aerosol forcing are assumed. In Figure S11.3, measurements are for the standard uncoupled inversion. Values in the square brackets are the best estimates of climate sensitivity for the respective inversion setups.

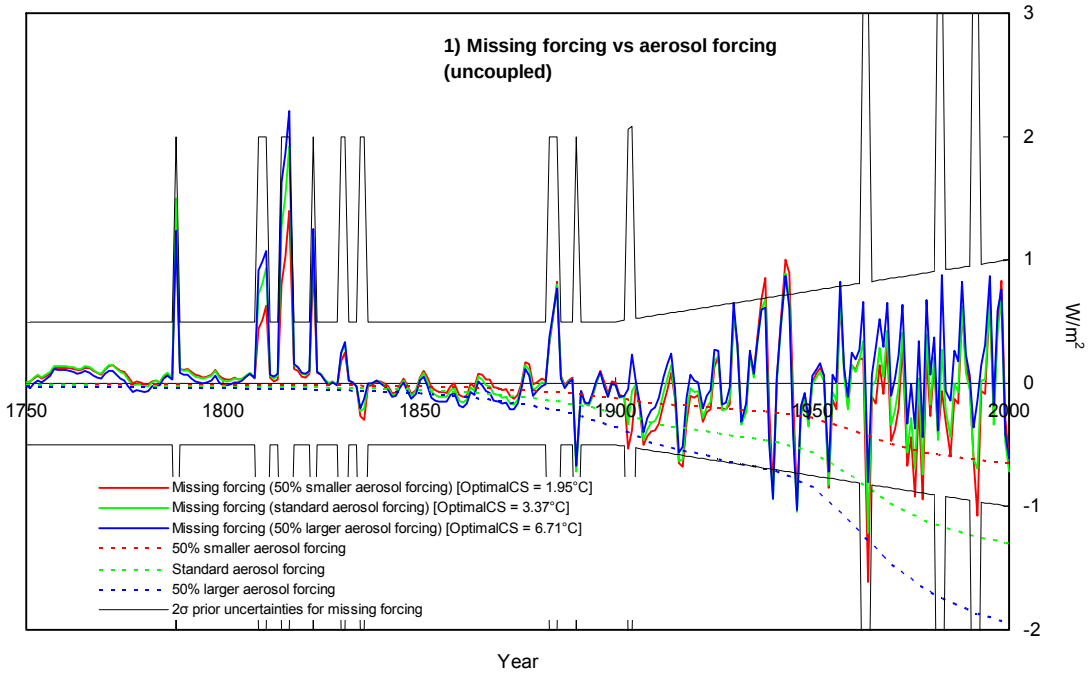


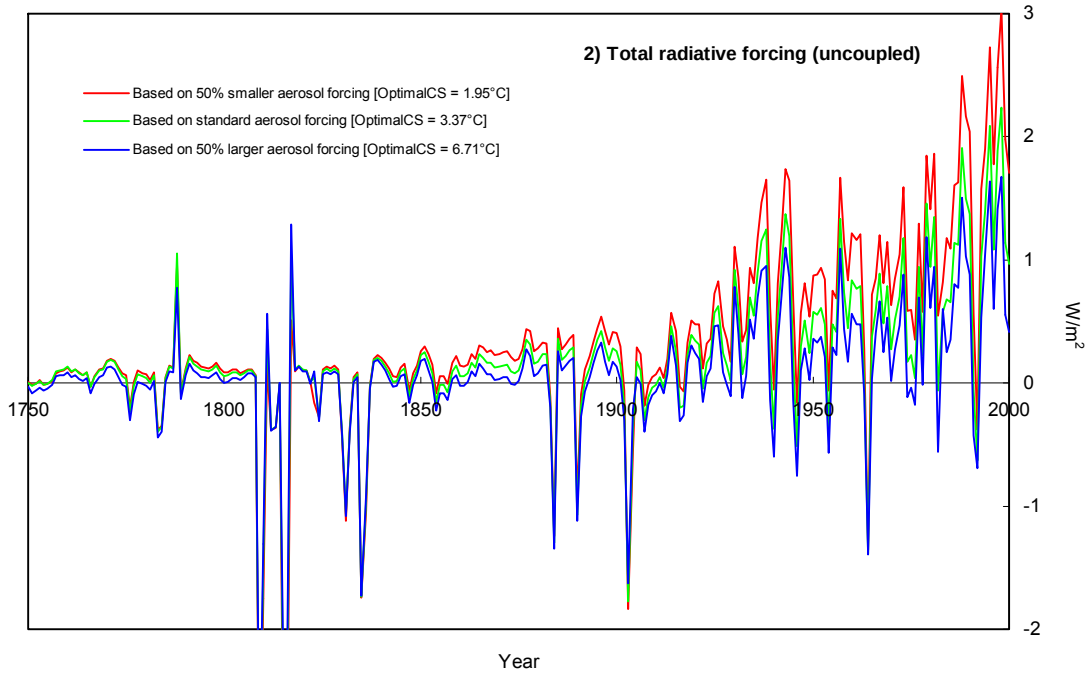

**Figure S11.** (Continued) Influence of prescribed aerosol forcing to missing forcing

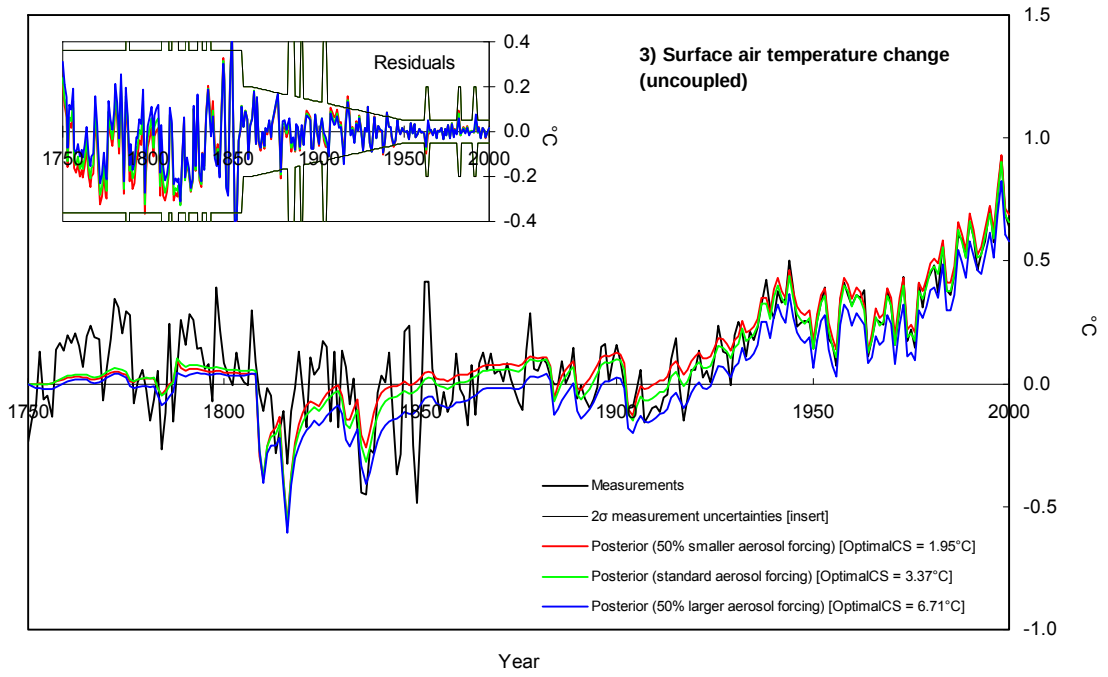

**Figure S12.** Influence of prescribed volcanic forcing to missing forcing

Shown below are the results of the ACC2 uncoupled inversions with different volcanic forcing prescribed (Ammann et al., 2003 (standard setup); Bertrand et al., 2002; Crowley et al., 2003). Values in the square brackets in the legends are the best estimates of climate sensitivity for the respective inversion setups. In Figure S12.3, measurements are for the uncoupled inversion using Ammann's volcanic forcing.

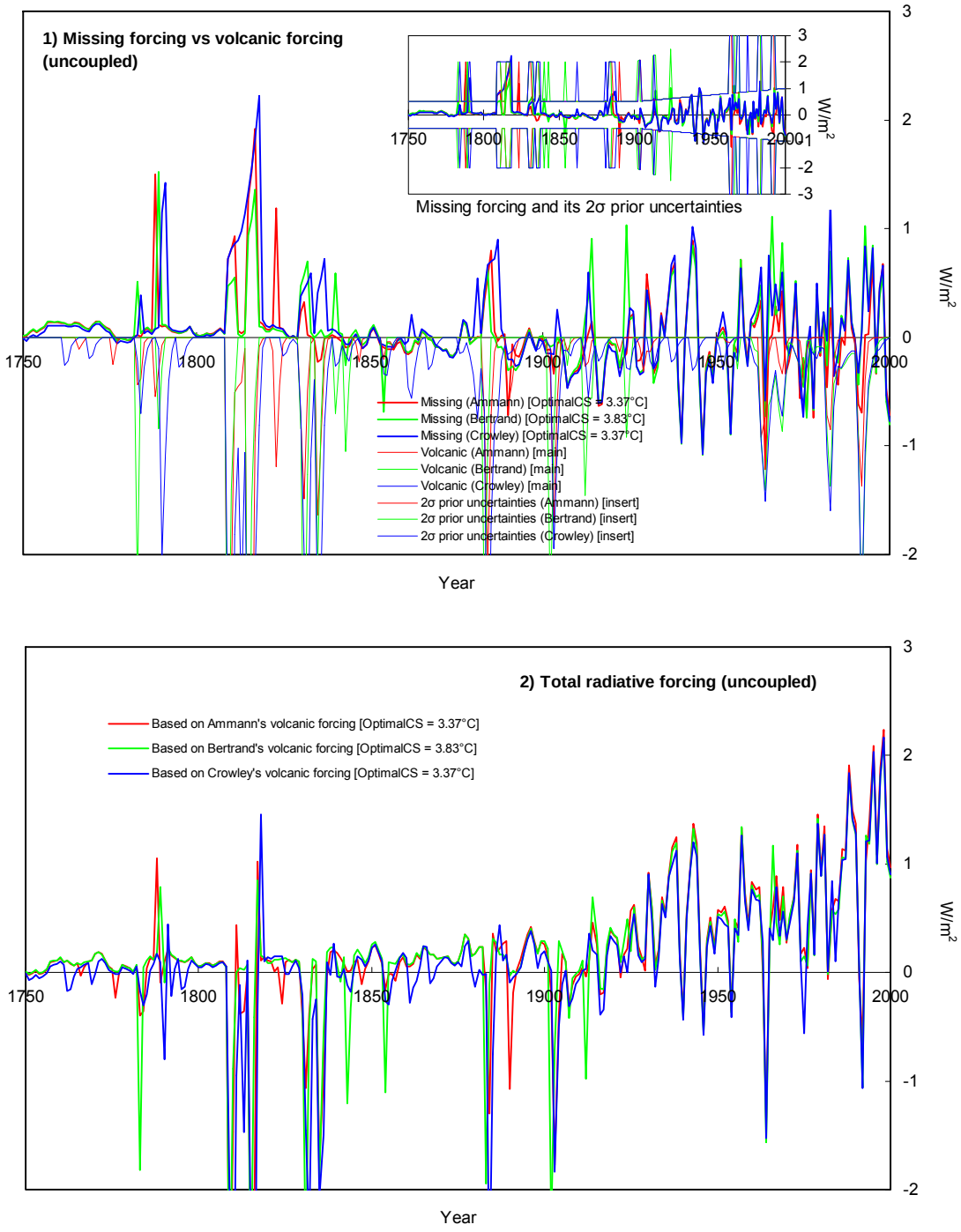

**Figure S12.** (Continued) Influence of prescribed volcanic forcing to missing forcing

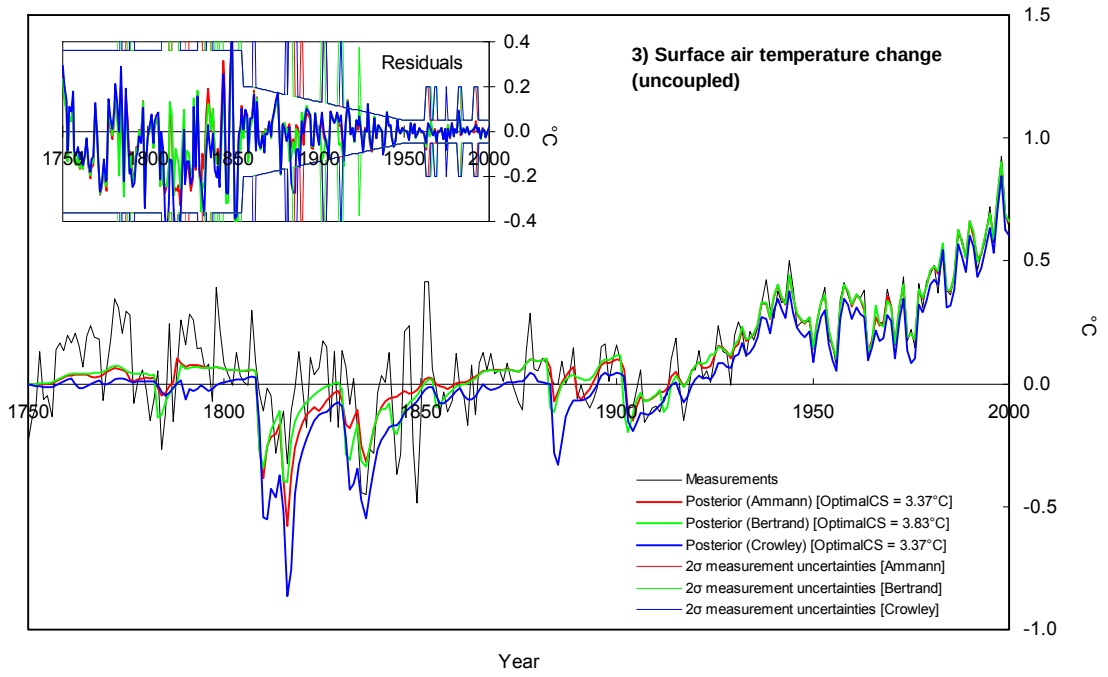

**Figure S13.** Influence of ENSO-driven temperature variability to missing forcing

The standard ACC2 uncoupled inversion is compared with an uncoupled inversion without accounting for the ENSO-driven variability in the temperature records. Values in the square brackets in the legends are the best estimates of climate sensitivity for the respective inversion setups. Measurements shown in Figure S13.2 are for the standard uncoupled inversion.

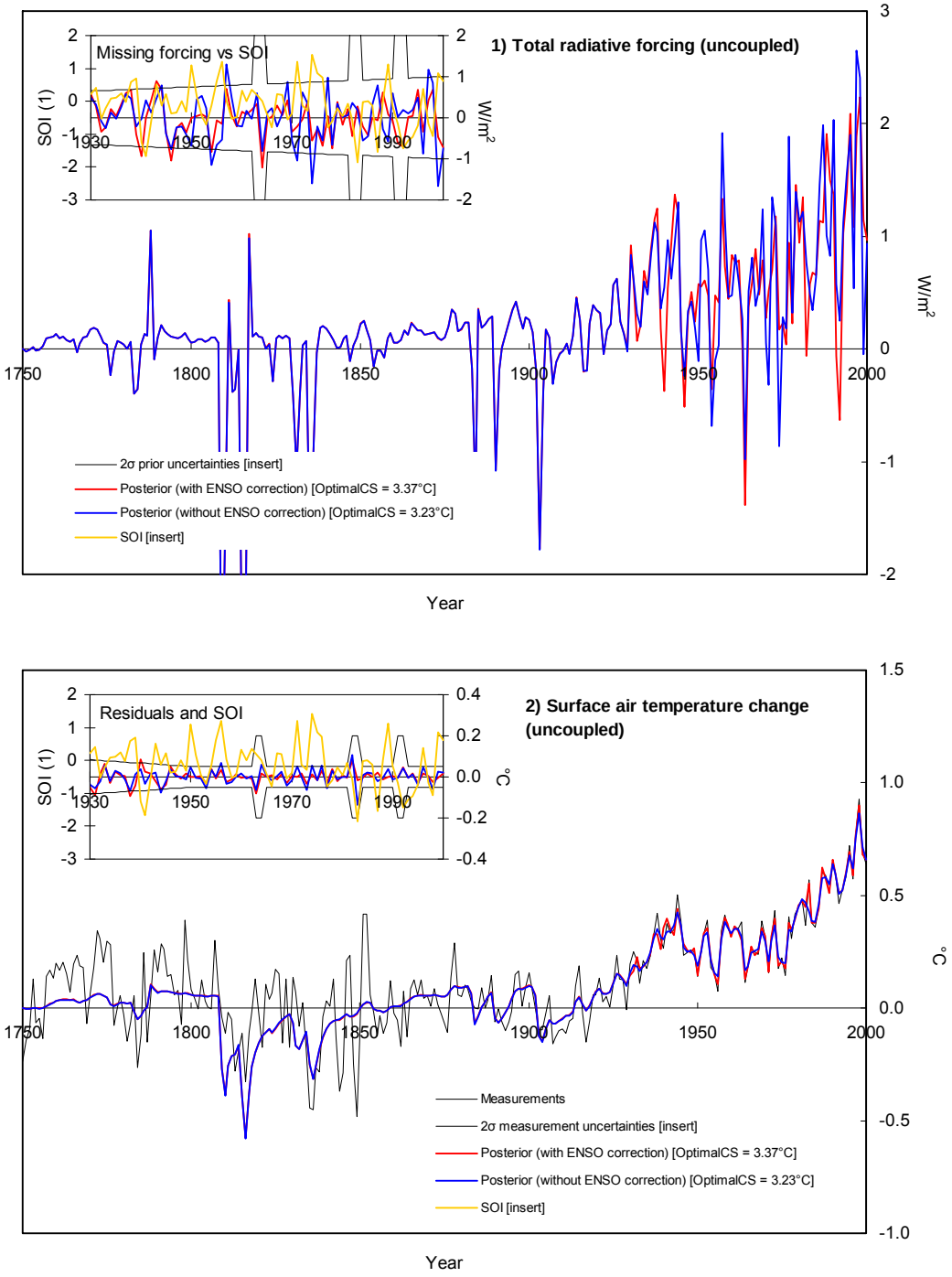

**Figure S14.** Changes in the cost function value with the changes in parameter values

Shown below are the final values of the cost function when inversions are performed with some key parameters fixed at different values. These experiments are done for fixed climate sensitivity (1, 3, 5, and 10°C). Note that the vertical scale for Figure S14.4 is different from others.

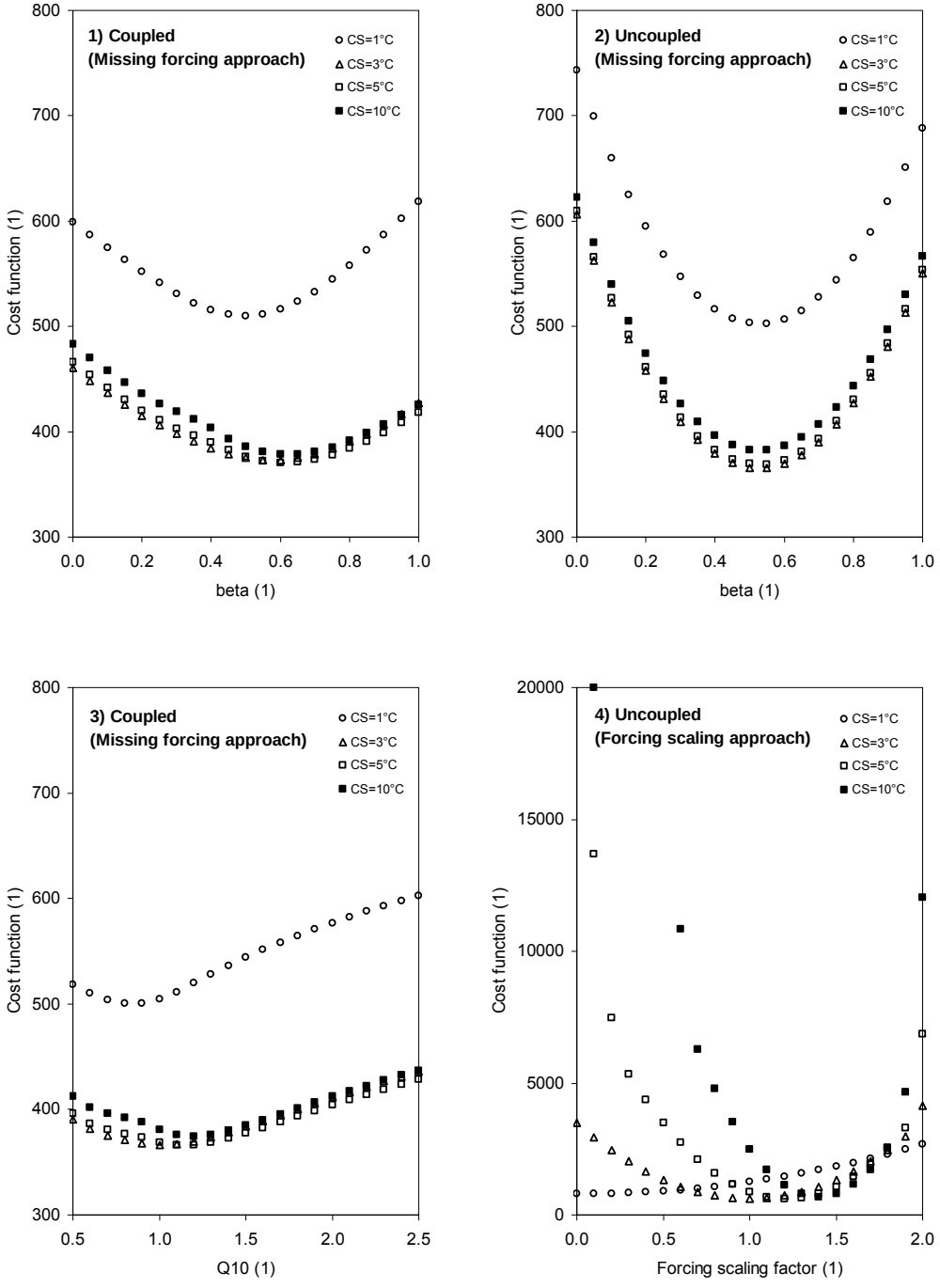

**Figure S15.** Influence of the AR(1) model to the inversion results

Figure S15.1 shows how the cost function curves in Figure 1 of the main article are influenced by the implementation of the AR(1) model for temperature residuals. The associated squared weighted residuals of selected time series are shown in Figure S15.2. Figures S15.3 to S15.6 are the radiative forcing and temperature change in the missing forcing-based and forcing scaling-based inversions with the climate sensitivity fixed at 1, 3, 5, and 10°C.

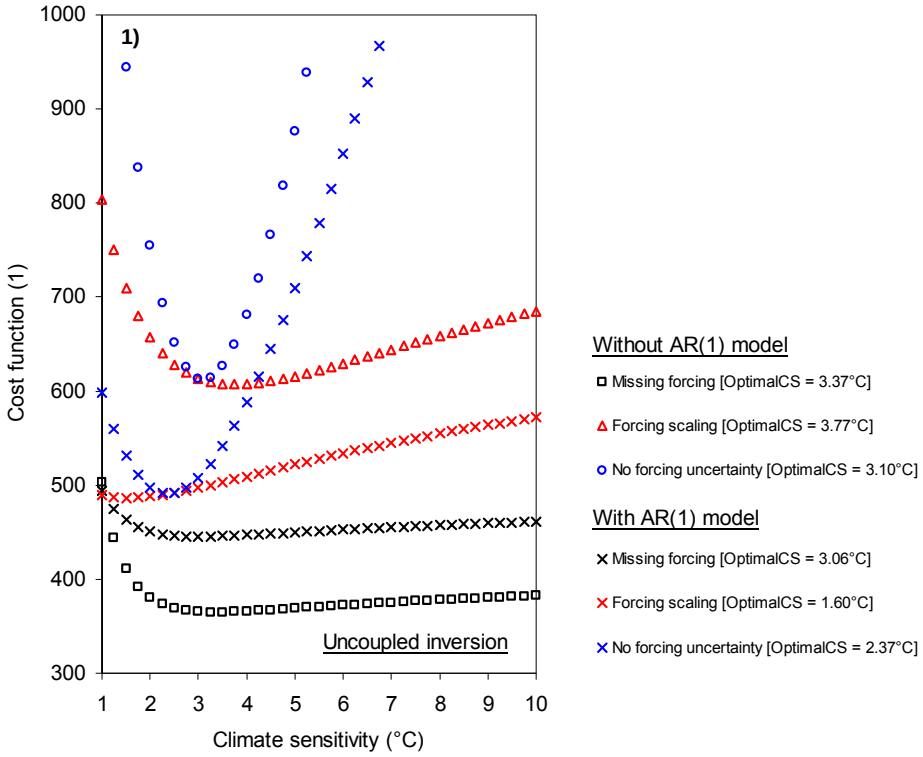

**Figure S15.** (Continued) Influence of the AR(1) model to the inversion results

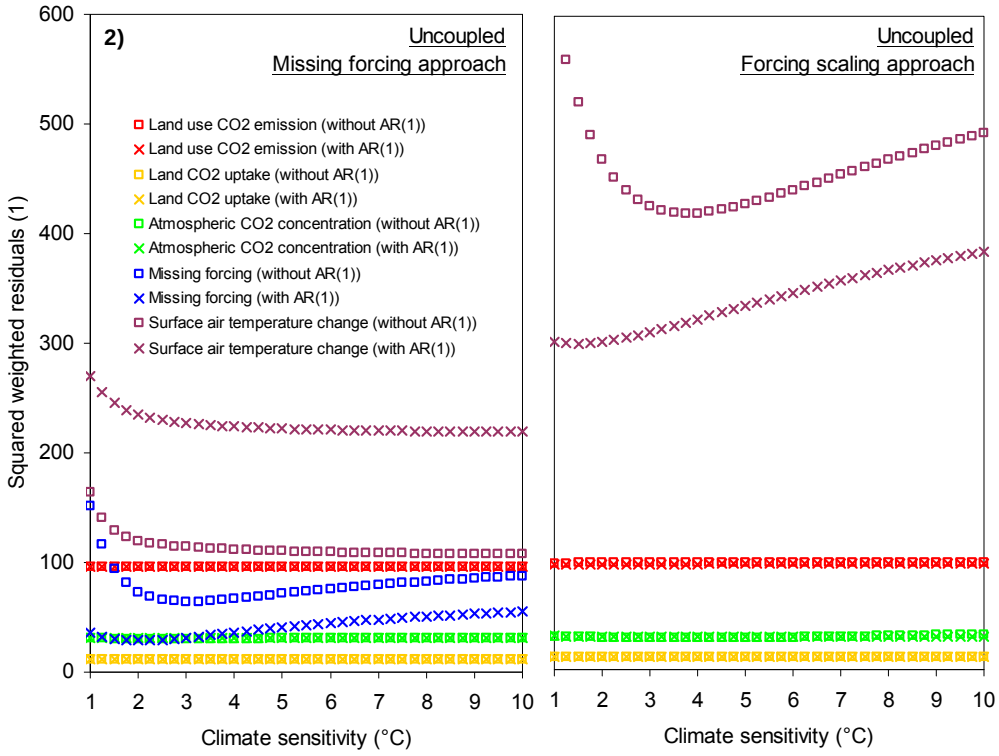

**Figure S15.** (Continued) Influence of the AR(1) model to the inversion results

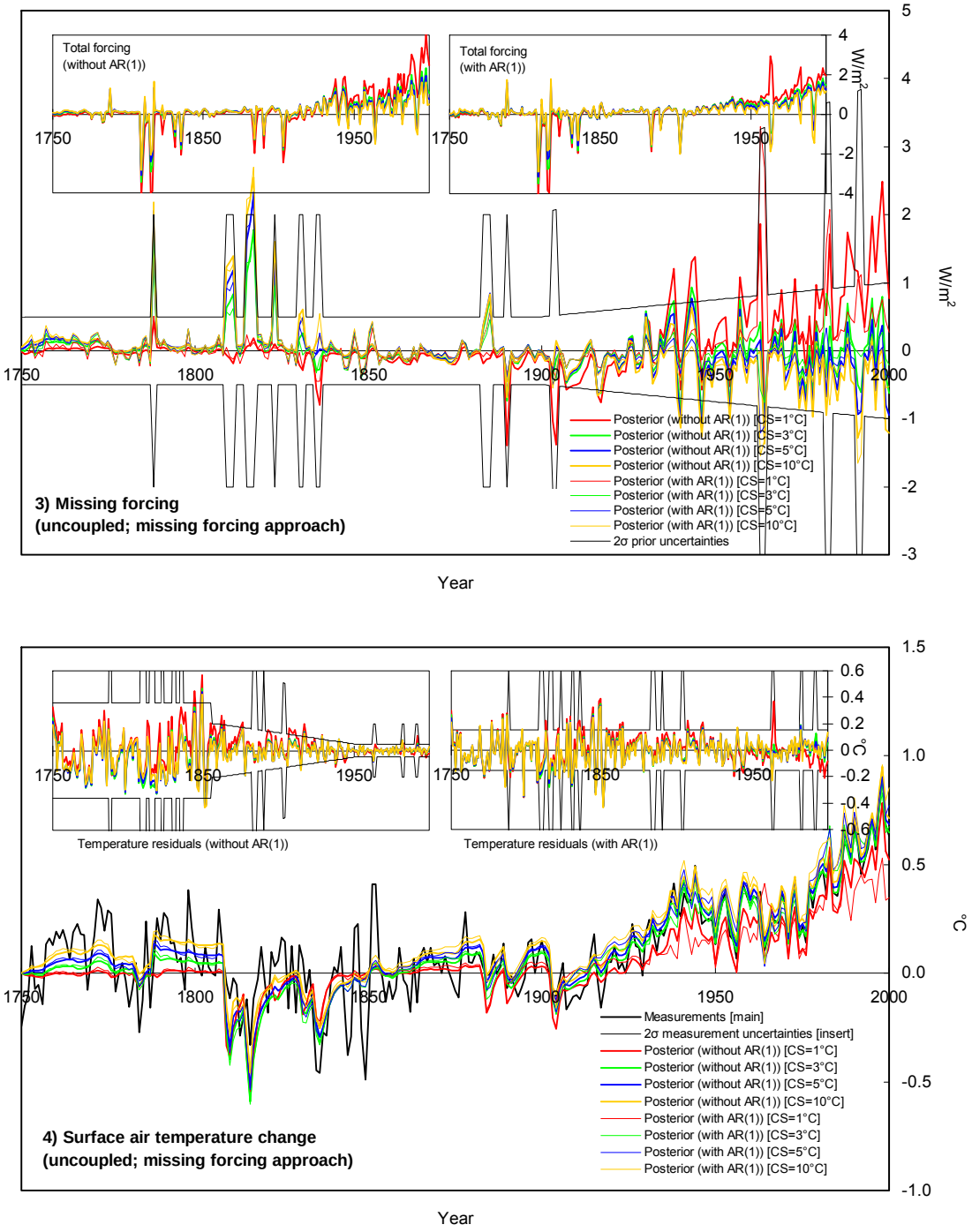

**Figure S15.** (Continued) Influence of the AR(1) model to the inversion results

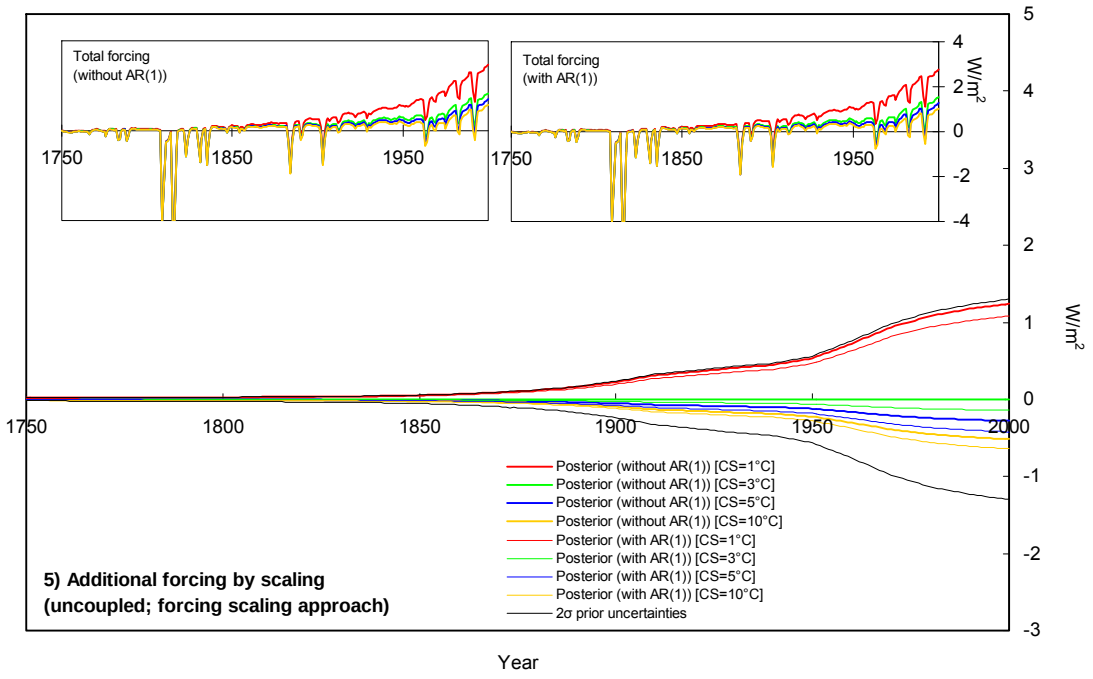


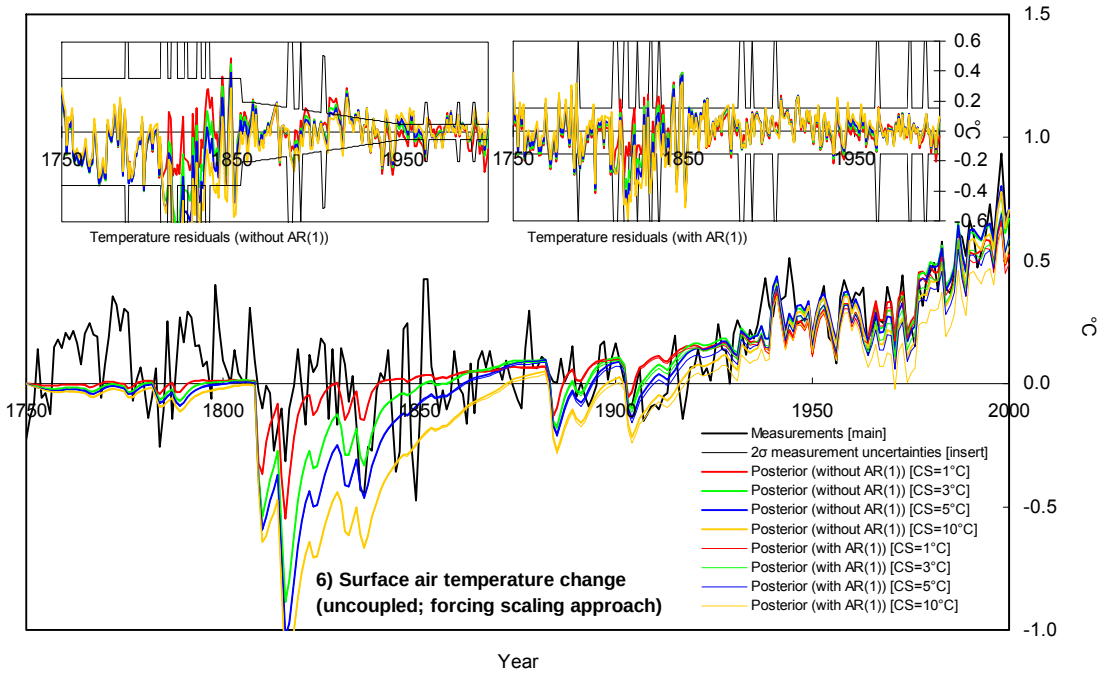

**Figure S16.** Influence of the AR(1) model to the temperature residuals

Figures S16.1a-p are the histograms of the temperature residuals in various ACC2 inversion results (missing forcing- and forcing scaling-based approach; climate sensitivity fixed at 1, 3, 5, 10°C; with/without the AR(1) model for temperature residuals). The bin width is determined by computing 40% of the standard deviation (e.g. Laws, 1997, p.215). Figures S16.2a-p show the corresponding spectrums of the temperature residuals.

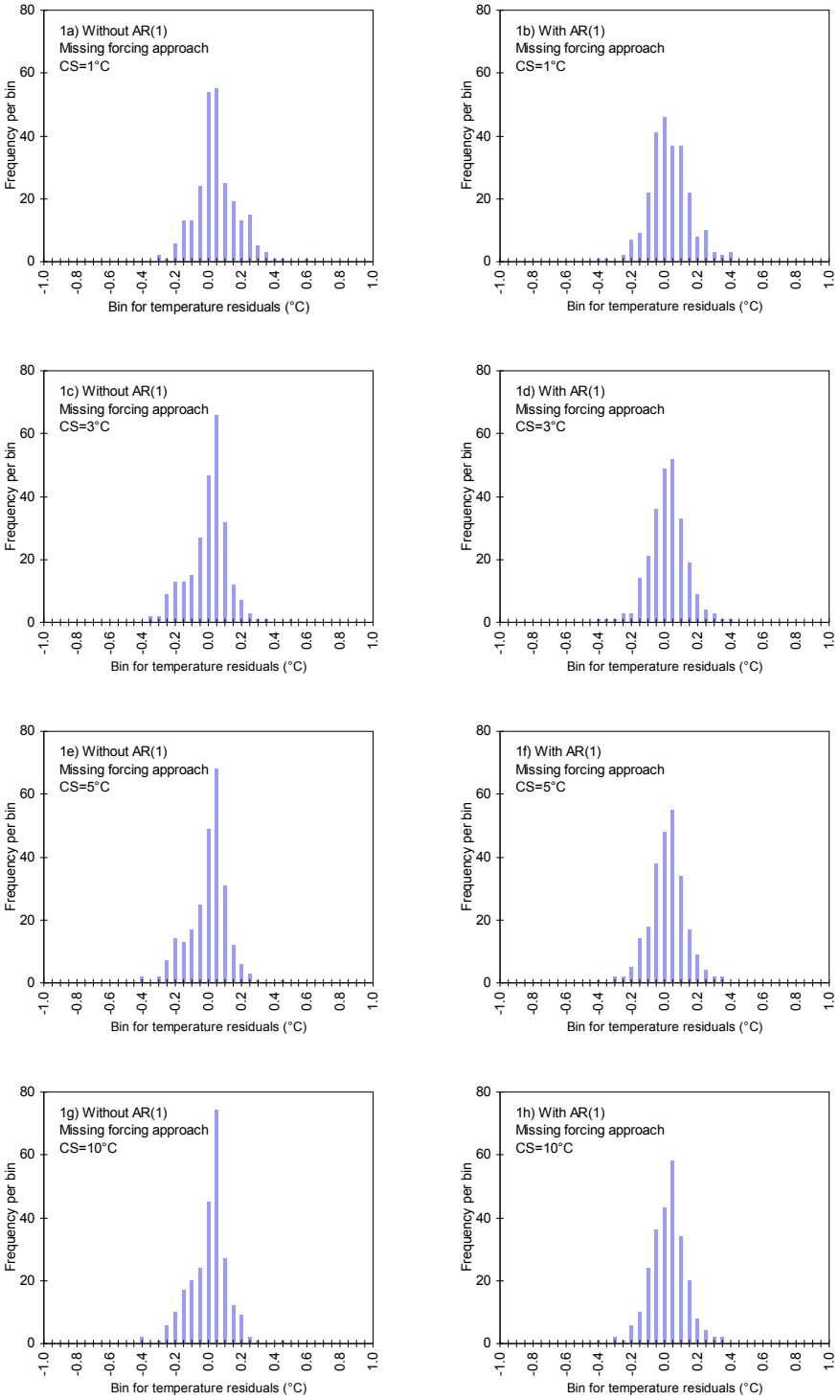

**Figure S16.** (Continued) Influence of the AR(1) model to the temperature residuals

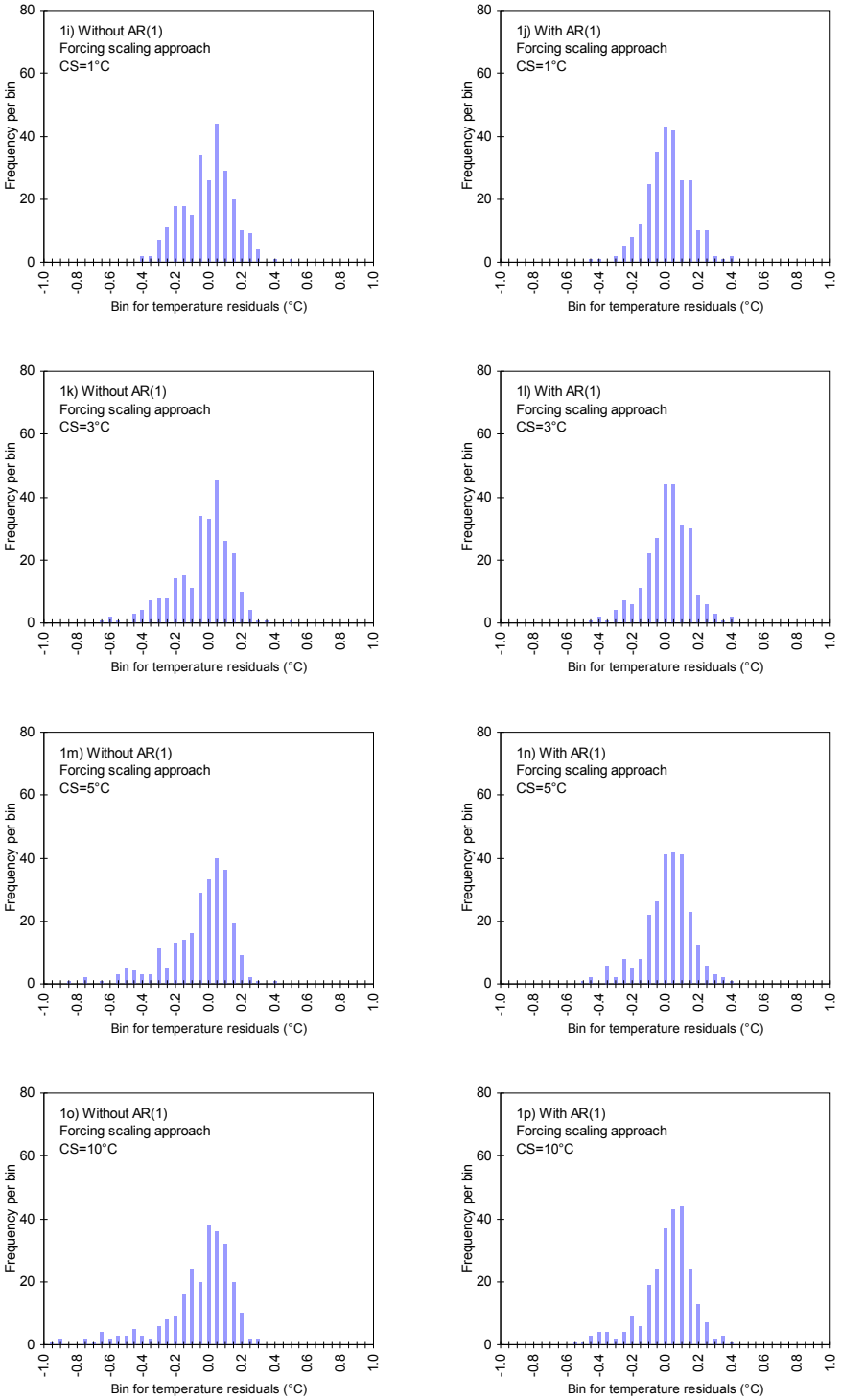

**Figure S16.** (Continued) Influence of the AR(1) model to the temperature residuals

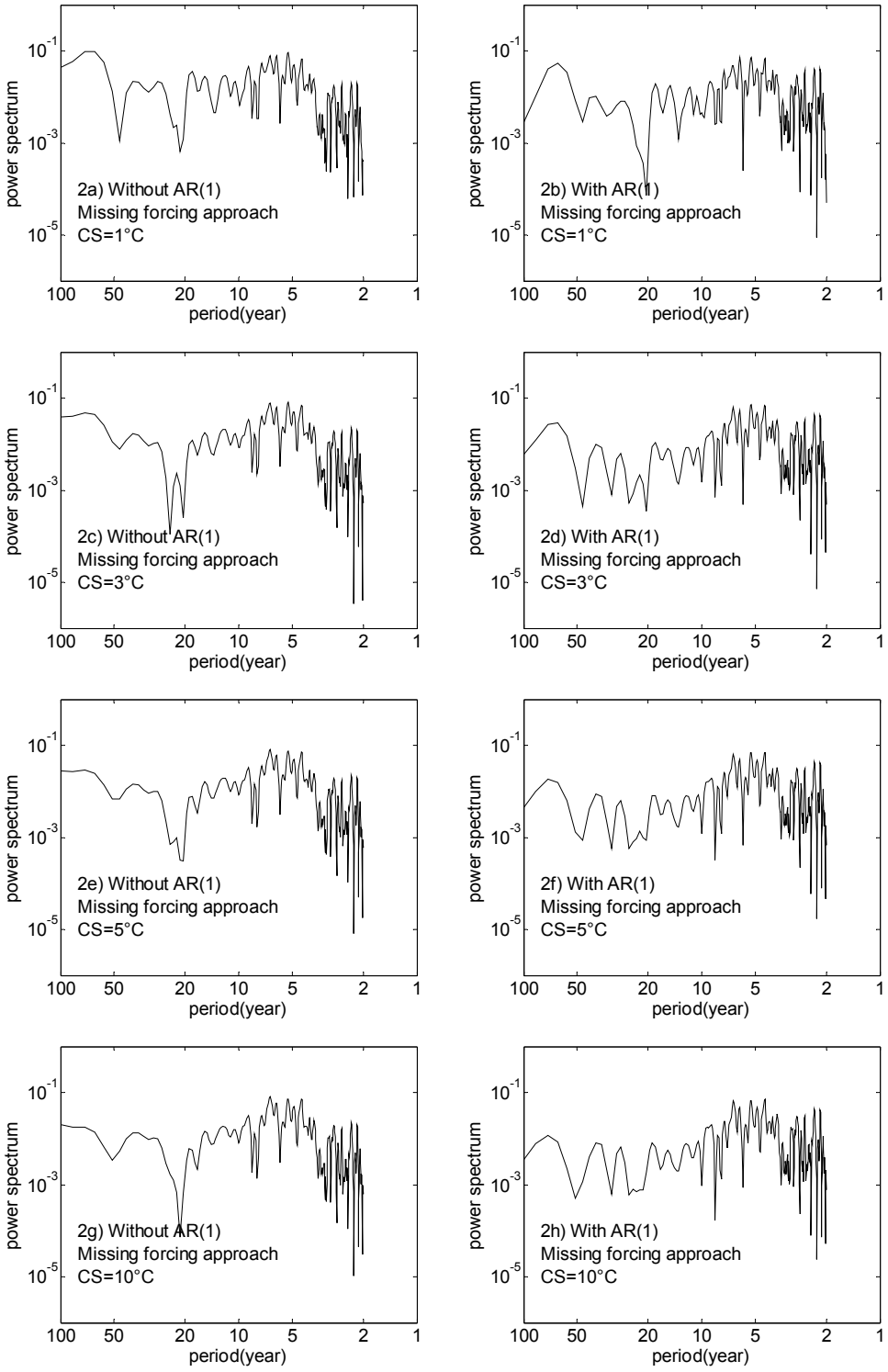

**Figure S16.** (Continued) Influence of the AR(1) model to the temperature residuals

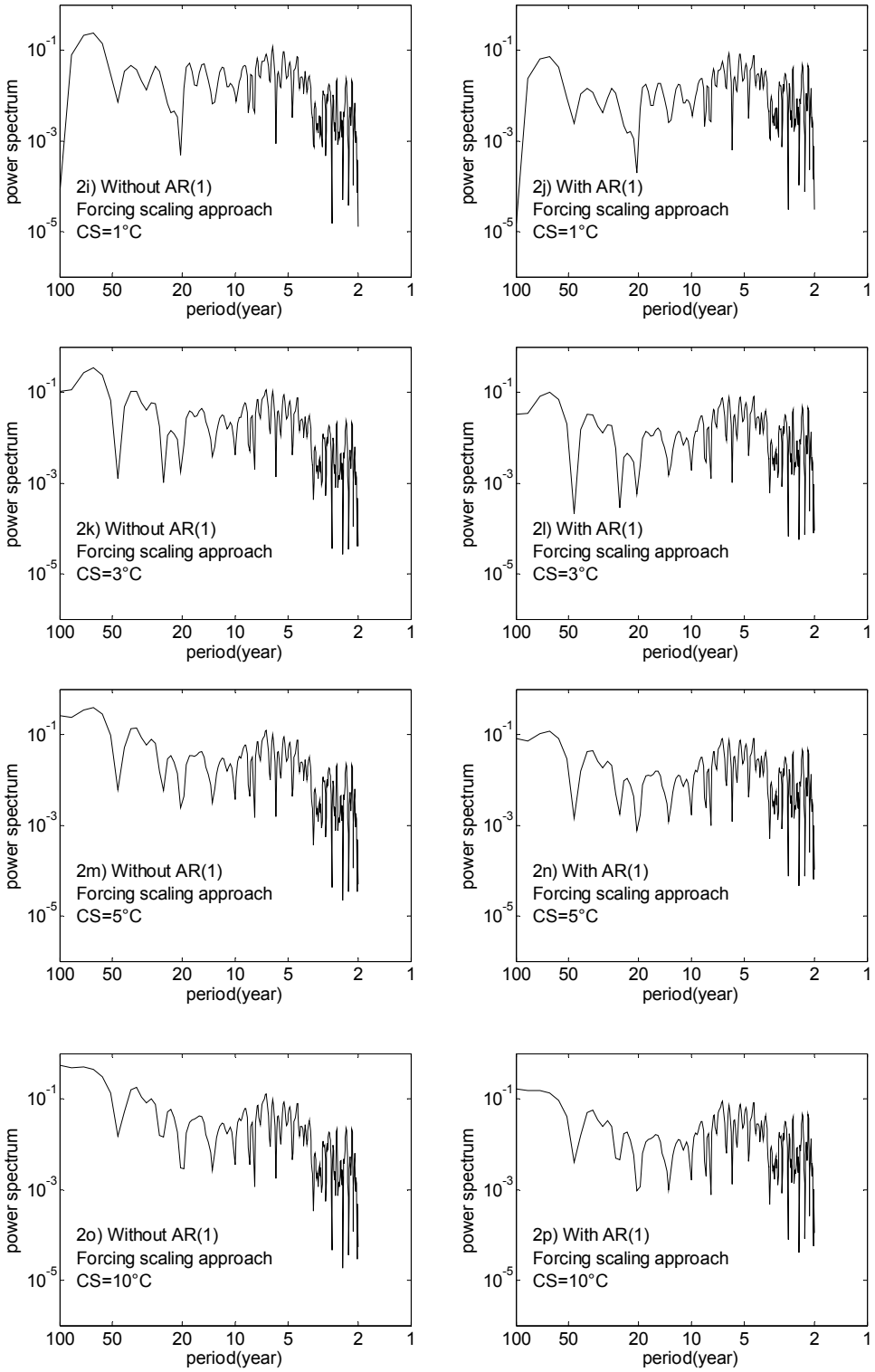

## REFERENCES FOR SUPPLEMENTARY INFORMATION


Ammann, C. M., G. A. Meehl, W. M. Washington, C. S. Zender (2003) A monthly and latitudinally varying volcanic forcing dataset in simulations of 20th century climate. *Geophysical Research Letters*, **30**(12), 1657, doi:10.1029/2003GL016875.

Bertrand C., M.-F. Loutre, M. Crucifix, A. Berger (2002) Climate of the last millennium: a sensitivity study. *Tellus A*, **54**, 221-244.

Box, G. E. P., G. M. Jenkins (1970) Time series analysis – forecasting and control. Holden-Day, San Francisco, California, USA. 553 pp.

Brovkin, V., A. Ganopolski, Y. Svirezhev (1997) A continuous climate-vegetation classification for use in climate-biosphere studies. *Ecological Modelling*, **101**, 251-261.

Collins, M., S. F. B. Tett, C. Cooper (2001) The internal climate variability of HadCM3, a version of the Hadley Centre coupled model without flux adjustments. *Climate Dynamics*, **17**, 61-81.

Crowley, T. J., S. K. Baum, K.-Y. Kim, G. C. Hegerl, W. T. Hyde (2003) Modeling ocean heat content changes during the last millennium. *Geophysical Research Letters*, **30**(18), 1932, doi:10.1029/2003GL017801.

Doney, S. C., K. Lindsay, I. Fung, J. John (2006) Natural variability in a stable, 1000-yr global coupled climate–carbon cycle simulation. *Journal of Climate*, **19**, 3033-3054.

Eden, C., R. J. Greatbatch, J. Lu (2002) Prospects for decadal prediction of the North Atlantic Oscillation (NAO). *Geophysical Research Letters*, **29**, 10, 1466, doi;10.1029/2001GL014069.

Etheridge, D. M., L. P. Steele, R. L. Langenfelds, R. J. Fransey (1996) Natural and anthropogenic changes in atmospheric $CO_2$ over the last 1000 years from air in Antarctic ice and firn. *Journal of Geophysical Research*, **101**, D2, 4115-4128.

Etheridge, D. M., L. P. Steele, R. J. Francey, R. L. Langenfelds (1998) Atmospheric methane between 1000 AD and present: evidence of anthropogenic emissions and climatic variability. *Journal of Geophysical Research*, **103**, D13, 15979-15993.

Forest, C. E., P. H. Stone, A. P. Sokolov, M. R. Allen, M. D. Webster (2002) Quantifying uncertainties in climate system properties with the use of recent climate observations. *Nature*, **295**, 113-117.

Frame, D. J., B. B. B. Booth, J. A. Kettleborough, D. A. Stainforth, J. M. Gregory, M. Collins, M. R. Allen (2005) Constraining climate forecast: the role of prior assumptions. *Geophysical Research Letters*, **32**, L09702, doi: 10.1029/2004GL022241.

Friedlingstein, P., P. Cox, R. Betts, L. Bopp, W. von Bloh, V. Brovkin, P. Cadule, S. Doney, M. Eby, I. Fung, G. Bala, J. John, C. Jones, F. Joos, T. Kato, M. Kawamiya, W. Knorr, K. Lindsay, H. D. Matthews, T. Raddatz, P. Rayner, C. Reick, E. Roeckner, K.-G. Schnitzler, R. Schnur, K.

Strassmann, A. J. Weaver, C. Yoshikawa, N. Zeng (2006) Climate–carbon cycle feedback analysis: results from the $C^4$MIP model intercomparison. *Journal of Climate*, **19**, 3337-3353.

Gitz, V., P. Ciais (2003) Amplifying effects of land-use change on future atmospheric $CO_2$ levels. *Global Biogeochemical Cycles*, **17**, 1024, doi:10.1029/2002GB001963.

Gregory, J. M., R. J. Stouffer, S. C. B. Raper, P. A. Stott, N. A. Rayner (2002) An observationally based estimate of the climate sensitivity. *Journal of Climate*, **15**, 3117-3121.

Gu, L., D. D. Baldocchi, S. C. Wofsy, J. W. Munger, J. J. Michalsky, S. P. Urbanski, T. A. Boden (2003) Response of a deciduous forest to the Mount Pinatubo eruption: enhanced photosynthesis. *Science*, **299**, 2035-2038.

Gurney, K. R., R. M. Law, A. S. Denning (2002) Towards robust regional estimates of $CO_2$ sources and sinks using atmospheric transport models. *Nature*, **415**, 626-630.

Hansen J., M. Sato (2004) Data sets used in GISS 2004 GCM. http://www.giss.nasa.gov/data/simodel/ghgases/GCM.html

Hegerl, G. C., T. J. Crowley, W. T. Hyde, D. J. Frame (2006) Climate sensitivity constrained by temperature reconstructions over the past seven centuries. *Nature*, **440**, 1029-1032.

Hoffert, M. I., A. J. Callegari, C.-T. Hsieh (1981) A box-diffusion carbon cycle model with upwelling, polar bottom water formation and a marine biosphere. In (ed.) B. Bolin. *Carbon cycle modelling (SCOPE 16)*. pp.287-305. John Wiley & Sons. 390 pp.

Houghton, R. A. (2003). Revised estimates of the annual net flux of carbon to the atmosphere from changes in land use and land management 1850-2000. *Tellus B*, **55**, 378-390.

Houtekamer, P. L., L. Lefaivre, J. Derome, H. Ritchie, H. L. Mitchell (1996) A system simulation approach to ensemble prediction. *Monthly Weather Review*, **124**, 1225-1242.

IPCC (2001) Climate change 2001: the scientific basis. Contribution of Working Group I to the Third Assessment Report of the Intergovernmental Panel on Climate Change [Houghton, J.T.,Y. Ding, D.J. Griggs, M. Noguer, P.J. van der Linden, X. Dai, K. Maskell, and C.A. Johnson (eds.)]. Cambridge University Press, Cambridge, United Kingdom and New York, New York, USA. 881 pp.

IPCC (2004) IPCC Workshop on describing scientific uncertainties in climate change to support analysis of risk and of options. National University of Ireland, Maynooth, Co. Kildare, Ireland. May 11-May 13, 2004. 138 pp.

IPCC (2007) Climate change 2007: the physical science basis. Contribution of Working Group I to the Fourth Assessment Report of the Intergovernmental Panel on Climate Change [Solomon, S., D. Qin, M. Manning, Z. Chen, M. Marquis, K.B. Averyt, M. Tignor and H.L. Miller (eds.)]. Cambridge University Press, Cambridge, United Kingdom and New York, New York, USA. 996 pp.

Jones, C. D., P. M. Cox (2001) Modeling the volcanic signal in the atmospheric $CO_2$ record. *Global Biogeochemical Cycles*, **15**, 453-465.

Jones, P. D., K. R. Briffa, T. P. Barnett, S. F. B. Tett (1998) Millennial temperature reconstructions. IGBP PAGES/World Data Center-A for Paleoclimatology Data Contribution Series #1998-039. NOAA/NGDC Paleoclimatology Program, Boulder, Colorado, USA.

Jones, P. D., M. E. Mann (2004) Climate over past millennia. *Review of Geophysics*, **42**, RG2002.

Jones, P. D., D. E. Parker, T. J. Osborn, K. R. Briffa (2006) Global and hemispheric temperature anomalies – land and marine instrumental records. In *Trends: a compendium of data on global change.* Carbon Dioxide Information Analysis Center, Oak Ridge National Laboratory, US Department of Energy, Oak Ridge, Tennessee, USA. http://cdiac.ornl.gov/

Keeling, C. D., T. P. Whorf (2005) Atmospheric $CO_2$ records from sites in the SIO air sampling network. In *Trends: a compendium of data on global change.* Carbon Dioxide Information Analysis Center, Oak Ridge National Laboratory, US Department of Energy, Oak Ridge, Tennessee, USA. http://cdiac.ornl.gov/

Kicklighter, D. W., M. Bruno. S. Dönges, G. Esser, M. Heimann, J. Helfrich, F. Ift, F. Joos, J. Kaduk, G. H. Kohlmaier, A. D. Mcguire, J. M. Melillo, R. Meyer, B. Moore III, A. Nadler, I. C. Prentice, W. Sauf, A. L. Schloss, S. Sitch, U. Wittenberg, G. Würth (1999) A first-order analysis of the potential role of $CO_2$ fertilization to affect the global carbon budget: a comparison of four terrestrial biosphere models. *Tellus B*, **51**, 343-366.

Knutti, R., T. F. Stocker, F. Joos, G.-K. Plattner (2002) Constraints on radiative forcing and future climate change from observations and climate model ensembles. *Nature*, **416**, 719-723.

Kohlmaier, G. H., H. Brohl, E. O. Siré, M. Plőchl, R. Reville (1987) Modelling stimulation of plants and ecosystem response to present levels of excess atmospheric $CO_2$. *Tellus B*, **39**, 155-179.

Kriegler, E. (2005) Imprecise probability analysis for Integrated Assessment of climate change. Ph.D. dissertation. Potsdam Universität, Germany. 256 pp. http://www.pik-potsdam.de/~kriegler/

Lal, R. (2005) Soil erosion and carbon dynamics. *Soil and Tillage Research*, **81**, 137-142.

Levitus, S., J. I. Antonov, T. P. Boyer, C. Stephens (2000) Warming of the world ocean. *Science*, **287**, 2225-2229.

Mackenzie, F. T., A. Lerman (2006) Carbon in the geobiosphere: Earth's outer shell. Springer, Dordrecht, The Netherlands. 402 pp.

Mann, M. E., P. D. Jones (2003) Global surface temperatures over the past two millennia. *Geophysical Research Letters*, **30**(15), 1820, doi:10.1029/2003GL017814.

Marland, G., T. A. Boden, R. J. Andres (2006) Global, regional, and national $CO_2$ emissions. In *Trends: a compendium of data on global change.* Carbon Dioxide Information Analysis Center, Oak Ridge National Laboratory, US Department of Energy, Oak Ridge, Tennessee, USA. http://cdiac.ornl.gov/

Masarie, K. A., R. L. Langenfelds, C. E. Allison, T. J. Conway, E. J. Dlugokencky, R. J. Francey, P. C. Novelli, L. P. Steele, P. P. Tans, B. Vaughn, J. W. C. White (2001) NOAA/CSIRO flask intercomparison project: a strategy for directly assessing consistency among atmospheric

measurements made by independent laboratories. *Journal of Geophysical Research*, **106**, D17, 20445-20464.

Meyer, R., F. Joos, G. Esser, M. Heimann, G. Hooss, G. Kohlmaier, W. Sauf, R. Voss, U. Wittenberg (1999) The substitution of high-resolution terrestrial biosphere models and carbon sequestration in response to changing $CO_2$ and climate. *Global Biogeochemical Cycles*, **13**, 785-802.

Räisänen, J. (2007) How reliable are climate models? *Tellus A*, **59**, 2-29.

Ricciuto, D. M., K. J. Davis, K. Keller (2008) A Bayesian synthesis inversion of carbon cycle observations: How can observations reduce uncertainties about future sinks? *Global Biogeochemical Cycles*, doi:10.1029/2006GB002908, in press.

Robock, A. (2005) Cooling following large volcanic eruptions corrected for the effect of diffuse radiation on tree rings. *Geophysical Research Letters*, **32**, L06702, doi: 10.1029/2004GL022116.

Stainforth, D. A., T. Aina, C. Christensen, M. Collins, N. Faull, D. J. Frame, J. A. Kettleborough, S. Knight, A. Martin, J. M. Murphy, C. Piani, D. Sexton, L. A. Smith, R. A. Spicer, A. J. Thorpe, M. R. Allen (2005) Uncertainty in predictions of the climate response to rising levels of greenhouse gases. *Nature*, **433**, 403-406.

Sundquist, E. T., L. N. Plummer (1981) Carbon dioxide in the ocean surface layer: some modelling considerations. In (ed.) B. Bolin. *Carbon cycle modelling (SCOPE 16)*. pp.259-269. John Wiley & Sons. 390 pp.

Tanaka, K., E. Kriegler, T. Bruckner, G. Hooss, W. Knorr, T. Raddatz (2007) Aggregated Carbon Cycle, Atmospheric Chemistry, and Climate Model (ACC2): description of the forward and inverse modes. Reports on Earth System Science No. 40. Max Planck Institute for Meteorology, Hamburg. 188 pp.
http://www.mpimet.mpg.de/wissenschaft/publikationen/erdsystemforschung.html

Tanaka, K. (2008) Inverse estimation for the simple Earth system model ACC2 and its applications. Ph.D. dissertation. Hamburg Universität. International Max Planck Research School on Earth System Modelling, Hamburg. 296 pp.
http://www.sub.uni-hamburg.de/opus/volltexte/2008/3654/

Tarantola, A. (2005) Inverse problem theory and methods for model parameter estimation. Society for Industrial and Applied Mathematics (SIAM), Philadelphia, USA. 342 pp.
http://www.ipgp.jussieu.fr/~tarantola/

Tjoelker, M. G., J. Oleksyn, P. B. Reich (2001) Modelling respiration of vegetation: evidence for a temperature-dependent Q10. *Global Change Biology*, **7**, 223-230.

Tol, R. S. J, A. F. de Vos (1998) A Bayesian statistical analysis of the enhanced greenhouse effect. *Climatic Change*, **38**, 87-112.

Trudinger, C. M. Trudinger, I. G. Enting, P. J. Rayner, R. J. Francey (2002) Kalman filter analysis of ice core data 2: double deconvolution of $CO_2$ and $\delta^{13}C$ measurements. *Journal of Geophysical Research*, **107**, D20, 4423-4446, doi:10.1029/2001JD001112.

van Aardenne, J. A., F. J. Dentener, J. G. J. Olivier, C. G. M. Klein Goldewijk, J. Lelieveld (2001) A 1 x 1 degree resolution dataset of historical anthropogenic trace gas emissions for the period 1890-1990. *Global Biogeochemical Cycles*, **15**, 909-928.

von Storch, H., F. W. Zwiers (1999) Statistical analysis in climate research. Cambridge University Press, Cambridge, United Kingdom. 484 pp.

Wang, G. (2005) Agricultural drought in a future climate: results from 15 global climate models participating in the IPCC 4th assessment. *Climate Dynamics*, **25**, 739-753.

Zellner, A., G. C. Tiao (1964) Bayesian analysis of the regression model with autocorrelated errors. *Journal of the American Statistical Association*, **59**, 763-778.